

THESIS

(1995)



3 1293 01410 1772

This is to certify that the
dissertation entitled
FLUORESCENT PROBES FOR MONITORING AND
CHARACTERIZING THE CRYSTALLIZATION
CONDITIONS OF LYSOZYME

presented by

Borlan Pan

has been accepted towards fulfillment
of the requirements for

Ph.D. degree in Chemical Engineering


Major professor

Date Sept. 27, 1995

LIBRARY

Michigan State University

PLACE IN RETURN BOX to remove this checkout from your record.
 TO AVOID FINES return on or before date due.

DATE DUE	DATE DUE	DATE DUE
OCT 25 2001 2026 0	_____	_____
_____ JAN 2 2004	_____	_____
_____	_____	_____
_____	_____	_____
_____	_____	_____
_____	_____	_____
_____	_____	_____

**FLUORESCENT PROBES FOR MONITORING AND
CHARACTERIZING THE CRYSTALLIZATION
CONDITIONS OF LYSOZYME**

By

Borlan Pan

A DISSERTATION

**Submitted to
Michigan State University
in partial fulfillment of the requirements
for the degree of**

DOCTOR OF PHILOSOPHY

Department of Chemical Engineering

1995

ABSTRACT

FLUORESCENT PROBES FOR MONITORING AND CHARACTERIZING THE CRYSTALLIZATION CONDITIONS OF LYSOZYME

By

Borlan Pan

The production of protein crystals for crystallographic structural determination largely relies on trial and error methods for determining optimal crystallization conditions. To expedite the screening and optimization of the protein crystallization process, methods are required that are able to monitor the molecular scale interactions occurring during nucleation and subsequent crystal growth in supersaturated solutions. Steady-state and time-resolved fluorescence and anisotropy measurements of protein-coupled fluorescent probes are applied to monitor and characterize the crystallization behavior of hen egg-white lysozyme (HEL).

The X-ray crystallographic structure of HEL co-crystallized with the organic anion orange II is first examined. The decreased amount of NaCl required to crystallize HEL and the decreased extent of the solvent structure indicate the participation of orange II in the crystallization process. Further investigations using 1-pyrene butyric acid (PBA) as a covalently bound fluorescence probe demonstrate that the fluorescence lifetimes of PBA and the rotational correlation times of HEL are dependent on the crystallization conditions.

The fluorescence from the non-covalently bound probe, 1-anilino-8-naphthalene sulfonic acid (ANS), is demonstrated to be a more practical method to dynamically monitor protein crystallization conditions of HEL *in*

situ. The use of this technique for the optimization of protein crystallization conditions is discussed. Finally, a comparison of the effects of various ionic precipitants on the fluorescence behavior of the ANS/HEL system provides information on the chemical mechanisms of HEL crystallization and is shown to be useful for the screening of crystallization conditions.

The results indicate that specific interactions between the HEL and anions are the central phenomenon involved in nucleation and crystallization. The binding of these anions is found to cause increased interactions between the protein and leads to a decrease in the rotational mobility. Subsequent nucleation and crystallization depends on the ability of these bound anions to participate in the formation of crystalline contacts between HEL molecules.

ACKNOWLEDGMENTS

The encouragement and support provided by the people associated with Michigan State University have contributed to my development over the years and made this work possible. I would like to thank my graduate advisor, Dr. Kris Berglund for his exceptional enthusiasm, dedication and guidance. I would also like to thank my parents, Dr. Keh-Ming and Su-Mei Pan and my dear friend, Elizabeth Gibson for being there throughout.

Thanks are also given to Dr. Daina Briedis, Dr. Daniel Nocera and Dr. Patrick Oriel for their useful suggestions, comments and criticisms while serving as my committee members. I would like to thank Dr. John Merrill and Dr. Donna Koslowsky for providing valuable discussions and assistance on protein separations. Dr. Mali Yin's work on the crystallographic refinement of the protein structures is also appreciated as is the assistance of Dr. Alexander Tulinsky and his coworkers. I would also like to acknowledge Dr. Tom Carter for his assistance with the spectroscopic instrumentation.

TABLE OF CONTENTS

LIST OF TABLES.....	viii
LIST OF FIGURES	ix
Chapter 1. Introduction and Background on Protein Crystallization	
Processes	1
Introduction	1
Background on Protein crystallization	4
History of Protein Crystal Growth and Crystallography	4
The Crystallization Process	7
Nucleation	8
Crystal Growth.....	12
Cessation of Crystal Growth	15
Intermolecular Interactions in Protein Association.....	16
Chapter 2. Current Experimental Techniques for Investigations on	
Protein Crystallization.....	24
Introduction	24
Macroscopic Methods	25
Static Light Scattering	31
Dynamic Light Scattering	32
Chapter 3. Fluorescence Techniques for Investigations on Protein	
Crystallization	40
Introduction	40
Fluorescence and Anisotropy Processes	42
Experimental Determination of Fluorescence Parameters	47
Applications of Fluorescence	50
Fluorescence of HEL	52
Chapter 4. The Effects of Co-Crystallization with Orange II on the	
Structure of Lysozyme.....	57
Abstract	57
Introduction	57
Material and Methods	59
Results	63
Effects on Crystallization	63
Comparison of the Structure of OHEL with 1HEL.....	63

Discussion	65
Chapter 5. Time-Resolved Fluorescence and Anisotropy of Covalently Coupled PBA for Monitoring the Crystallization Conditions of Lysozyme.....	70
Abstract	70
Introduction	71
Experimental Methods	73
Labeling of HEL with PBA	73
Sample Preparation	74
Fluorescence Measurements	74
Data Analysis	75
Results	77
Chromatography and PAGE of PBA-Lys.....	77
Fluorescence Measurements of PBA-HEL.....	78
Effects of NaCl	80
Effects of Ammonium Acetate and Ammonium Sulfate	83
Discussion	86
Chapter 6. Time-Resolved Fluorescence and Anisotropy of Non-Covalently Bound ANS for Monitoring the Crystallization Conditions of Lysozyme.....	90
Abstract	90
Introduction	90
Experimental.....	93
Solution Preparation.....	93
Fluorescence Measurements	93
Results.....	95
Response of ANS Fluorescence to Solution Conditions	95
Response of the Rotational Correlation Times to Solution Conditions.....	99
Monitoring the Progress of Batch Crystallization.....	102
Monitoring of Vapor Diffusion Crystallization.....	104
Discussion	105
Chapter 7. The Effects of Precipitants on the Time-Resolved Fluorescence and Anisotropy of ANS for Characterizing Lysozyme Crystallization	110
Abstract	110
Introduction	110
Experimental.....	112
Solution Preparation.....	112
Fluorescence Measurements	113
Results.....	114
Fluorescence Properties of ANS in HEL solutions.....	114
Comparison of Salt Effects at 3.6 % HEL.....	115
Effects of HEL Concentration	119
Discussion	121

Chapter 8. Summary and Conclusions127
 Conclusions127
 Recommendations for Further Research 130

APPENDIX A. Tabulated Data for Chapter 5133

APPENDIX B. Tabulated Data for Chapter 6146

APPENDIX C. Tabulated Data for Chapter 7169

LIST OF REFERENCES..... 190

LIST OF TABLES

	Page
Table 3.1. Amino acid sequence of hen egg white lysozyme.	52
Table 3.2. Tryptophan fluorescence parameters for 0.1% HEL.	54
Table 4.1. Summary of x-ray diffraction and refinement statistics for orange II lysozyme (OHEL) and lysozyme (1HEL, from [98]).	60
Table 4.2. Co-crystallization of HEL with orange II. Values of [NaCl] are the concentrations in the reservoir and values of [Orange II] are the initial concentrations in the hanging drop. X _n indicates the presence of crystals where n is the number of crystals, ppt indicates precipitate and + indicates relatively many. Qualitative descriptions are given in the parenthesis indicating small (sm), large (lg) and irregular (irr) crystals.	61

LIST OF FIGURES

	Page
Figure 1.1. Schematic illustration of the processes involved in nucleation and amorphous precipitation as described by classical nucleation theory.	9
Figure 1.2. The morphology of tetragonal HEL crystals. The faces are labeled as (101) and (110).	14
Figure 2.1. Schematic diagram of vapor diffusion trial. Typically a 4x6 grid of these trials are performed in one tray.	26
Figure 2.2. Schematic illustration of the crystallization behavior for HEL. The data points are measured solubility data at pH 4.6, 25° C [36]. The line through the points represent the solubility limit. Above this is a metastable zone where nucleation does not occur. In the X region, crystallization occurs. Above this region, immediate precipitation is observed. (Adapted from reference [8])	28
Figure 3.1. Photochemical processes in fluorescence spectroscopy.	42
Figure 3.2. Photoselection in fluorescence anisotropy. The arrows in the box represent the absorption dipole moments of the fluorescent probes. Bold arrows indicate that absorption occurs.	45
Figure 3.3. Time-resolved fluorescence and anisotropy instrumentation.	48
Figure 3.4. HEL α -carbon atoms showing the main polypeptide chain (from reference [91]).	53
Figure 3.5. Effect of NaCl concentrations on the tryptophan a) fluorescence lifetimes and b) rotational correlation times of 2% HEL solutions.	55
Figure 4.1 Structure of Orange II.	59

Figure 4.2. Structures of a) OHEL co-crystallized with orange II and b) 1HEL (from Reference [98]) showing the protein and associated solvent atoms.	62
Figure 4.3. a) Average root mean square difference between the residues of OHEL and 1HEL. The models were overlaid by a least-squares procedure minimizing the rms difference between the backbone atoms. b) Thermal factors for OHEL and 1HEL.	64
Figure 5.1. The structure of 1-pyrene butyric acid (PBA).	73
Figure 5.2. Time-dependent fluorescence intensity decays of free PBA at 23°C in 50 mM sodium borate buffer at pH 8.5. Also shown is the fit through the total fluorescence decay data. I_{V_V} and I_{V_H} are virtually indistinguishable because of the fast rotational rate of the relatively small PBA. Each channel represents a time interval of 0.197 ns.	78
Figure 5.3. Time-dependent fluorescence intensity decays of 0.02% PBA-HEL at 23°C in 50 mM sodium acetate buffer at pH 4.6. The fits are shown as the solid lines through the data points. The difference in I_{V_V} and I_{V_H} is due to the fluorescence anisotropy of the conjugated PBA. Each channel represents a time interval of 0.197 ns.	79
Figure 5.4. Dependence of the a) fluorescence lifetimes of and b) rotational correlation times of PBA-HEL on NaCl concentrations at 2% (□) and 4% (○) HEL. The X and ppt symbols represents crystallization or precipitation, respectively. The + symbols represent the relative amounts formed to show increasing supersaturation.	81
Figure 5.5. Effects of the ionic strength of NaCl on the rotational correlation times of PBA-HEL at 2% (□) and 4% (○) HEL.	82
Figure 5.6. Dependence of the a) fluorescence lifetimes and b) rotational correlation times of PBA-HEL on HEL concentrations at 2% (□) and 5% (○) NaCl. See Figure 5.4 for an explanation of the X and ppt symbols.	83
Figure 5.7. Dependence of the a) fluorescence lifetimes and b) rotational correlation times of PBA-HEL on salt concentrations at 4% HEL. The (○), (Δ) and (□) represent solutions containing NaCl, NAc and NS, respectively.	84
Figure 5.8. Effects of the ionic strength with NaCl (○), NAc (Δ) and NS (□) on the rotational correlation times of PBA-HEL at 4% HEL.	85
Figure 6.1. Structure of ANS.	92

Figure 6.2. Time resolved fluorescence decay curves for 10^{-4} M ANS in 3.6 % HEL.	96
Figure 6.3. Response of the fractional pre-exponential factors A_1 (\circ), A_2 (\bullet), A_3 (\square) and A_4 (\blacksquare) on NaCl concentrations for 3.6 % HEL.	97
Figure 6.4. Response of the combined fractional contributions from A_1 and A_2 (FA_{12}) of HEL associated ANS to the ionic strength of NaCl (a) and NS (b). For a), symbols represent 1.0 (\triangle), 2.0 (\diamond), 3.6 (\square) and 5.0 % (\circ) HEL. For b), symbols represent 2.1 (\diamond), 3.6 (\square) and 4.3 % (\circ) HEL. X indicates the formation of crystals, XC indicates crystalline spherulites and ppt indicates precipitation. The + symbols represent relative amounts formed.	98
Figure 6.5. Response of the long rotational correlation times (ρ_1) of HEL associated ANS to the ionic strength of NaCl (a) and NS (b). For a), symbols represent 1.0 (\triangle), 2.0 (\diamond), 3.6 (\square) and 5.0 % (\circ) HEL. For b), symbols represent 2.1 (\diamond), 3.6 (\square) and 4.3 % (\circ) HEL. See Figure 6.4 for explanations of the other symbols.	101
Figure 6.6. Monitoring the batch crystallization of HEL. The (\circ) symbols represents HEL concentrations from A^{281} measurements of diluted aliquots taken at the indicated times. The (\square) symbols are the FA_{12} values in a) and the ρ_1 values in b) from in situ fluorescence measurements.	103
Figure 6.7. Monitoring the progress of a HEL vapor diffusion crystallization trial using ANS fluorescence with a) FA_{12} and b) ρ_1.	105
Figure 7.1. Effects of the ionic strength of NS (\circ), NaP (\square), pH 4.6 NAc (\diamond), NaCl (\triangle) and NaSCN (∇) salts on the a) FA_{12} and b) ρ_1 fluorescence parameters and crystallization behavior of 3.6% HEL solutions. X indicates the formation of crystals and XC indicates crystalline clusters. The + symbols represent relative amounts formed.	117
Figure 7.2. Effects of the ionic strengths on the a) FA_{12} and b) ρ_1 fluorescence parameters and crystallization behavior of 3.6% HEL solutions at pH 7.7 (\circ), 6.4 (\square) and 4.6 (\diamond). See Figure 7.1 for an explanation of the other symbols.	118

Figure 7.3. Effects of HEL concentrations on the a) FA₁₂ and the b) ρ_1 fluorescence parameters and crystallization behavior of 0.86 ionic strength NS (○), NaP (□), pH6.4 NAc (◇), NaCl (△), NaSCN (▽) and 0.86M concentration NS (○) solutions. See Figure 7.1 for an explanation of the other symbols.

119

Chapter 1

Introduction and Background on Protein Crystallization Processes

Introduction

To determine the three dimensional structure of proteins using X-ray crystallography, diffraction quality protein crystals must be obtained. The goal is to find conditions that will gradually increase the level of supersaturation until only a few nuclei are formed that will grow into single crystals. Presently, the production of these crystals largely relies on trial and error methods for determining optimal crystallization conditions. Although this method has produced many suitable crystals in the past, the disadvantages of the trial and error approach are well known [1]. Typically, the search for optimal conditions is performed by screening a multitude of conditions among which include the choice of precipitants, the protein concentrations, pH and temperature. The choice of successive experimental trials is governed by a combination of skill, intuition and chance. Protein crystallization is at present still an art more than it is a science.

In these empirical trials, suitable conditions for crystallization are known only after the crystals are formed. Evaluating the efficacy of these conditions relies on macroscopic observations on which further crystallization trials are based. Only limited information on the physico-chemical process of crystallization is obtained from macroscopic observations and results in an inefficient strategy for finding optimal conditions. These traditional methods are particularly disadvantaged by the long experimental time periods,

ranging from days to months, or occasionally years, before the results of the trials are known. Furthermore, the optimization of conditions once a suitable precipitant is found is hindered by the lack of active control over the solution properties which mediate nucleation and subsequent crystal growth. A better understanding of the interactions occurring between the protein, solvent and precipitant components is required to achieve a more rational and efficient search of protein crystal growth conditions.

To expedite the screening and optimization of the protein crystallization process, methods are required that are able to monitor the molecular scale interactions occurring during nucleation and subsequent crystal growth in supersaturated solutions. Measurements of the microenvironmental properties of fluorescence probes provide a means by which the dynamic interactions between protein molecules, the solvent and other additives can be measured prior to the actual appearance of crystals.

The microenvironments of fluorescence probes are strongly influenced by solution conditions. In turn, the fluorescence lifetimes and rotational correlation times of these probes are affected by the probe microenvironment. Hence, measurements of these fluorescence properties are able to provide information on the solution conditions leading to supersaturation. Time-resolved techniques allow the direct measurement of the fluorescence lifetimes and rotational correlation times. Time-correlated single photon counting is a high resolution method that is often used to measure the time-dependent fluorescence decays. From these decays, the fluorescence and rotational parameters can be extracted. In this work, *in situ* techniques using the steady-state and time-resolved fluorescence of probe molecules are developed and demonstrated to be a flexible and sensitive alternative to current methods.

The fundamental processes involved in protein crystal growth are first reviewed. A summary of the techniques used to investigate and screen protein crystallization conditions then follows. From this background information, the predominant issues and needs involved in protein crystallization are illustrated. Much of the previous work has focused on the crystallization properties of hen egg-white lysozyme (HEL) and results concerning this protein will be emphasized in the review. To enable comparison with the available chemical, structural and crystallization data, HEL has also been chosen for the current work. The results are presented in the following studies:

- 1) The X-ray crystallographic structure of HEL co-crystallized with the organic anion orange II is examined. The effects of this co-crystallization agent on the determined structure of HEL itself was found to be minimal. However, the perturbed crystallization behavior and the decreased extent of the solvent structure indicate the participation of orange II in the crystallization process.
- 2) Investigations using 1-pyrene butyric acid (PBA) as a covalently bound fluorescence probe demonstrate that the fluorescence lifetimes of PBA and the rotational correlation times of HEL are dependent on the crystallization conditions.
- 3) Fluorescence measurements of the non-covalently bound probe, 1-anilino-8-naphthalene sulfonic acid (ANS), are demonstrated to be a practical method to dynamically monitor protein crystallization conditions of HEL *in situ*. The use of this technique for the optimization of protein crystallization conditions is discussed.

- 4) A comparison of the effects of various ionic precipitants on the fluorescence behavior of ANS in HEL solutions provides information on the chemical mechanisms of HEL crystallization and is shown to be useful for the screening of crystallization conditions.

In summary, methods using fluorescence spectroscopy have been developed to monitor the interactions of proteins for a more efficient screening and optimization of protein crystallization conditions. Through these studies, the mechanisms of HEL crystallization have also been investigated. These mechanisms most likely involve the neutralization of the repulsive positive potential on the surface of HEL by anion binding and a subsequent chemically specific nucleation step mediated by the bound anions. A combination of physical measurement techniques and chemical knowledge of protein-solvent and protein-protein interactions promises to be a more rational and efficient strategy than the traditional methods for the production of protein crystals.

Background on Protein crystallization

History of Protein Crystal Growth and Crystallography

The history of protein crystallization is replete with serendipitous and inadvertent discoveries using trial and error approaches for obtaining protein crystals. This situation has not presently changed, although the need for more rational and efficient methods is now being realized. A comprehensive survey of the historical progress of protein crystallization is found in MacPherson's review [2]. Here, we present a summary of the empirical progress made in protein crystallization.

In the mid to late 1800's, hemoglobin became the first subject for the systematic study of protein crystallization. By pressing the blood of earthworms between two glass slides and allowing the liquid to slowly evaporate, flat plate-like crystals were obtained [3]. The crystallization of hemoglobin from several other animal species was accomplished by more or less fortuitous means. Subsequent studies on the crystallization of plant reserve proteins and albumins produced several procedures for protein crystallization that are now common. These procedures include temperature variation, dialysis against solutions of low ionic strength and the use of organic additives. Another common procedure, salting-out with ammonium sulfate and magnesium sulfate, originated in the crystallization of hen egg and horse serum albumins [4].

Efforts to crystallize enzymes made by J.B. Sumner in the early 1900's demonstrated that enzymes were in fact proteins. Through this work, Sumner successfully crystallized concavallin A, concavallin B and urease from the Jack Bean [5]. An illustration of the serendipitous nature of protein crystallization is seen in Stacey Howell's accidental crystallization of canavallin [6]. After leaving a beaker containing a solution of canavallin on his bench top for a week, Howell returned to find a disagreeable odor along with rhombohedral crystals growing on the bottom of the beaker. The native canavallin molecules had apparently been cleaved by bacterial proteases into products that would crystallize whereas the native canavallin would not. This ability of proteolytic products to crystallize has since been found to occur with many other proteins.

Further incentive for progress in understanding protein crystallization processes was provided by the advent of X-ray crystallography for structural determination. Until the development of X-ray crystallography, protein

crystallization was primarily used for purifying proteins from extracts or demonstrating the purity of protein preparations [2]. Since the 1930's, the growth of large single crystals for use in X-ray diffraction studies has largely supplanted the use of crystallization for separations. Until the 1970's, the supply of protein crystals was more than adequate for the needs of structural determination.

However, advances in the methodology and instrumentation of X-ray crystallography have greatly reduced the effort and time required to solve protein structures [1]. Recombinant DNA technology now allows the production of sufficient quantities of protein for study. Synchrotron radiation sources are able to provide X-ray beams with greater intensities and a wider range of specific wavelengths to produce clearer diffraction patterns. Electronic area detectors and automated diffractometers also allow the rapid collection of diffraction patterns into digital form. In probably the most significant advancement, improved computer hardware, algorithms and graphics allow for the amenable analysis and visualization of diffraction data. These advances have resulted in the rapid determination and refinement of the three-dimensional coordinates of proteins. However, this is the case only after large and well-ordered protein crystals have been obtained.

Unfortunately, the progress seen in the methodology of X-ray structural determination has not paralleled progress in the fundamental and technical aspects of protein crystallization. Hence, the growth of suitable crystals has become the "bottle-neck" in the determination of protein structures. Most current efforts to crystallize proteins rely on the same methods used early in the history of protein crystal growth. That is, by trial and error methods where hundreds or thousands of experimental trials are conducted to find the optimal conditions. Investigators have tried many

varied means such as subjecting the protein solution to the addition of metal ions, the addition of polymers, gels, containerless growth cells, and microgravity environments in space in efforts to grow protein crystals. Through these empirical macroscopic studies heuristic rules have been developed but protein crystallization remains a process involving more intuition and chance than scientific methodology. The situation is such because an understanding of the fundamental aspects of the association and aggregation processes in protein crystallization is lacking.

The Crystallization Process

Protein crystallization is a complex process affected by a variety of interacting parameters in a continuously evolving and non-ideal multicomponent system. By considering the processes that are common to protein crystallization, the pertinent parameters and effects can be isolated. The growth of protein crystals involves three distinct interdependent stages: 1) Nucleation of crystals 2) Post-nucleation crystal growth and 3) Cessation of crystal growth. Although the theoretical treatment of protein crystallization is by no means complete, the current views on protein crystallization processes are presented as a starting point for further investigations. For a more comprehensive survey of the various aspects of protein crystallization, reviews are found in Arakawa and Timasheff's theoretical treatment of protein solubility [7], Feher and Kam's article on nucleation and growth [8], Boistelle and Astier's article on crystallization mechanisms [9], Mcpherson's treatment of the general principles [9-11] and Ollis and Whites article from a more utilitarian viewpoint [12].

Nucleation

A necessary condition for the nucleation and growth of crystals is that the concentration of protein in the growth solution must be greater than the solubility concentration. This non-equilibrium supersaturated condition results in a chemical potential of the protein solute that is greater than at equilibrium conditions and provides the driving force for phase transition. The parameter $\beta = C/C_s$ is commonly used to describe the degree of supersaturation in a protein solution where C_s is the solubility concentration and C is the actual concentration of the protein. With this relationship, the chemical potential driving force, $\Delta\mu$, is,

$$\Delta\mu = k_B T \ln(\beta) \quad (1.1)$$

where k_B and T are Boltzman's constant and temperature, respectively.

Several means of achieving supersaturation are available which decrease solubility limit of the protein by changing the solution properties [9, 13]. These methods include 1) the increase or decrease of the temperature, 2) evaporation of the solvent, 3) the addition of other soluble species or 4) a change of pH. Although these methods are the most commonly used, many variants to these methods are also seen. Not only is the supersaturation important in the final quality of the crystals, but also the path taken towards this state.

Regardless of the specific technique used, once supersaturation is achieved, this far from equilibrium condition causes the association of protein molecules. Nucleation occurs as the protein molecules aggregate into a suitable structural configuration that will continue to grow into protein crystals. Nucleation theory was first applied to proteins by Feher and Kam [8] and is now the most commonly accepted view of the initial events in

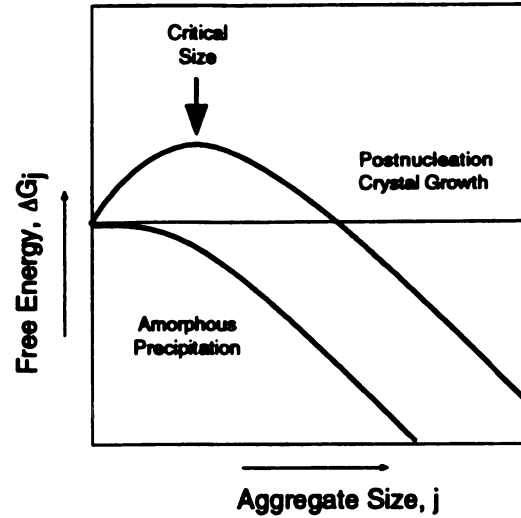


Figure 1.1. Schematic illustration of the processes involved in nucleation and amorphous precipitation as described by classical nucleation theory.

protein crystallization. Two possibilities in the tendency towards equilibrium are the nucleation of crystal growth centers and the formation of amorphous aggregates.

According to the classical nucleation theory, a distribution of small aggregates initially forms to produce a state of quasi-equilibrium. To form a crystal nucleus that continues into post-nucleation growth, the aggregate size must surmount a free energy barrier formed by two competing free-energy terms as illustrated in Figure 1.1,

$$\Delta G_j^o = -vjG_b + \beta j^\gamma G_s \quad (1.2)$$

where G_b is the bulk energy/unit volume and G_s is the energy/unit surface area relative to the values in solution. v is the volume of the molecule and vj gives the total volume of the aggregate. The total surface area is given by βj^γ , where β and γ depend on the shape of the aggregate. For a spherical

aggregate, $\beta=(36\pi v^2)^{1/3}$ and $\gamma=2/3$. The first term on the right hand side represents the bulk driving force for nucleation and increases as the size of the nucleus increases. The second term arises as a consequence of dangling bonds on the surface of the nucleus causing inhibition of further nucleus growth. This surface energy term increases with an increase in the surface area of the nucleus. As the nucleus develops through local fluctuations in the local concentration, the ratio of the surface area to volume decreases allowing the volume term to dominate.

Under this framework, the mechanism encountered with crystal nucleation contrasts with the formation of an amorphous precipitate [14]. Amorphous aggregates are assumed to be approximated by a one dimensional chain of protein molecules where the addition of monomers only occur at the ends. Because the bulk driving force dominates throughout the range of aggregate sizes, a small surface free energy term contributes little to the total free energy. Hence, no free energy barrier is present and the amorphous aggregate rapidly forms without the need for a nucleation event as seen in Figure 1.1. The precise chemical nature of the structural configuration is unclear at this time, but is crucial to understanding the formation of protein crystals.

Application of the theory of homogenous vapor phase nucleation to the batch crystallization of lysozyme leads to a rationalization for conditions leading to either crystallization or amorphous aggregation. The protein aggregation process has been described as the successive association and dissociation of monomers to a growing aggregate, A_j , composed of j monomers by the reaction,



For a crystalline aggregate, the structure of the nucleus is assumed to be a compact spherical cluster, while for amorphous precipitation, a linear polymer is formed. The equilibrium constants for the crystalline j-mer is then given by,

$$K_j = \frac{k_j^f}{k_{j+1}^b} = \frac{C_{j+1}}{C_j C_1} = \exp \left[- \frac{d\Delta G_j^o}{dj} / k_B T \right] \quad (1.4)$$

$$= \exp \left\{ - [\nu G_B + \gamma \beta j^{\gamma-1} G_s] / k_B T \right\}$$

where C_j is the concentration of the j-mer. Assuming that the aggregate is spherical so that $\gamma=1/3$, K_j can be expressed in terms of K_1 and K_∞ ,

$$K_j = K_1 \left(\frac{K_\infty}{K_1} \right)^{1-j^{-1/3}} = K_\infty \left(\frac{K_1}{K_\infty} \right)^{j^{-1/3}} \quad (1.5)$$

From this relation, it is expected that $K_\infty^{XTAL}/K_1^{XTAL} \gg 1$ under crystallizing conditions. Under conditions favoring amorphous aggregation, it is expected that $K_j \approx K_1 \approx K_\infty$, or $K_\infty^{AMOR}/K_1^{AMOR} \approx 1$ since the free energy does not depend on the size of the aggregate. It has been suggested that by measuring K_1 and K_∞ for a particular condition, it is possible to predict whether crystals will grow or an amorphous aggregate will be formed.

By considering the kinetics of the aggregation process, further information on the time dependence of the nucleation process is obtained. Results from the numerical calculations indicated that after a relatively short time period, a quasi-equilibrium is attained where C_j remains constant for j less than the critical nucleus size of j^* . For the crystallizing solution, $C_j(t)$ must then proceed toward the true equilibrium values. Once a critical nucleus size is reached, the rate of monomer association becomes equal to the rate of dissociation. Thus, the growth of the nucleus is governed by a random

addition process rather than being driven by a free energy gradient. From vapor phase nucleation theory, the estimated delay time is then,

$$\tau_D = (\Delta j^*)^2 (k_{j^*}^b)^{-1} \quad (1.6)$$

where Δj^* is the number of monomer additions to the critical nucleus needed for the energy difference to become of the order $k_B T$ and the approximate time of each addition is given by $(k_{j^*}^b)^{-1}$. As the protein concentration is increased, the Δj^* that must be accomplished for the energy difference to become of the order $k_B T$ decreases drastically and nucleation occurs more readily. For the formation of amorphous aggregates, no time delay should occur.

There are two principle mechanisms of crystal nucleation. Homogenous nucleation occurs when nuclei spontaneously form in the bulk phase as described above. In the case of heterogeneous nucleation, the nuclei form onto solid substrates such as the walls of the container, a dust particle or a seed crystal. The degree of supersaturation required to produce homogenous nucleation is generally greater than with heterogeneous nucleation. This effect occurs because contact with the solid substrate decreases the surface area in contact with the solution and subsequently decreases the surface free energy term. Eventually, a critical nucleus size may be achieved and depending on random fluctuation events, either the nucleus will continue to grow into a crystal or dissipate back into a prenucleation cluster.

Crystal Growth

After a nucleus has been formed, the postnucleation growth of protein crystals continues by the transport of protein to the crystal surface followed by their ordered incorporation into the crystal lattice. According to the

periodic boundary chain theory [15-17], crystal growth can occur at three different types of faces: 1) flat faces, where growth occurs in a two dimensional plane, 2) stepped faces, where growth occurs along a linear array and 3) kinked faces, where growth occurs by the direct incorporation of the molecule onto the lattice corner. No nucleation mechanism is required for growth onto kinked faces, whereas a one dimensional nucleation mechanism is needed for growth onto stepped faces and a two dimensional nucleation event is required for the flat faces. Consequently, the growth rates of the flat faces are less than the growth rates of the stepped faces which are, in turn, less than the growth rates of the kinked faces. Since the kinked and stepped faces grow at a relatively faster rate than the flat faces, the kinked and stepped faces eventually disappear and the growth rate of the crystal is determined by the growth rate of the flat faces.

Two primary mechanisms are involved with the growth of flat faces. These mechanisms are growth by two dimensional nucleation and growth by spiral dislocation. With the two dimensional nucleation mechanism, molecules must diffuse onto the surface of the crystal and become adsorbed. Once the two dimensional nucleus has formed a large enough layer, additional molecules can then be incorporated along the edges. More than one nucleation event can occur so that multiple layers may eventually intersect or grow on top of one another. The spiral dislocation mechanism occurs when a screw dislocation appears on the flat face providing a step or a sequence of steps that can spread from the center. Growth occurs by the lateral growth from the spiral steps until the crystal edge is reached where upon a new layer has been added to the crystal face.

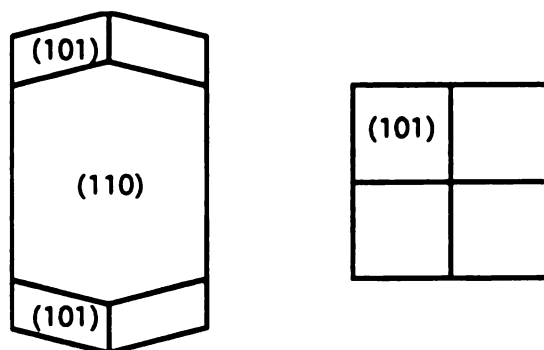


Figure 1.2. The morphology of tetragonal HEL crystals. The faces are labeled as (101) and (110).

Most of the theories on protein crystal growth have been derived from the small molecule crystal growth theories. However, there are important differences involved with proteins [18]. Because of the larger size and greater complexity, there are relatively few specific contact sites and more possible non-specific contact points. The energies per bond are also much lower if the surface area is taken into account. Several attempts at understanding the mechanism of HEL crystallization have been made by measuring the growth of the tetragonal crystal form. The classical form of the HEL crystal used in many protein crystallization studies is illustrated in Figure 1.2. Growth rate measurements are made on the 101 and 110 faces which define the morphology of this crystal.

Fiddis et. al. [19] concluded that tetragonal lysozyme crystals grew by a mechanism of spontaneous surface nucleation instead of by screw dislocation. In subsequent growth studies using electron microscopy, Durban and Feher found that growth by the two dimensional mechanism only occurs at higher values of supersaturation ($>1\%$ HEL) [20]. At lower protein supersaturations ($<0.8\%$ HEL) growth occurred by a defect mediated mechanism. These results were in agreement with their studies using visual

examination of growth rates where the effect of NaCl concentration was also investigated [18]. At greater NaCl concentrations, the solubility of HEL decreases. This lower solubility indicates stronger bonding in the crystals and thus should predict a greater surface energy. However, the surface energy was found to decrease as the solubility decreased. Similar results were found by Forsythe and Pusey [21] with the effect of decreased temperatures. The reasons for these observations are not clear, but may involve the formation of preformed aggregates which are directly incorporated into the crystal.

Although crystal growth mechanisms determine the growth rate of the flat faces, they do not define the actual structure of the crystal. Both internal and external factors play crucial roles in determining the actual crystal morphology or habit. Internal factors include the structure of the protein molecule along with the bonds in the crystal. External factors include the level of supersaturation and the solution composition including salt concentration, pH, temperature and impurities in the protein preparation. For example, HEL may exist in a variety of forms depending on the crystallization conditions and the composition of the solution [22]. Aside from the tetragonal form, orthorhombic, monoclinic, and triclinic crystal forms may also result under different growth conditions. Many of the internal and external factors may be modified to produce protein crystals of a suitable morphology and size.

Cessation of Crystal Growth

A problem encountered in obtaining large crystals is the eventual cessation of protein crystal growth even when the protein concentration is not depleted. This behavior has been observed experimentally, but the cause is not well understood. Previous studies have shown that proteins crystals

grown under similar conditions reach approximately the same terminal size depending on the rate of crystal growth [8]. Crystals that were reduced in size by cutting or dissolving grew again to approximately the same size when placed in the original growth conditions. Furthermore, impure protein preparations produce smaller crystals than pure protein solutions. Several explanations have been given to explain this behavior. The most generally accepted reason for the cessation of growth is through the poisoning of growth sites by impurities in solution. Errors would be successively incorporated into the lattice until growth could no longer occur. However, this would not explain why a microgravity environment can produce larger crystals. Hence, convection current in the protein solution should also play a role in causing cessation of growth [23]. A scenario where both impurities and convection synergistically contribute has been suggested [20]. Another explanation involves colloid stability theory, where the electrostatic interface potential between the crystal and the solution builds up to a point where further incorporation is inhibited [24]. As with the other aspects of protein crystallization, a thorough understanding and the ability to control cessation of growth is as of yet lacking.

Intermolecular Interactions in Protein Association

Further investigations of the forces and dynamics involved in protein association needs to be accomplished in order to understand and control the complex processes involved in protein crystallization. By examining the microscopic aggregation and ordering behavior responsible, a connection with the macroscopic behavior may be made. This connection is made possible by modeling the molecular processes involved and relating these processes to the bulk macroscopic behavior. The extent of the models must be compromised by

the limitations of an incomplete theory on the fundamental nature of intermolecular forces and dynamics, the finite computational resources available and insufficient experimental techniques for measuring these molecular interactions. To begin, the molecular forces involved in protein association are examined.

Four general types of molecular interactions are responsible for the structure and function of biological molecules as well as the aggregation behavior. These are electrostatic forces, dispersion forces, hydrogen bonding interactions and so called hydrophobic interactions. Together, through the actions of these forces, the interaction of protein solutes with the aqueous solvent lead to dynamic association and organization and ultimately, the macroscopic thermodynamic and kinetic behavior of crystallizing protein solutions. Protein-solvent interactions balance against protein-protein interactions to determine whether the protein molecules will remain in solution, randomly aggregate to form amorphous precipitate or spontaneously order to form crystals.

The most dominant and long-range interactions are due to electrostatic forces. These interactions originate from the attraction or repulsion of charges particles in a particular environment. Actually, all four of the types of interactions mentioned above are ultimately due to charge effects, but in the context of protein association, electrostatic forces are considered to arise only from ionic species. Attempts to model behavior of ions in dilute ionic solution has lead to some degree of success, although a complete understanding at higher ionic concentrations is yet to be obtained.

In a salt solution, where the ions are presumably dissociated, a central ion causes a local polarization in the concentration of ions with opposite charge so that the concentration of oppositely charged ions is higher near the

cent

fun

pot

giv

a c

lin

po

av

be

w

pe

a

t

p

b

s

s

c

c

central ion and decays to the bulk value away from the central ion. The fundamental relationship between charge density, ρ_r , and electrostatic potential, ψ , is given by the Poisson-Boltzmann (PB) equation,

$$\frac{1}{r^2} \frac{d}{dr} \left(r^2 \frac{d\psi}{dr} \right) = -\frac{4\pi}{\epsilon} \rho_r, \quad (1.7)$$

given here for a spherically symmetric geometry, where r is the distance from a central ion and ϵ is the dielectric permittivity of the solvent. By solving the linearized form of the PB equation with the assumption that the charge polarization caused by a central reference ion can be approximated with an average charge distribution profile, the first successful model of ionic behavior in solutions was arrived at with the Debye-Huckel equation,

$$\log f_{\pm} = -\frac{A(z_+z_-)I^{\frac{1}{2}}}{1 + BaI^{\frac{1}{2}}} \quad (1.8)$$

where f_{\pm} is the activity coefficient of the ion, z_+ and z_- are the respective positive and negative valences of an ionic salt, I is the ionic strength given by,

$$I = \frac{1}{2} \sum c_i z_i^2 \quad (1.9)$$

and A and B are constants. The finite size of an ion is taken into account with the parameter a , representing the radius of the central ion. This equation provides an adequate theoretical description for dilute solutions of ions but at higher concentrations the theory fails.

An examination of the effects of salt concentration on the experimental solubility of protein solution may provides an explanation as to why the simple treatment is inadequate. In general, the solubility of proteins is enhanced with low salt concentrations. This behavior is termed salting-in and can be explained by treating the protein as a charged species with the Debye-

Hückel theory. The ionic atmosphere surrounding the protein decreases the electrostatic free energy causing an increase in the solubility. As the salt concentration is increased, however, a point is reached where the solubility begins to decrease [25]. The solubility of proteins in this regime can be described by modifying the Debye-Hückel equation,

$$\log \frac{S}{S_0} = \frac{A(z_+z_-)I^{\frac{1}{2}}}{1 + BaI^{\frac{1}{2}}} - K_s I \quad (1.10)$$

The salting-out behavior with higher salt concentrations is due to two effects [7]. First, the addition of salt ions to aqueous solutions causes the formation of hydration sheaths of ordered water molecules around the ions. This binding of water molecules by the salt ions decreases the amount of water available for the primary solvation of the protein molecules. The second effect is due to the secondary solvation of the protein molecules [26]. The replacement of water molecules by a protein solute of lower dielectric constant causes an effective decrease in the orientational polarizability of the solvent that leads to a repulsion of the salt ions. Consequently, an increase in the free energy causes a decreased solubility of the protein.

London dispersion or Van Der Waals interactions cause a short range attraction between protein molecules. While electrostatic forces are caused by discrete charged species, dispersion forces arise from fluctuations in the electron densities within molecules and can be termed electrodynamic. Dispersion forces arise when an instantaneous fluctuation in the electron density of one molecule forms an dipole moment. This dipole moment induces the formation of an instantaneous dipole moment in another molecule. The dipole moments of the two molecules become correlated and lead to an overall attractive force. Dispersion forces vary with the distance, r , between two

molecules as r^{-6} . At very close distances, the electronic densities of the molecules overlap and repulsion occurs. At greater distances, the phases of the electromagnetic field propagating between dipoles become out of phase and causes a retardation effect so that the dispersion forces vary with r^{-7} . Although dispersion forces are small for small molecules, the strength of dispersion interactions become significant in the case of macromolecules.

In aqueous solutions, hydrogen bonding and hydrophobic interactions become significant. The resemblance of the average structure of water to a diamond lattice results from the intermolecular hydrogen bonding between water molecules. Intramolecular and intermolecular bonds within proteins are also determined by direct hydrogen bonding. Hydrogen bonding forces arise from the interactions between the permanent dipole moments of polar molecules. Because of this geometric constraint, hydrogen bonds are dependent on the orientation of the dipoles, the strongest interaction occurring with a linear alignment of the dipoles. Generally, the optimal distances occur at around 3 Å with an energy between -3 and -6 kcal/mol.

Hydrophobic interactions are an indirect result of hydrogen bonding. Although not completely understood, these interactions between nonpolar molecules are entropic in origin and are a consequence of the structuring of water around a nonpolar molecule. Aggregation of nonpolar molecules cause a relative increase in the entropy of water because of the greater number of microstates that unstructured water molecules possess. The hydrophobic interaction is involved in protein folding, the specific association of multimeric proteins and also the nonspecific crystallization and precipitation behavior of proteins.

Protein molecules, with sizes larger than 1 nm in diameter, may be regarded as colloidal particles. Hence, colloid stability theory may be applied

to protein associations [24, 27, 28] by approximating globular proteins as lyophobic particles or sols. According to this model, whether protein molecules will remain in solution as a stable suspension or will aggregate depends on a balance between the repulsive electrostatic forces and the attractive dispersion forces. The theoretical treatment was developed independently by Derjaguin and Landau and by Verwey and Overbeek and is known as the DLVO theory.

In the DLVO theory, the electrostatic interaction of charged colloid particles is due to a diffuse double layer of opposite charge surrounding the particle [29]. For two spheres of equal radius, a , at a center to center distance, r , the potential energy due to electrostatic repulsion, $U_r(r)$, is given as,

$$U_r(r) = 2\pi\epsilon a\psi_0^2 \ln[1 + \exp(-\kappa s)] \quad (1.11)$$

where ψ_0 is the surface potential of the particle and $s=r-2a$. Dispersion forces are responsible for the attractive interactions. The potential energy due to the dispersion interactions may be approximated by the expression

$$U_a(r) = -\frac{Aa}{12s} \quad (1.12)$$

where A is known as the Hamaker constant, which is dependent on the material of the particles.

Three distinct cases are possible: 1) At low salt concentrations, a primary potential energy minimum is present at the surface of the particle with a large potential barrier gradually decreasing away from the particle. In this case, the particles repel each other and can not aggregate. 2) At intermediate ionic strengths, a secondary minimum is present with a smaller potential energy barrier. The particles may more easily approach each other

to the distance of the secondary potential energy well. 3) At high ionic strengths, the potential energy barrier is nonexistent and aggregation occurs rapidly. In addition to changing the ionic strength, the behavior of aqueous colloid dispersions may be manipulated by altering the dielectric constant by mixing other solvents such as ethanol and by altering surface charge with the binding of charged species or changing the pH.

In analogy with protein solutions, these three cases correspond to 1) a stable protein solution, 2) a metastable protein solution and 3) amorphous precipitation of the protein. For the second case, the secondary potential well may allow interacting protein molecules to orient in a more favorable position for crystallization to proceed [28]. A configuration may be achieved where a collection of protein molecules are held together in the secondary potential well. Nucleation may occur as the favorably oriented particles in the collection collapses into the primary well.

This model of protein crystallization is most likely an oversimplification of the actual process. The structure of proteins are not well described as simple spherical objects with a uniformly charged surface. Protein surfaces are rough, with crevices and convolutions. The dynamic structural fluctuations observed in proteins also affect crystallization behavior. Charged amino acids and other polar groups are distributed non-uniformly and interact with one depending on the stereospecificity and chemical properties. Proteins are composed of flexible structural domains with segments that are mobile and loose. For example, the structure of lysozyme can be approximated with two lobes that bend at a hinge [30]. Even this model oversimplifies the reality. The molecular forces that drive protein association must be coupled with the dynamic aspects of protein polypeptide chains in order to achieve a complete physical picture.

Protein crystallization must involve the interaction of the different processes examined above. Electrostatic forces are long range interactions that may enhance or decrease the solubility of proteins. In the colloid picture of particle interactions, electrostatic forces only cause a repulsion between protein particles. Dispersion forces, on the other hand, result in an attractive interaction between protein particles. The structuring of water by hydrogen bonding is exerted indirectly through hydrophobic interactions. Hydrogen bonding also occur between protein molecules and with the solvent constituents. All of these more fundamental structural and chemical mechanisms are coupled with the dynamic motions of proteins to determine whether crystals can be produced. At this time, theoretical and computational limitations preclude the prediction of the crystallization behavior of proteins. Hence, a mechanistic understanding of nucleation, crystal growth and cessation of growth lies in the domain of experimental methods.

Chapter 2

Current Experimental Techniques for Investigations on Protein Crystallization

Introduction

Since the realization that a trial and error approach to the crystallization of proteins has proven to be inadequate, there has been an impetus towards developing improved techniques and a deeper understanding of this process. Many of these studies have been geared towards the development of assays to predict whether given crystallization conditions will promote favorable crystal growth. Some workers have investigated methods to predict crystallization conditions, while others have focused on a more fundamental understanding of the processes involved. All of these approaches require techniques to probe or deduce the interactions of proteins in the solution phase. In this chapter, the methods used for screening, characterizing and measuring aggregation behavior are reviewed along with a presentation of selected results obtained by previous studies. Macroscopic measurements of protein and solute concentrations and thermodynamics have provided information on the solubility and solute behavior of crystallizing protein solutions.

Spectroscopic methods, including light scattering and fluorescence, provide a microscopic view of the solution behavior of interacting proteins. Such methods provide details on the space and time scales that are not accessible to traditional macroscopic techniques and are thus valuable in understanding the mechanisms of protein crystal growth. Light scattering

has been extensively used to monitor and characterize the protein crystallization process. However, this method is inherently limited in its specificity and sensitivity. In contrast, fluorescence spectroscopy is a highly sensitive technique that is able monitor the behavior of specific components in solution. More recently, investigations have used electron microscopy and scanning microscope techniques to investigate the surface [20, 31, 32] and internal properties in protein crystals. X-ray crystallography also provides means by which the specific interactions between protein molecules and the associated solvent shell including other solutes may be visualized. The principles of the macroscopic, light scattering and, in the following chapter, fluorescence methods are presented along with applications pertinent to protein crystallization.

Macroscopic Methods

The screening, characterization and analysis of protein crystallization processes has overwhelmingly relied on macroscopic measurements. These traditional methods use the visual inspection of crystal growth to screen a wide array of experimental conditions in the hopes that some form of crystals will result. In the event that crystals are obtained, successive trials are conducted to progressively narrow the range of conditions needed to optimize the crystal growth properties. However, many important proteins still may not form well ordered crystals under the screened conditions and the structural determination is subsequently abandoned. This situation makes the development of techniques able to crystallize such proteins crucial and demonstrates the importance of understanding the mechanisms involved in protein crystal growth.

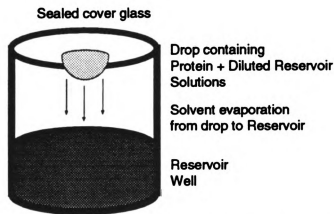


Figure 2.1. Schematic diagram of vapor diffusion trial. Typically a 4x6 grid of these trials are performed in one tray.

The hanging drop method, as illustrated in Figure 2.1, is by far the most common technique used to grow crystals because of the gradual attainment of supersaturation. This method involves a combination of solvent evaporation and the addition of a soluble precipitant. A hanging drop containing the protein and diluted reservoir solution is suspended above the reservoir well which contains a higher concentration of the precipitant. In this way, the water in the drop and in the reservoir will equilibrate by vapor diffusion. Consequently, the protein and precipitant concentrations in the drop will gradually increase to create supersaturating conditions. The soluble precipitant is usually a salt such as ammonium sulfate, but polymers such as polyethylene glycol (PEG) and organic solvents such as methanol or 2-methyl-2,4-pentanediol (MPD) are often used. Variants to the hanging drop method include dialysis, gel growth and the use of controlled evaporation.

The traditional methods for the screening of crystal growth conditions has been classified into two groups. The so called “brute force” technique relies on the assumption that if enough combinations of parameters are tested, crystals will eventually result [33]. The use of robotics is particularly

amenable to this strategy. Although many crystals have been obtained using this method, the primary disadvantage is the large amounts of protein which must be consumed. For the 20 independent variables that may affect the crystallization behavior, 10^6 different conditions are possible if only two different values are assumed for each variable [8]. This technique has also been criticized in that the value of human intelligence and skill is minimized.

The other traditional approach, which has gained wide acceptance, is the “multiple factorial” [34] method. This procedure involves screening a set of conditions which have been successful in crystallizing other proteins. For the purpose of choosing conditions, a Biological Macromolecule Crystallization Database is available for more than 1000 crystal forms and over 600 macromolecules [35]. The selected conditions represent a statistical sampling of precipitants, buffers and the other parameters known to affect crystallization. Because of the randomness associated with this technique, it has also been termed the “shotgun” approach. A major disadvantage of this method lies in the difficulty of interpreting the outcomes. If no crystals result, the trials do not provide adequate physico-chemical information for a further choice of conditions. Proteins preparations are diverse in their crystallization behavior, even among those that appear to be closely related. It is likely that the small subset of possible conditions used in the statistical screening methods will not lead to the crystallization of some or possibly most proteins.

Because of the complexity of the protein crystallization process, it is unlikely that the empirical screening approach will be completely supplanted. However, knowledge of the effects of the physical and chemical properties of the protein and the interactions with the precipitants and solutions on crystallization behavior will be helpful in choosing proper experimental conditions. For example, it is generally conceded that hydrophobic

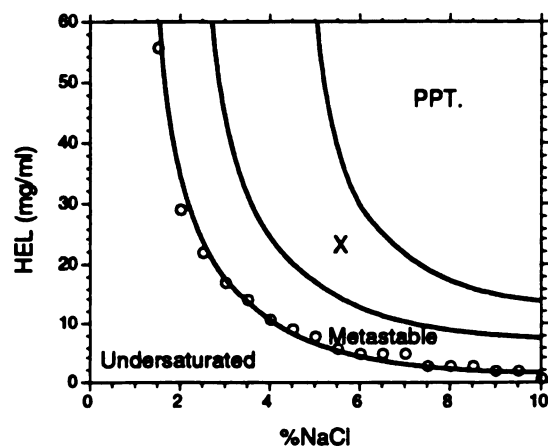


Figure 2.2. Schematic illustration of the crystallization behavior for HEL. The data points are measured solubility data at pH 4.6, 25° C [36]. The line through the points represent the solubility limit. Above this is a metastable zone where nucleation does not occur. In the X region, crystallization occurs. Above this region, immediate precipitation is observed. (Adapted from reference [8])

interactions are non-specific, while hydrogen bonding and electrostatic interactions require specific complementary. If the surface interaction properties of the proteins can be characterized, the choice of possible conditions may be reduced. Macroscopic methods have played an important role in characterizing some of the interactions involved in protein crystallization.

The crystallization of hen egg-white lysozyme (HEL) by sodium chloride illustrates the progress made by macroscopic measurements and observations. The primary means of characterizing the behavior of protein solutions is the phase diagram as illustrated in Figure 2.2. The solubility relationships for tetragonal HEL in sodium chloride solutions has been determined [36]. From direct observations of batch HEL solutions, the protein association behavior ranges from immediate precipitation within seconds at

high supersaturation to the formation of well ordered crystals within hours near the metastable limit to a completely stable solution at low levels of supersaturation.

Using solubility measurements, direct ion pairing has been found to play an important role in the crystallization of HEL. The crystallization of the basic proteins HEL and erabutoxin b did not show behavior that was characteristic of salting out when thiocyanate and other organic anions were used as the precipitants [37]. In fact, the effectiveness of salts for crystallizing HEL was found to follow the reverse order of the lyotropic (or Hoffmeister) series. This result may be an indication that crystallization and amorphous precipitation proceed by different mechanisms. At pH 4.5, histidine, lysine, arginine and terminal amino groups are generally protonated to give basic proteins a positive charge [38, 39]. Presumably, the positive charges on the protein were neutralized by the negatively charged precipitants thereby decreasing the protein solubility. Subsequent data showed that the binding of Cl^- is highly exothermic [40]. The ensuing protein aggregation involved the release of Cl^- into the solution with a lower rate of heat release. Such results show the significance of anion binding in the crystallization of HEL.

Recently, the use of ligands for the co-crystallization of proteins have resulted in an improvement in crystal growth techniques. Studies on the use of organic anions to induce the precipitation of HEL show a strong electrostatic binding of these ligands to HEL [41]. This binding was also accompanied by heat production and resulted in the co-crystallization of HEL with the ligands. Many examples illustrate the use of small organic ligands to facilitate the crystallization of proteins [11]. These include the use of phenol for the crystallization of insulin [42] and thymol for the crystallization of

chymotrypsin [43]. An example that not only illustrates the use of macromolecular ligand binding for crystallization, but also underscores the importance of understanding protein crystallization processes, is seen in the crystallization of the reverse transcriptase protein from the human immunodeficiency virus (HIV-1) [44]. Attempts to crystallize the homogenous protein with salts had only yielded crystals that diffracted to 9 Å resolution. Upon the introduction of oligonucleotide ligands, crystals diffracting to 2.6 Å could be obtained. Another interesting use of ligands, involves the co-crystallization of the glycoprotein tissue factor with the Fab fragment from immunoglobins [45, 46]. With this method, crystals were obtained that diffracted to about 2.0 Å resolution.

From such studies, it is possible to postulate the mechanisms responsible for ligand induced crystal growth [41]. The conformational mobility of many proteins leads to a high water content both in the protein and in crystals, resulting in their inability to form high quality crystals. Ligands may act to reduce the repulsive forces between protein particles, provide contact points as well as tighten the conformation of proteins. Additionally, ligands may become incorporated into the crystal, forming a scaffolding to further reduce mobility.

Macroscopic methods have long been the primary technique for the analysis of protein crystallization trials and experiments. Although many important results have been obtained using these methods, the macroscopic viewpoint is only able to detect the bulk properties of the solution and provide subjective visual observations of the outcomes of crystallization trials. Because of these limitations, the causative microscopic and molecular processes responsible for protein crystallization and aggregation can only be

inferred. Thus, other techniques better suited to investigating the small scale structure and interaction are required.

Static Light Scattering

Of the methods used to investigate the microscopic solution behavior involved in the crystallization of proteins, light scattering has been the most common. Through the use of light scattering techniques, information on the molecular weight, aggregate size and polydispersity may be obtained. Static light scattering measures the intensity of light scattered from a population of particles as detected at an angle from the incident beam [47]. Dynamic light scattering (DLS), also known as photon correlation spectroscopy or quasi-elastic light scattering, measures the molecular motions due to thermal fluctuations. Both techniques have been widely used to investigate protein-protein interactions and predict conditions that are favorable for protein crystallization.

Although static light scattering is commonly used to measure the molecular weight of non-interacting macromolecules, this technique has had some successes for the study of interacting particles. For protein crystallization the molecular interactions at high protein concentrations can not be neglected and other analyses must be used. By comparing the relative intensity of scattered light from crystallizing HEL solutions, Pusey was able to estimate the equilibrium constants for the formation of dimers and tetramers [48]. The concentration of monomers, dimers and tetramers could then be estimated as a function of the total protein concentration.

It was found that the monomer and dimer concentrations eventually reached a constant value while the tetramer concentration continued to increase as the total protein concentration increased. Comparison of the

aggregate concentration profiles with the crystal face growth rate showed that the constant monomer and dimer concentrations did not correlate with the increasing crystal face growth rate. This result suggested that HEL crystal growth proceeds by the addition of pre-formed tetrameric or higher aggregates rather than by the addition of monomers or dimers. Although the simplifying assumptions made in this study limited the amount of information that could be obtained, it demonstrated the importance of the solution behavior not only on nucleation, but also the crystal growth process.

Dynamic Light Scattering

DLS is able to detect the brownian motion of particles in solution by measuring the time dependent fluctuations of the scattered light intensity [49]. These fluctuations are analyzed by using the autocorrelation function, $G_2(\tau)$, given by,

$$G_2(\tau) = \frac{\langle I(q, t + \tau) I(q, t) \rangle_t}{\langle I(q, t) \rangle_t^2} \quad (2.1)$$

In its generalized form, $G_2(\tau)$ can be expressed as,

$$G_2(\tau) = A + b[G_1(\tau)]^2 \quad (2.2)$$

where A is the baseline, b is an instrument constant which depends on the geometry of the optics and $G_1(\tau)$ is the first order autocorrelation function. For a polydisperse mixture of N aggregates or particle sizes, $G_1(\tau)$ is a sum of exponential terms given by,

$$G_1(\tau) = \sum_{i=1}^N a_i \exp(-q^2 D_i \tau) \quad (2.3)$$

where a_i is the contribution from species i and D_i is the translational diffusion coefficient of species i . The hydrodynamic radius of species i , $R_{h,i}$, is often expressed in terms of the D_i by the Stokes equation,

$$R_{h,i} = \frac{k_B T}{6\pi\eta D_i} \quad (2.4)$$

where k_B is the Boltzmann constant, T is the temperature and η is the hydrodynamic viscosity. From these relations, it is possible to obtain the particle size distribution in a solution provided that the individual decay components can be extracted from the experimentally measured autocorrelation function.

The use of DLS in the study of protein crystallization and aggregation has become widespread. Studies begun in the late 1970's first offered a kinetic explanation of how equilibrium constants of association influenced whether the outcome of a crystallization trial would result in crystal growth or amorphous aggregation. Subsequent studies have investigated the use of DLS as a diagnostic method for predicting the outcome of particular crystallization conditions. Recently, the focus has shifted to the goal of obtaining a deeper understanding of the molecular interactions involved in crystallization. The progression from early findings to the current state is outlined here.

The pioneering work of Kam, Shore and Feher laid the groundwork for the use of DLS in further studies of protein crystallization [14]. Using classical nucleation theory, as outlined in chapter 1, to study the prenucleation behavior of HEL solutions, they rationalized the formation of crystalline and amorphous aggregates under different conditions. 5% (w/v) sodium chloride was used as the precipitant in the solutions promoting the growth of tetragonal crystals, while 30% (w/v) ammonium sulfate was used

for the formation of amorphous aggregates. Conditions were at pH=4.2 and a temperature of 20°C. Values of the equilibrium constants for the addition of a monomer to another monomer, K_1 , and for addition to large aggregates, K_∞ , were determined using dynamic light scattering for both conditions [50].

For the case of crystallization, it was found that $K_1 \approx 0.065$ (% w/v)⁻¹, $K_\infty \approx 2.3$ (% w/v)⁻¹ and $K_\infty / K_1 \approx 35$. For amorphous precipitation, $K_1 \approx 0.5$ (% w/v)⁻¹, $K_\infty \approx 7.5$ (% w/v)⁻¹ and $K_\infty / K_1 \approx 1.5$. These results are consistent with the theoretical model that $K_\infty / K_1 \gg 1$ for crystallization and $K_\infty / K_1 \approx 1$ for amorphous precipitation. However, this simple model may not completely describe crystallization behavior, as the conditions that were compared could be considered to be limited. In experiments with phosphoglucosyltransferase, both crystallizing conditions using polyethylene glycol 400 and amorphous precipitating conditions using ammonium sulfate gave $K_\infty / K_1 \approx 30$ [50].

Several subsequent studies have examined the use of DLS as a general diagnostic method for predicting whether a particular solution would form crystals. Mikol, et. al. applied DLS to investigate the crystallization of aminoacyl-tRNA synthetase [51]. The average diffusion coefficient was measured and by the Stokes-Einstein equation the apparent hydrodynamic radius, R_h , was calculated. Interactions between protein molecules that were detected before reaching saturation were indicative that conditions were not favorable for crystallization. Similar results were reported with HEL and jack bean concanavalin A. It was concluded that a monodisperse distribution is a necessary but not sufficient condition for crystal growth. Other studies by Kadima, et. al. comparing the aggregation behavior of insulin [52] and concanavalin [53] showed similar results.

More recent uses of DLS as a diagnostic of protein crystallization have refined the data analysis procedures. Zulaf and D'Arcy used the obtained particle size distributions for the aggregation behavior of 15 different proteins [54]. In all cases where narrow unimodal (monodisperse) distributions were observed, crystals resulted, while in no cases where more complicated multimodal distributions were observed did crystals grow. Thibault, et. al. used DLS to measure the particle size distributions for the crystallization of several aminoacyl-tRNA synthetases. Two effects were observed in amorphously aggregating systems as the precipitant concentrations increased: A) an increase in the scattering intensity corresponding to large aggregates and B) a shift in the monomer peak. Under conditions where either effect A or B occurred crystallization was not observed.

Subsequent studies have focused on the use of DLS to follow the dynamics of nucleation in an effort to diagnose whether conditions are favorable for crystallization. Mikol, et. al. used DLS to follow the crystallization of HEL [55]. In this case, nucleation was achieved by lowering the temperature of the solution. As crystallization proceeded, the apparent hydrodynamic radius, $R_{h,app}$, increased from $\sim 22\text{\AA}$ to a maximum value of $\sim 33\text{\AA}$ and then decreased as tetragonal crystals became visible. The variance of the measurements remained small indicating that the distribution of aggregate sizes was fairly monodisperse. These results did not reveal the presence of a measurable number of large critical nuclei. Thus, it was suggested that protein crystal growth occurs by the addition of either monomers or small aggregates.

Another study using DLS with the cumulant method of analysis also followed the course of HEL crystallization, but instead, the results were interpreted in terms of the measured friction factor [56]. In this case,

supersaturation was achieved by using sodium chloride as the precipitant. The increase in the friction factor from undersaturated solutions to supersaturated solutions was attributed to an increase in molecular interactions rather than the presence of large aggregates.

Skouri, et. al. have investigated DLS from HEL solutions for conditions that favor crystallization and amorphous aggregation [57]. The intermolecular interactions were found to be greater in undersaturated solutions of ammonium sulfate as compared to undersaturated solutions of sodium chloride. Again, ammonium sulfate was used as the solution favoring amorphous aggregation and sodium chloride as the solution favoring crystallization. A temperature quenching of HEL solutions containing sodium chloride showed a bimodal distribution. The fast relaxation mode was attributed to the monomer, while the slow relaxation mode was attributed to the presence of aggregates with a radius of about 260 nm. The time evolution of the modes indicated a slow growth in the aggregates whereas the monomer concentration remained constant over a long period of time.

In other studies by Georgalis, et. al., a bimodal distribution was also observed for crystallizing conditions with sodium chloride and for precipitating conditions with ammonium sulfate [58, 59]. The slow relaxation mode was attributed to the growth of a fractal aggregates while the fast relaxation mode was attributed to the presence of the monomer. These aggregates were classified as either CRAGGS (precrySTALLine aggregates) or PRAGGS (Precipitating aggregates) [60]. The CRAGGS exhibited a fractal dimension close to that expected for diffusion limited cluster aggregation. A maximum in R_h was also observed as the concentration of sodium chloride increased.

Malkin and Mcpherson applied DLS to the investigation of aggregates of satellite tobacco mosaic virus (STMV), ferritin, apoferritin and pumpkin seed globulin [61]. Under conditions favoring crystallization, there were no observed increases in R_h during an initial induction period. After this period, a sharp increase in the aggregate sizes up to μm R_h values were observed. In the case of amorphous precipitation, a slow increase in R_h of the aggregates took place followed by a sharp increase to μm sizes.

Sazaki, et. al. combined DLS with scanning electron microscopy (SEM) in their studies on the crystallization of thermolysin [62]. A linear increase in the average size of the aggregates was observed using DLS as the crystallization progressed. The size distribution showed three peaks at 3-6 nm, 100 nm, and >500 nm diameter. From the SEM images, crystalline precipitates were found to be composed of small spherical particles that roughly corresponded to the size of the 100 nm peak. They proposed a mechanism for thermolysin growth which proceeded through the initial formation of primary particles of 15-200 nm diameter. This is followed by crystal growth occurring through the attachment of the primary particles.

To summarize, the DLS results have shown that there are typically two or more peaks in the size distribution of supersaturated solutions. The diameter corresponding to the largest sized peaks increases as time progresses. There is also some evidence that the aggregation pathways leading to amorphous precipitation are different than those leading to crystalline precipitation. However, this evidence is not conclusive. Further data is required to determine the properties of the interacting proteins and the structures that are formed during nucleation and crystal growth. Although DLS has provided a large amount of data concerning protein crystallization, this technique is becoming limited with respect to

characterizing the chemical features involved in solutions of associating proteins.

A more complete physico-chemical description of protein crystal growth is required to explain the behavior of supersaturated solutions. The most compelling limitations for the practical implementation of DLS are the low sensitivity, low specificity and inflexibility of this technique for measurements of a range of protein interactions under crystallization conditions. Because the primary transport property measured by DLS is the bulk translational diffusion, changes in protein dynamics due to molecular scale interactions with protein and solvent molecules may not be adequately resolved. Although measurements of rotational motions may be much more sensitive to such interactions, DLS is not generally suitable for such measurements [63]. A lack of specificity is another characterizing feature of DLS that is due to the nature of measuring bulk fluctuations of optical inhomogeneities. These effects are manifested in the undesired scattering of light from sources such as reflections, convection currents, large particles and scattering from the solvent itself [64]. Although some of these effects may be ameliorated by careful sample preparation, interference from the solvent and other constituents represents the most severe limitation to protein crystallization applications.

The solutions used for protein crystallization contain a complex and concentrated mixture of interacting protein, precipitant and buffer agents that may confound DLS measurements [65]. Crystallization trials typically contain additives, including high concentrations of inorganic salts or organic precipitants, high molecular weight polymers, such as polyethylene glycol, and detergents in the case of membrane and otherwise hydrophobic proteins, that may interfere with DLS measurements. Furthermore, the appearance of

crystals, precipitates and other sources of turbidity intrinsic to the process of protein crystallization may give rise to multiply scattered light [59]. The feasibility of monitoring and controlling protein crystal growth techniques depends on the development of other methods that are able to circumvent the practical limitations of DLS. Steady-state fluorescence and time-resolved fluorescence (TRF) spectroscopy provide techniques that are able to supplement or supplant current techniques in the ability to measure a wider range of protein interaction parameters with molecular scale sensitivity and resolution.

Chapter 3

Fluorescence Techniques for Investigations on Protein Crystallization

Introduction

The methodology and techniques associated with fluorescence spectroscopy have now been developing for over thirty years and is in wide use for investigating a diverse variety of phenomena including protein conformation and dynamics, lipid membrane dynamics, polymer dynamics and solvation interactions [66-77]. Fluorescence methods are able to probe many aspects of biophysical systems including the structure and dynamics of the interactions seen in protein crystallization. However, it is surprising that a technique like fluorescence that is well suited to the study of molecular behavior in solutions has been applied to such a limited extent for the study of protein crystallization. In this section, the aspects of protein crystallization behavior that can be determined using fluorescence spectroscopy will be examined.

Information on the local environmental, structural and dynamic influences acting on a fluorescent probe is obtained through the use of fluorescence spectroscopy. For the study of protein dynamics, the fluorescent probe may be an *intrinsic* chromophore, such as the amino acids tryptophan, tyrosine and phenylalanine, incorporated in the native structure of the protein itself. Alternatively, it may be associated covalently or non-covalently by conjugating an *extrinsic* fluorophore to the protein. A wide variety of

extrinsic probes are available and the particular choice that is used depends on matching the probe properties to the specific application.

The microenvironment in which the probe is located also exerts its influence on the fluorescence behavior. For example, the polarity of the solvent and collisional quenchers in solution influences the fluorescence behavior of the probe. The effects of different probe environments may then be interpreted in terms of solvent accessibility. Additionally, the rotational motion of the fluorophore influences the relative intensities of the vertically and horizontally polarized emission. By conjugating the probe to protein molecules, the rotational dynamics of the probe are influenced by the rotational motions of the protein and its interactions. It is evident that fluorescence methods can provide a wealth of structural and dynamic information pertinent to protein crystallization.

Although steady-state fluorescence measurements are able to provide some information on the probe environment and dynamics, time-resolved fluorescence techniques are able to more directly quantify the relevant parameters. Complicating experimental factors due to contaminating emissions, temperature and viscosity variations can be more directly separated from the physical effects of interest. With time-resolved fluorescence techniques, the decay profile of the probe is measured and the extracted decay lifetimes related to photophysical processes. Similarly, the time dependent difference of the vertical and horizontal polarization results in the rotational correlation times of the probe. In the case of heterogeneous samples, multiple lifetimes and rotational correlation times may be obtained.

Here, the theoretical and experimental aspects of measuring fluorescence lifetimes and rotational correlation times are discussed. It will be demonstrated how time-resolved fluorescence spectroscopy can be used to

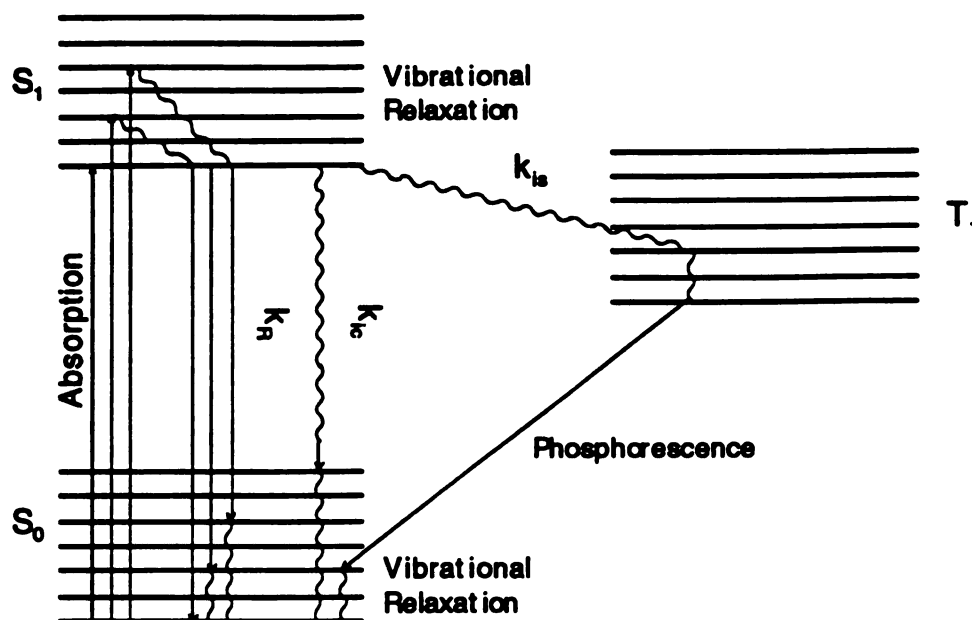


Figure 3.1. Photochemical processes in fluorescence spectroscopy.

obtain information on dynamic protein crystallization behavior on the nanometer length and nanosecond time scales. The structural and spectroscopic properties of hen egg white lysozyme (HEL) are also reviewed.

Fluorescence and Anisotropy Processes

The initial event in the fluorescence process is the electronic excitation of a fluorophore caused by the absorption of a photon. Following this event, a relaxation occurs back to the ground state through spontaneous emission and other nonradiative pathways. The photon absorption event occurs on the time scale of femtoseconds. It is too rapid to permit the observation of the dynamics occurring with protein interactions. Fluorescence, however, occurs on time scales ranging from picoseconds to hundreds of nanoseconds. Because of the slower time scales, it is possible to follow the dynamics of protein interactions. The process of fluorescence is illustrated in Figure 3.1, where S_0

and S_1 are the ground singlet state and excited singlet state, respectively, and n_0 and n_1 are the populations in these states. In the absence of nonradiative relaxation pathways, the rate of depopulation of level S_1 is given by,

$$\frac{dn_1}{dt} = -A_{10}n_1 \quad (3.1)$$

where A_{10} is the Einstein coefficient for spontaneous emission. The intrinsic fluorescence lifetime, τ_R , and the intrinsic fluorescence rate constant, k_R , of the excited state, S_1 , is related to the Einstein coefficient by,

$$\tau_R = \frac{1}{k_R} = \frac{1}{A_{10}} \quad (3.2)$$

However, the processes of internal conversion, intersystem crossing and a number of excitation quenching mechanisms contribute to a decrease in the actual observed fluorescence lifetime.

These nonradiative processes can be useful in characterizing the effects of the probe microenvironment in biophysical systems. The rate constant for internal conversion, k_{ic} , depends upon the dissipation of excitation energy through solvent collisions or internal vibrations. Intersystem crossing at a rate of k_{is} , occurs when the electron converts from the excited singlet state, S_1 , to the excited triplet state, T_1 . Phosphorescence from T_1 to S_0 can then occur with extremely long lifetimes. However, phosphorescence is rarely observed under the conditions used in biological studies because of the competition by internal conversion or quenching. Quenching processes result from collisions or energy transfer interactions with other molecular species in solution. In the case of collisional quenching, diffusion of quenchers results in a bimolecular de-excitation reaction with a rate constant, $k_q(Q)$. Together,

these processes influence the total depopulation rate, k_F , from energy level S_1 to define the observed fluorescence lifetime, τ_F ,

$$\tau_F = \frac{1}{k_F} = \frac{1}{k_R + k_{ic} + k_{is} + k_q(Q)} \quad (3.3)$$

The total rate for the depopulation of state S_1 , is given by,

$$\frac{dn_1}{dt} = -k_F n_1 \quad (3.4)$$

Solving this differential equation gives the expression for the time dependent population of S_1 ,

$$n_1(t) = n_1(0) \exp(-t / \tau_F) \quad (3.5)$$

where $n_1(0)$ is the initial population of S_1 . For an infinitely short excitation pulse, the intensity of light emitted at time, t , is proportional to the rate of depopulation from S_1 and the fraction of depopulation of S_1 due to fluorescence, ϕ_F ,

$$I_{\text{tot}}(t) \propto \phi_F \frac{dn_1}{dt} = (n_1(0) / \tau_R) \exp(-t / \tau_F) \quad (3.6)$$

where,

$$\phi_F = \tau_F / \tau_R \quad (3.7)$$

In the case where a mixture of fluorescent components is present in the sample, the time dependent fluorescence intensity following an impulse excitation is given by [73],

$$I_{\text{tot}}(t) = \sum_{k=1}^p A_k \exp(-t / \tau_k) \quad (3.8)$$

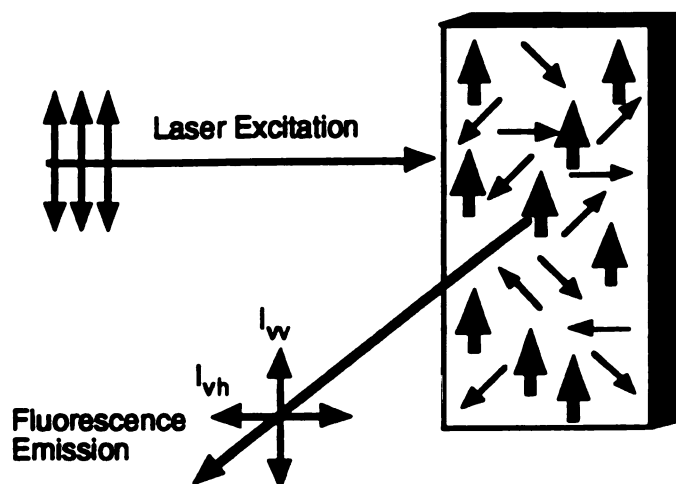


Figure 3.2. Photoselection in fluorescence anisotropy. The arrows in the box represent the absorption dipole moments of the fluorescent probes. Bold arrows indicate that absorption occurs.

where p is the total number of components, A_k , the pre-exponential factor, is proportional to the concentration of component k and τ_i is its fluorescence lifetime.

The rotational motions of the fluorophores in solution can be detected by using a linearly polarized excitation source as shown in Figure 3.2 [47]. Through a process of photoselection, a population of fluorescent probes with their absorption dipole moments oriented in the direction of polarization is preferentially excited. The probability of photon absorption is proportional to $\cos^2 \theta$, where θ is the angle between the absorption dipole moment and the axis of polarization. Because of the anisotropic orientations of the excited probes, the orientation of the fluorescence emission will also be anisotropic. The time dependent vertically, $I_{vv}(t)$, and horizontally, $I_{vh}(t)$, polarized emission intensities from a vertically polarized excitation source defines the fluorescence anisotropy [78],

The
rep
abs
em

The
For
of
bet

mo
rot

wh
anc
rot

wh
hyd
med
and

$$R(t) = \frac{I_{\parallel}(t) - I_{\perp}(t)}{I_{\parallel}(t) + 2I_{\perp}(t)} \quad (3.9)$$

The numerator of this expression is the difference decay. The denominator represents the total fluorescence, $I_{\text{tot}}(t)$, and is the fluorescence seen in the absence of polarization effects. For an angle ξ between the absorption and the emission dipole moments, the initial anisotropy is given by,

$$r_0 = (3\cos^2 \xi - 1)/5 \quad (3.10)$$

Thus, the maximum value of the anisotropy is 2/5 while the minimum is -1/5. For molecules acted on by the randomizing forces in solution, the orientation of the molecules eventually become isotropic. At long times, the difference between $I_{\parallel}(t)$ and $I_{\perp}(t)$ disappears so that the anisotropy approaches zero.

The rotational diffusion experienced by a protein is reflected in the motion of the attached fluorescence probe. For a spherical particle, the rotational diffusion is described by the equation,

$$\frac{dW(\theta, \phi, t)}{dt} = D_{\text{rot}} \nabla^2 W(\theta, \phi, t) \quad (3.11)$$

where $W(\theta, \phi, t)$ is the time dependent probability of a particular orientation and D_{rot} is the rotational diffusion coefficient [76]. D_{rot} is related to the rotational friction coefficient, f_{rot} , by,

$$D_{\text{rot}} = \frac{k_B T}{f_{\text{rot}}} = \frac{k_B T}{6V_h \eta} \quad (3.12)$$

where k_B is Boltzman's constant, T is the absolute temperature, V_h is the hydrodynamic volume of a non-interacting sphere and η is the viscosity of the medium. From the initial distribution of the orientations of the excited probes and the fluorescence decay, the fluorescence anisotropy is given by,

$$R(t) = r_0 \exp(-t/\rho) \quad (3.13)$$

where ρ is the rotational correlation time defined by,

$$\rho = \frac{1}{6D_{rot}} = \frac{V_h \eta}{k_B T} \quad (3.14)$$

The rotational correlation time is a measure of the time required for the randomization of the orientational anisotropy. For a spherical particle with a rigidly attached fluorescence probe, the anisotropy is given by an exponential decay. The multicomponent anisotropic decay is similar to the case of multicomponent fluorescence decay,

$$R(t) = \sum_{i=1}^n B_i \exp(-t/\rho_i) \quad (3.15)$$

where B_i is the fractional contribution of the component i .

Experimental Determination of Fluorescence Parameters

The experimental apparatus for performing time-resolved fluorescence measurements is illustrated in Figure 3.3. A vertically polarized light pulse originating from a laser, impinges upon the sample causing the absorption of photons. As the excited fluorophores relax back to the ground state, the time dependent fluorescence emission is detected. The dye laser system consists of a mode-locked Nd:YAG laser and a synchronously pumped, cavity dumped dye laser. The output from the dye laser is frequency doubled and passed through a polarization rotator and a vertically oriented polarizer before encountering the sample.

The fluorescence emission is collected through collimating lenses, a rotatable emission polarizer and then a depolarizer before entering the monochromator. A reversed mode time-correlated single photon counting apparatus is used to collect the data [79]. This instrument uses a time to

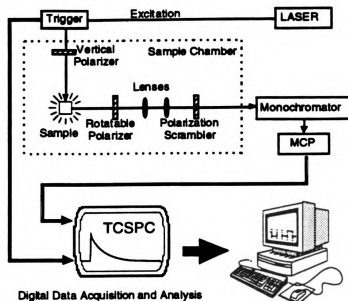


Figure 3.3. Time-resolved fluorescence and anisotropy instrumentation.

amplitude converter which outputs a voltage that is proportional to the time delay between the excitation signal and a detected fluorescence emission signal. The reversed timing mode uses the emission photon signal as the START input. The excitation signal is delayed by a specified time interval and is used as the STOP input. A multichannel analyzer increments the count in the channel corresponding to the elapsed time. Over the course of the measurement, a histogram representing the fluorescence decay as a function of time is constructed.

The analysis of time-resolved fluorescence data involves fitting the fluorescence decay to a sum of exponential components by taking into account the finite pulse shape of the excitation source. When a pulse with a finite duration is used for excitation, the experimentally observed fluorescence decay profile, $I_{\text{obs}}(t)$, is a convolution of the excitation pulse, $L(t)$, with the intrinsic fluorescence response, $I_{\text{tot}}(t)$,

$$I_{tot,obs}(t) = \int_0^t L(t-s)I_{tot}(s)ds. \quad (3.16)$$

$I_{tot}(s)$, must be extracted from the convoluted fluorescence profile usually using a least squares fitting procedure [80-83]. From equation 3.8, this expression may be written as,

$$I_{tot,obs}(t) = \int_0^t L(s) \sum_{k=1}^p A_k \exp\left(-\frac{(t-s)}{\tau_k}\right) ds \quad (3.17)$$

In this procedure values of A_i and τ_i are varied until the reduced sum of squares,

$$\chi^2 = \left(\frac{1}{N-1}\right) \sum_{i=1}^N \frac{[I_{obs,i} - I_{calc,i}]^2}{\sigma_i^2} \quad (3.18)$$

is minimized. $I_{obs,i}$, $I_{calc,i}$ and σ_i^2 are the observed intensity, calculated intensity and variance, respectively, for the discrete time channel i and N is the total number of channels.

$R(t)$ is also distorted by the excitation pulse profile, but $R(t)$ cannot be directly fit to the observed decay. Instead, the r_j and ρ_j values are found by numerically fitting the experimentally measured vertically, $I_{vv,obs}$, and horizontally, $I_{vh,obs}$, polarized emission using previously determined parameters for I_{tot} [83, 84]. From equation 3.9, the total fluorescence decay, $I_{tot}(t)$, and the anisotropy decay, $R(t)$, are related to the nondistorted emission curves by,

$$I_{vv}(t) = \frac{1}{3} I_{tot}(t) [1 + 2R(t)] \quad (3.19a)$$

$$I_{vh}(t) = \frac{1}{3} I_{tot}(t) [1 - R(t)] \quad (3.19b)$$

Convolution with the instrument response function, $L(t)$, gives

$$I_{vv,obs}(t) = \int_0^t L(t-s)I_{vv}(s)ds \quad (3.20a)$$

$$I_{vh,obs}(t) = \int_0^t L(t-s)I_{vh}(s)ds \quad (3.20b).$$

From equations 3.8, 3.15 and 3.20, these expressions can be rewritten as,

$$I_{vv,obs}(t) = \frac{1}{2} \sum_{k=1}^p \left\{ F^k(t) + 2 \sum_{l=1}^q \int_0^t L(s)C_k \exp\left(-\frac{(t-s)}{\theta_k}\right)ds \right\} \quad (3.21a)$$

$$I_{vh,obs}(t) = \frac{1}{2} \sum_{k=1}^p \left\{ F^k(t) - \sum_{l=1}^q \int_0^t L(s)C_k \exp\left(-\frac{(t-s)}{\theta_k}\right)ds \right\} \quad (3.21b)$$

where,

$$F^k(t) = \int_0^t L(s)A_k \exp\left(-\frac{(t-s)}{\tau_k}\right)ds \quad (3.22a)$$

$$\theta_k = \left(\frac{1}{\tau_k} + \frac{1}{\rho_l} \right)^{-1} \quad (3.22b)$$

$$\text{and } C_k = A_k B_l \quad (3.22c).$$

Suitable computer programs using an iterative least-squares deconvolution procedure have been developed to fit the experimentally observed I_{tot} parameters [80, 81]. These values are then used to simultaneously fit the $I_{vv,obs}$ and $I_{vh,obs}$ curves [83]. The Marquardt-Levenburg algorithm is used to minimize the χ^2 values for the fluorescence decay curves by adjusting the fluorescence parameters and for parameters taking into account the scattered light and time shift of the excitation pulse [85].

Applications of Fluorescence

Fluorescence spectroscopy has become a useful tool for the investigation of macromolecular structure, dynamics and interactions in solutions. Properties of protein bound fluorescent probes have been measured and information gained on the structure, conformation and interactions of proteins in numerous studies using conventional steady-state and time-

resolved fluorescence methods [67, 68, 74]. For example, solution studies on immunoglobins have investigated antigen-antibody binding by measuring the quenching of ligands, immunoglobulin flexibility by measuring the fluorescence anisotropy of bound fluorophores, and intermolecular distances using energy transfer. Studies of muscle proteins used fluorescence anisotropy to detect the flexibility of myosin and used energy transfer to determine the effect of calcium on muscle contraction. Other areas where the use of fluorescence is widespread has been in the study of lipid micelles [68, 86] and polymer dynamics [71]. Fluorescence spectroscopy has become established as a powerful tool for the experimental investigation of a wide variety of the physical properties of molecules in solution.

Only recently has fluorescence spectroscopy been used to investigate the crystallization behavior of proteins [87-89]. Jullien and coworkers studied protein interactions in the crystallization of ribonuclease A by monitoring the steady-state fluorescence anisotropy. The measured anisotropy was found to increase as the protein concentration increased. Rotational correlation times were calculated assuming that the lifetime remained constant. The effects of precipitating agents on crystallization were interpreted in terms of the virial coefficient, α ,

$$\rho' = \rho(1 + \alpha C) \quad (3.23)$$

where ρ' and ρ are the measured effective and infinite dilution values of the rotational correlation times, and C is the protein concentration. The virial coefficient was found to increase sharply under conditions that were favorable for protein crystallization.

In further studies with time-resolved fluorescence, a maximum entropy data analysis scheme was used to calculate a rotational correlation time

Table 3.1. Amino acid sequence of hen egg white lysozyme.

1	LYS	VAL	PHE	GLY	ARG	CYS	GLU	LEU	ALA	ALA	ALA	MET	LYS
14	ARG	HIS	GLY	LEU	ASP	ASN	TYR	ARG	GLY	TYR	SER	LEU	GLY
27	ASN	TRP	VAL	CYS	ALA	ALA	LYS	PHE	GLU	SER	ASN	PHE	ASN
40	THR	GLN	ALA	THR	ASN	ARG	ASN	THR	ASP	GLY	SER	THR	ASP
53	TYR	GLY	ILE	LEU	GLN	ILE	ASN	SER	ARG	TRP	TRP	CYS	ASN
66	ASP	GLY	ARG	THR	PRO	GLY	SER	ARG	ASN	LEU	CYS	ASN	ILE
79	PRO	CYS	SER	ALA	LEU	LEU	SER	SER	ASP	ILE	THR	ALA	SER
92	VAL	ASN	CYS	ALA	LYS	LYS	ILE	VAL	SER	ASP	GLY	ASN	GLY
105	MET	ASN	ALA	TRP	VAL	ALA	TRP	ARG	ASN	ARG	CYS	LYS	GLY
118	THR	ASP	VAL	GLN	ALA	TRP	ILE	ARG	GLY	CYS	ARG	LEU	

distribution [90]. In the presence of high ammonium sulfate concentrations, a bimodal distribution was observed. The rotational correlation time of the aggregate peak varied between two and three times that of the monomer peak. This aggregate peak appeared to be a stable intermediate in the crystallization process and is possibly a symmetrical dimer of the ribonuclease. Although light scattering methods have been far more extensively used to study protein crystallization, these results represent only the beginnings for the use of fluorescence techniques in investigations of protein crystallization. Clearly, fluorescence methods have not yet been fully exploited for the study of protein crystallization.

Fluorescence of HEL

HEL has been the subject of a majority of the previous research done on protein crystallization and is also one of the better characterized proteins [91]. To enable comparison with previous results this protein was chosen as the model system in this current work. Lysozyme was first discovered by Alexander Fleming because of a cold [92]. A drop from Fleming's nose had fallen onto an agar plate resulting in the clearance of the microbial colonies. The ability of the substance to lyse bacterial cells led to the enzyme's name. It accomplishes this lytic action by hydrolyzing the β -(1-4)-glycosidic linkage of

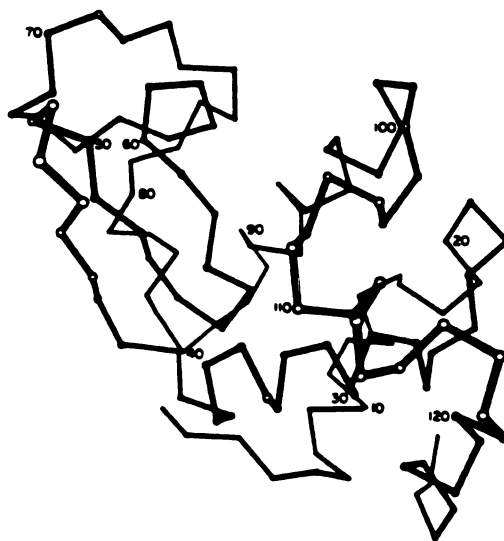


Figure 3.4. HEL α -carbon atoms showing the main polypeptide chain (from reference [91]).

the tetra-sacharides found in bacterial cell walls. Lysozyme is found in the tissues and secretions of animals and plants, but is the most plentiful in egg whites.

HEL is a relatively small protein with a molecular weight of 14,300 and consists of 129 amino acid residues. The amino acid sequence of HEL is shown in table 3.1. There are 17 basic residues and 9 acidic residues in HEL. The isoionic point of is 11.1 and at pH 4.6 it carries a charge of +10 [38, 39]. HEL was the first enzyme structure that was determined using X-ray crystallography [93]. The alpha carbon backbone is illustrated in Figure 3.4. The overall shape of the protein molecule can be can be approximated as a prolate spheroid with dimension of about 4.5 X 3.0 nm. A substrate binding cleft separates the molecule into two lobes [30]. The larger lobe (residues 5-36 and 98-129) consists primarily of α -helices while the smaller lobe (residues 40-94) has a β -sheet structure.

Table 3.2. Tryptophan fluorescence parameters for 0.1% HEL.

Lifetimes	λ_1	λ_2	λ_3	τ_1	τ_2	τ_3
2 Components	0.27	0.73		3.28	0.76	
Vos. et. al.	0.25	0.75		3.23	1.28	
3 components	0.16	0.49	0.35	3.30	1.00	0.26
Vos. et. al.	0.02	0.56	0.42	6.25	2.18	0.70
Anisotropy	B_1	B_2	ρ_1	ρ_2		
1 Component	0.21		3.08			
Vos. et. al.	0.22		3.80			
2 Components	0.20	0.06	3.48	0.10		

The intrinsic fluorescence of HEL has been previously investigated. There are a total of six tryptophans in the protein. However, from steady-state fluorescence measurements, it was found that 80 % of the fluorescence intensity comes from Trp-62 and/or Trp-108 [94]. There also appears to be energy transfer from Trp-108 to Trp-62. The time-resolved fluorescence lifetimes of HEL have been measured by Vos, et. al [95] and are seen in Table 3.2. Measurements of the fluorescence anisotropy indicated a single rotational correlation time component of 3.8 ns. This value is too low to describe the overall rotational motion of HEL and may be a result of internal motions in the protein.

To determine whether crystallization conditions have an influence on the intrinsic fluorescence behavior, we have measured the effects of sodium chloride concentrations in HEL solutions. The time-correlated single photon counting apparatus was used as described earlier. An excitation wavelength of 300 nm from the frequency doubled output of an R6G dye was used and the emission collected at a wavelength of 340 nm. The total fluorescence lifetimes were fit to a three component model. The fluorescence lifetimes and

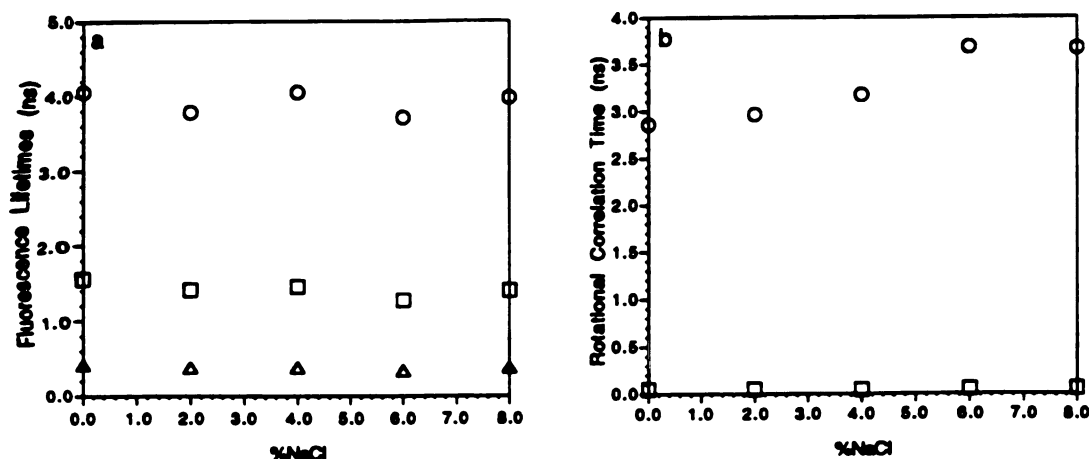


Figure 3.5. Effect of NaCl concentrations on the tryptophan a) fluorescence lifetimes and b) rotational correlation times of 2% HEL solutions.

rotational correlation times of 0.1% HEL in 0 % sodium chloride are shown in table 3.2. The two longest lifetimes agree with the two component fits obtained by Vos, et. al. However, we also observed a shorter lifetime component. As seen in Figure 3.5a, the fluorescence lifetimes of 2 % HEL solutions are not significantly affected by the sodium chloride concentration.

It appears that a two component fit to the anisotropy decay is able to separate the long and short contributions that do not appear in a one component fit. The rotational correlation times of the tryptophan residues in HEL are shown in Figure 3.5b. Because there is little effect of the changes in the solution conditions on the rotational correlation times, the intrinsic fluorescence of HEL does not appear to be suitable for the measurement of crystallization conditions. There are other practical difficulties in using intrinsic fluorescence for monitoring protein crystallization as well. The high concentration of protein present in the sample causes complete absorption of the excitation beam leading to an inner filtering effect. The wavelength of

excitation source causes photobleaching and denaturation of the protein if the intensity is too strong. Attenuating the power of the beam results in decreased signal. Furthermore, the relatively short lifetimes of tryptophan present measurement difficulties.

To solve these problems we must turn to the use of extrinsic probes. To begin, we investigate the effect of the binding of anionic ligands on the crystallographic structure of HEL. From there, two different classes of fluorescence probes are applied to the problems of protein crystallization. A covalently bound probe is first used to demonstrate that the overall rotational transport properties of HEL provide information on the crystallization conditions. However, the labeling procedure used consumes valuable protein material and is also not amenable to routine use. An alternative technique using non-covalently bound fluorescent probes is demonstrated to be a practical way to optimize and dynamically monitor crystallization conditions. With this novel technique, the chemical effects of various precipitants on the physical behavior of the protein are investigated. Applications to the screening of protein crystallization conditions are discussed.

Chapter 4

The Effects of Co-Crystallization with Orange II on the Structure of Lysozyme*

Abstract

To investigate the effects of organic anionic ligands on protein crystallization, the structure of hen egg-white lysozyme (HEL) co-crystallized with orange II was determined at 2.1 Å resolution. This structure was compared with a previously determined HEL structure from a crystal without orange II. Orange II was not found in a specific location and did not significantly perturb the structure of the protein itself. However, differences in the solvent shell and the crystallization behavior were evident. It is possible that these differences are due to increased hydrophobic interactions from weakly associated orange II.

Introduction

The nucleation and subsequent growth of protein crystals results from the association of the proteins through a combination of electrostatic, Van Der Waals, hydrodynamic, hydrogen bonding and hydrophobic interactions [96]. These interactions are manipulated by altering solution conditions to facilitate the assembly of protein molecules into nucleation centers which eventually grow into macroscopic crystals. This process is usually achieved by increasing the concentration of an appropriate crystallization agent thereby driving the solution into a state of increasing supersaturation where

* Submitted to the Journal of Crystal Growth.

nucleation and subsequent crystal growth can occur. The precipitating agents are responsible for changing the solvation properties of the protein leading to the increased protein-protein bonds which must result if crystals are to form. However, the nature of these interactions and their roles in nucleation are not well understood.

Previous investigations have examined the role of ions on the crystallization behavior of hen egg-white lysozyme (HEL). Interactions with anions are known to affect the solubility of HEL according to the reverse order of the lyotropic series [97]. HEL readily crystallizes out of solutions containing sodium chloride, but ammonium sulfate is considered to be an unsuitable crystallization agent. It has also been suggested that a matrix coprecipitation and co-crystallization reaction with organic ligands could improve the crystallization process [41]. Such ligands could participate in crystallization in two ways. First, the ligands could act as conformational tighteners which decrease the conformational mobility of proteins. Secondly, these ligands may participate in the crystallization process by generating hydrophobic interactions between ligands to form a matrix. This process was termed matrix coprecipitation.

We further investigate the role of organic ions in protein association and crystallization by determining the X-ray crystallographic structure of HEL co-crystallized with orange II. Orange II is an anionic organic ligand with a hydrophobic moiety as illustrated in Figure 4.1. The effects of orange II on the crystallization and precipitation behavior in the presence of NaCl are examined. A comparison between the structures of the HEL crystallized in the presence of orange II (OHEL) is made with HEL crystallized in the absence of orange II (1HEL). The results do not indicate significant differences in the structure of the protein itself. However,

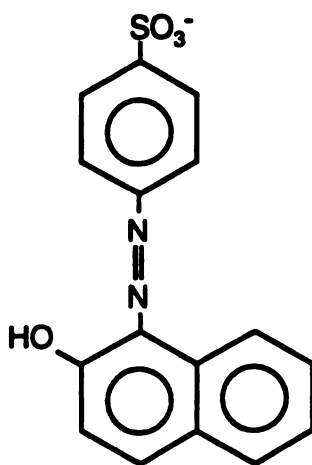


Figure 4.1 Structure of Orange II.

differences in the solvent structure were observed. These differences suggest that orange II provides additional interactions between the proteins.

Material and Methods

Three times crystallized and lyophilized HEL was obtained from Sigma and orange II was obtained from Aldrich. All solutions were made with 10 mM sodium acetate buffer at pH 4.6. The orange II was purified by recrystallization from a water/1-propanol solution. The HEL was dissolved in the buffer and filtered through a 0.45 μm filter. In the crystallization trials, HEL was co-crystallized with orange II using NaCl as a precipitant in hanging-drop vapor diffusion experiments. 10 μl drops containing HEL and orange II and 5 μl of the reservoir solution were equilibrated against a 1 ml reservoir of the limiting NaCl concentration. The limiting NaCl concentrations in the reservoir were 0, 2, 3 and 4%. For the initial concentration of 2% HEL, initial orange II concentrations were 0.2, 0.4, 0.6, 0.8, 1.0 and 1.2 mM. Crystallographic quality crystals were obtained from initial orange II concentrations of 0.8 mM with a limiting NaCl concentration

Table 4.1. Summary of x-ray diffraction and refinement statistics for orange II/lysozyme (OHEL) and lysozyme (1HEL, from [98]).

	OHEL	1HEL
Cell Constants:		
a,b (Å)	79.1	79.1
c (Å)	38.1	37.9
Unique Reflections	7,097	10,276
Resolution limit (Å)	2.1	1.7
R-value	0.165	0.152
Deviation, Bonds (Å)	0.018	0.019
Deviation, Angle (Degree)	3.3	2.4

of 3%. A crystal with approximate dimensions of 1.0 mm x 0.45 mm was used for the collection of X-ray data.

Three-dimensional X-ray diffraction data were collected at room temperature with a Siemens Xentronics area detector and graphite monochromated Cu K α radiation generated by a Rigaku RU200 X-ray generator operating at 7.5 kW. The crystal-detector distance was 13.0 cm, with a detector swing angle at 5.0°, and a scan range of 0.2° per frame. Each frame was collected for 200 s, with diffraction extending to 2.08 Å. The XENGEN [99] suite of programs was used for intensity data reduction. A total of 12,679 reflections were measured, of which 7,097 were unique. A summary of the statistics for the data set is shown in Table 4.1.

Patterson rotational/translation molecular replacement methods were used to solve the phase problem and the structure of OHEL. The atomic coordinates of HEL, stripped of solvent, from the Brookhaven Protein Data Bank file 1LYZ were employed as a search model for HEL/orange II. The rotational/translational search was performed using X-PLOR [100] on data between 7.0-2.8 Å resolution and $|F| > 2\sigma(|F|)$. Rigid body refinement of the

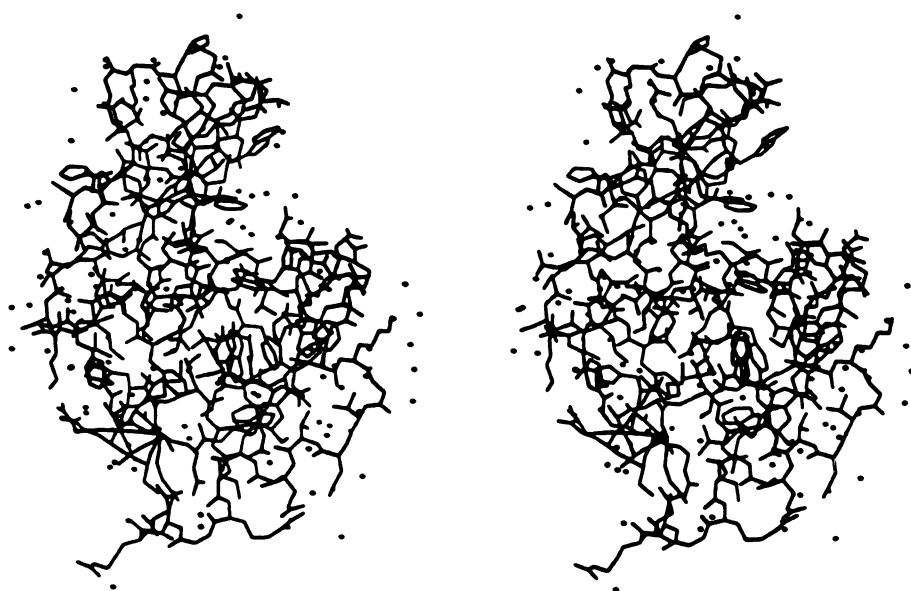
Table 4.2. Co-crystallization of HEL with orange II. Values of [NaCl] are the concentrations in the reservoir and values of [Orange II] are the initial concentrations in the hanging drop. Xn indicates the presence of crystals where n is the number of crystals, ppt indicates precipitate and + indicates relatively many. Qualitative descriptions are given in the parenthesis indicating small (sm), large (lg) and irregular (irr) crystals.

[NaCl] (%)	[Orange II] (mM)					
	0.2	0.4	0.6	0.8	1	1.2
0	Clear	Clear	ppt	ppt+	ppt+	ppt+
2	Clear	Clear	X3 (irr)	ppt+	ppt+	X+ (sm)
3	Clear	Clear	X3 (irr)	X2 (lg)	X (lg)	X+ (sm)
4	X+ (sm)	X3 (irr)	X+	X (irr)	X (irr)	X+ (sm)

P4₃2₁2 solution reduced the crystallographic residual from 0.48 to 0.28. Refinement was carried out using the restrained least-squares method with the program PROFFT [101].

After 89 cycles of refinement the residual was reduced to 0.165 for data with $|F| > 2\sigma(|F|)$ between 4.50 and 2.10 Å resolution (6753 reflections). The solvent sites were chosen only if the highest density persisted in the electron density map throughout the final stages of refinement. 107 water molecules were included in the final model (OHEL). Inspection of the electron density map of the HEL/orange II did not reveal any regions where the orange II could be tightly bound.

a



b

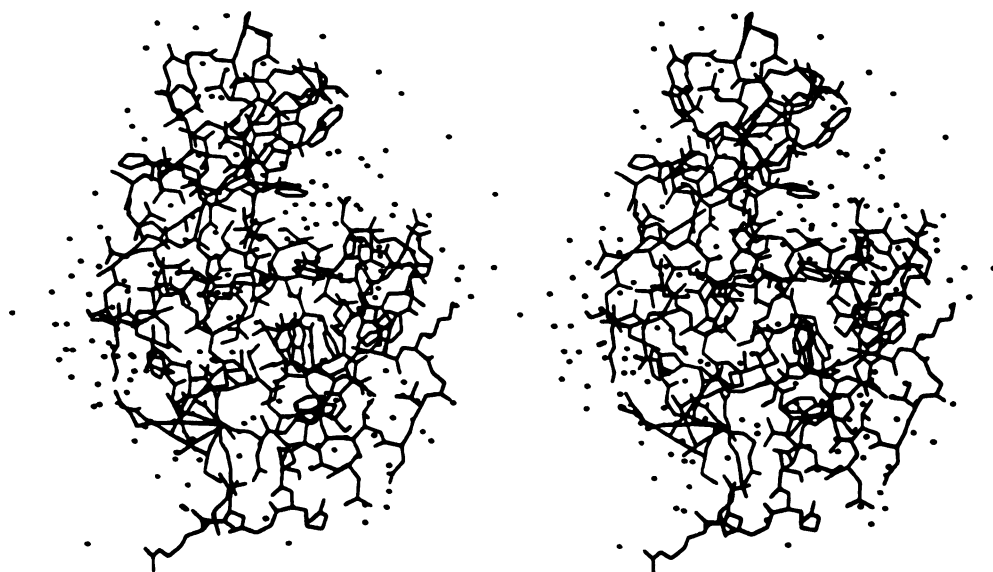


Figure 4.2. Structures of a) 0HEL co-crystallized with orange II and b) 1HEL (from Reference [98]) showing the protein and associated solvent atoms.

Results

Effects on Crystallization

The addition of orange II to HEL solutions was observed to affect the conditions under which crystals grow. Results of the crystallization trials are shown in Table 4.2. In general, the addition of orange II appears to decrease the concentration of NaCl required for the formation of crystals. Orange II itself, at initial concentrations of 0.6 to 1.2 mM (final concentrations approximately 1.8 to 3.6 mM), acts as an effective precipitant. However, only amorphous precipitates were formed in the presence of orange II alone. The crystallization of HEL with NaCl does not appear to be significantly altered at initial orange II concentrations below 0.6 mM (final concentration approximately 1.8 mM). As the NaCl concentration increases from 2 to 4 %, crystal growth occurs. The crystals that grew were of the familiar tetragonal morphology and were colored by the orange II. The optimal concentration for the co-crystallization of HEL with orange II was in the range of 3 % NaCl and initial orange II concentrations of 0.8 to 1.0 mM for an initial HEL concentration of 2 %.

Comparison of the Structure of OHEL with 1HEL

The structure of OHEL is compared with HEL crystallized from NaCl alone (1HEL). The structure used for comparison was determined by Wilson, et. al. [98] and is indexed as 1HEL in the Brookhaven Protein Data Bank. The 1HEL crystals were grown from an initial drop containing 10 μ l of 2 % HEL in 200 mM sodium acetate, pH 4.4, and 5 μ l of a 4 % NaCl reservoir solution. OHEL is isomorphous with 1HEL possessing identical cell dimensions of $a = b = 79.1 \text{ \AA}$ and a slightly smaller cell dimension of $c = 37.9 \text{ \AA}$. The number of unique reflections obtained were less in the case of

OHE

stru

in F

devi

fit a

corr

diff

surf

refin

facte

oran

HEL

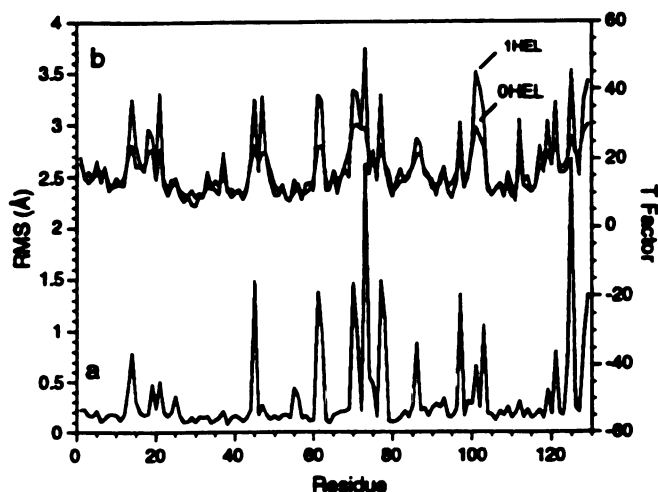


Figure 4.3. a) Average root mean square difference between the residues of OHEL and 1HEL. The models were overlaid by a least-squares procedure minimizing the rms difference between the backbone atoms. b) Thermal factors for OHEL and 1HEL.

OHEL as compared to 1HEL and is reflected in the resolution of the structures.

The structures of OHEL and 1HEL are shown with the solvent atoms in Figure 4.2. The protein structures of OHEL and 1HEL are similar. RMS deviations between the backbones atoms were minimized by a least-squares fit and calculated to be 0.614 Å. As seen in Figure 4.3, these differences also correspond to regions where the thermal factors are greatest. The largest differences are in the ARG side-chains which lie on the solvent exposed surfaces of HEL. A maximum thermal factor of 30 Å² was used in the refinement of OHEL and accounts for the differences in the average thermal factors for each residue. The structure of HEL grown in the presence of orangeII does not appear to be significantly different from the structure of HEL grown from NaCl only.

In contrast, the distribution of the solvent molecules between the two structures appears to be significantly different. A thorough search of the difference electron-density in the vicinity of the protein did not reveal any large continuous regions indicating specific binding of orange II. From this result, it appears that orange II is not strongly bound at specific locations to HEL in the crystal. However, it is possible that orange II may be bound at partial occupancy. There are significantly fewer solvent molecules in the structure of OHEL. A total of 107 water molecules were placed in the electron density surrounding OHEL, compared to 185 water molecules surrounding 1HEL. Of the 185 waters observed in 1HEL, 88 had thermal factors greater than 50\AA^2 . It is possible that many of the water molecules in 1HEL were observed because of the greater number of reflections used in the refinement.

In their comparison of crystal structures of T4 lysozyme at low, medium and high ionic strengths, Matthews, et. al. [102] found that the number of solvent molecules increased from the low, to medium to high ionic strength crystal structures. Their observations suggested that some of the solvent molecules present in the structure were actually bound ions at partial occupancy. In the structure of OHEL, some of the solvent molecules in the structures of HEL could also be bound chloride or orange II ions at partial occupancy. The decreased number of solvent molecules found in OHEL as compared to 1HEL may be due to the decreased ionic strength of the conditions used to grow OHEL crystals. From this assertion, it is likely that there are fewer ions bound to OHEL than to 1HEL.

Discussion

Insight into the crystallization mechanisms of proteins may be gained by examining the structural results together with previous results on the

effe

ora

bel

to

in

the

san

dis

pro

co-o

mat

spec

exp

sign

chlo

OHE

inve

T4 ly

show

stren

Simil

inhibi

phospl

tetrabo

showed

effects of precipitants on HEL crystallization. Although the addition of orange II to HEL solutions does affect the aggregation and crystallization behavior of HEL in solution, co-crystallization with orange II does not appear to alter the structural properties of the HEL molecule itself. The differences in the protein structure between 1HEL and OHEL lie in regions where the thermal factors are also high. These differences may be attributed to the same factors leading to large thermal factors including static and dynamic disorder.

In the model proposed by Conroy and Lovrien an initial tightening of the protein conformation by ligand binding is followed by a coprecipitation and co-crystallization process where the co-crystallizing ligands participate in a matrix stabilizing the crystal structure [41]. Orange II was not found to be specifically bound to HEL in the crystal. However, chloride ions also do not explicitly appear in the structure of 1HEL [93]. Because there is no significant difference in the protein structures with orange II and in sodium chloride only, conformational tightening does not appear to be occurring with OHEL.

Our results appear to be in accordance with previous structural investigations on the effect of solvent environments. The X-ray structures of T4 lysozyme under conditions of high, medium and low salt concentrations showed that the salt bridges in the protein are not affected by the ionic strength [102]. Differences were observed primarily in the solvent shell. Similar results are seen in other proteins such as bovine pancreatic trypsin inhibitor where the crystal structures were grown in different potassium phosphate concentrations [103]. A comparison of the structures of HEL in the tetragonal form and in the trigonal form obtained from 0.23 M sodium nitrate showed that differences were limited to regions of intermolecular contact in

the crystal [104]. Furthermore, structural differences in the native and low humidity forms of HEL were also found primarily in the solvent content [105].

However, it is evident from the crystallization trials and the difference in the distribution of solvent molecules around the HEL molecule that orange II does have an effect on the crystallization process. Orange II is an efficient precipitating agent, causing decreases in solubility at concentrations in the range of 2 mM. The crystallization trials show that orange II by itself does not lead to the nucleation of crystals and only results in the formation of amorphous precipitate. By taking into account the chemical interactions of orange II and HEL, further insight into the mechanism of HEL crystallization may be obtained.

At pH 4.6, HEL is known to highly charged with approximately +10 protons [38, 39]. Because of this property, anions are likely to interact with the positively charged groups on the protein. The effect of ion pairing on the crystallization of HEL was explained in terms of the polarizability of the ions as described by Pearson [106]. In this scheme, "soft" ions are more polarizable with a large size and low ionic charge, whereas "hard" ions are small and highly charged. The ability of various anions in decreasing the solubility of HEL can be related to their association constants with the positively charged residues.

It is likely that the role of orange II in the precipitation of HEL is related to the mechanism by which the "soft" inorganic anions cause protein-protein interactions. In precipitation reactions, Conroy and Lovrien found that close to one molecule of organic anion is bound for each cationic charge on the HEL [41]. Orange II could bind through specific ionic interactions between the sulfonate group and the positively charged residues of HEL. The

aromatic residues could then facilitate protein-protein interactions through hydrophobic interactions. Through these hydrophobic interactions, polymerization between HEL molecules would result in the large scale precipitation of the protein from the solution. Orange II would then simultaneously neutralize the charges on HEL eliminating the repulsive electrostatic forces and provide contact points for interprotein interactions mediated by the hydrophobic moiety.

However, such contact may not be suitable for crystallization. Indeed, for the crystallization of membrane proteins, hydrophobic contacts are explicitly avoided by using detergents [107]. The protein-protein interactions resulting from the molecular contacts of orange II are likely to be disordered since hydrophobic interactions are not in general directional. Multiple numbers of orange II bound to HEL would serve to randomly bind other similarly hydrophobically shielded HEL molecules, resulting in amorphous aggregation. The presence of sodium chloride appears to engender other interactions which lead to nucleation.

From fluorescence anisotropy studies, it was found that concentrations of sodium chloride which increases the rotational correlation times to intermediate values are the most favorable for HEL crystallization (Chapters 5 to 7). These conditions cause HEL to participate in protein-protein interactions but still allow sufficient mobility so that precipitation does not occur. Under optimal crystallization conditions, it is likely that although the proteins are able to interact with one another through a diminishing of the repulsive forces, there is enough mobility that the protein may reorient to form the specific interactions leading to nucleation. The interactions caused by orange II alone may not engender the favorable reorientation required for nucleation. The decrease in the amount of NaCl required to grow crystals in

the presence of orange II may indicate additional interactions imposed by orange II.

The absence of any definite location in the crystallographic structure for either orange II or sodium chloride suggest that the role of anions in the crystallization of HEL is not that of a specifically bound ligand which participates directly in forming crystal contacts. Rather, their role appears to be more diffuse. It is possible that the anions serve to stabilize the structure of the crystal. This lends support to a general concept of matrix co-crystallization. However, orange II in particular does not appear to be favorably involved in this process and may actually increase the disorder in the crystal by contributing non-directional hydrophobic interactions. The sodium chloride appears to alleviate these contributions. Thus, the balance between non-specific hydrophobic interactions and more specific ionic interactions appears to be important in the crystallization of HEL.

Chapter 5

Time-Resolved Fluorescence and Anisotropy of Covalently Coupled PBA for Monitoring the Crystallization Conditions of Lysozyme*

Abstract

Time-resolved fluorescence and anisotropy measurements of trace amounts of 1-pyrenebutyric acid labeled hen egg-white lysozyme (PBA-HEL) were used to characterize hen egg-white lysozyme (HEL) crystallization conditions. The effects of sodium chloride and protein concentrations on the fluorescence lifetimes and rotational correlation times of the labeled protein were examined. These results were compared with the effects of the salts ammonium acetate and ammonium sulfate. Addition of protein precipitants caused increases in the rotational correlation times which were attributed to a combination of steric, hydrodynamic, general electrostatic and specific ionic interactions. This decrease in the rotational mobility of HEL appears to be a necessary but not sufficient condition to allow the formation of specific interactions leading to crystallization. The results demonstrated that fluorescence measurements are effective in characterizing and monitoring protein crystallization processes prior to the appearance of macroscopic crystals.

* Submitted to the Journal of Crystal Growth.

Introduction

To expedite the screening and optimization of protein crystal growth conditions, advanced methods are required that are able to monitor protein interactions during nucleation and crystal growth in supersaturated solutions. Through the measurement of the microenvironmental properties of the protein and other solution constituents, spectroscopic techniques provide a means by which intermolecular interactions in solution can be monitored prior to the appearance of macroscopic crystals or precipitates. Information on the physical chemical processes involved in the protein-protein and protein-solvent interactions leading to crystallization may be obtained.

Steady-state fluorescence, time-resolved fluorescence and fluorescence anisotropy represent powerful optical spectroscopic techniques for monitoring the dynamics of macromolecular interactions in solution [66-68, 73]. Fluorescence techniques rely on the spontaneous emission of light by excited state probe molecules which are sensitive to the local environment of the probe. Specific information on the microenvironment of the fluorescent probe, either free in solution or coupled to a macromolecule, can be obtained from changes in the peak intensities and wavelengths in the steady-state spectra [72]. Furthermore, measurements of the rotational transport properties of the fluorophores, obtained from fluorescence depolarization techniques, are highly sensitive to molecular scale interactions [108, 109].

Time-resolved techniques are able to directly separate and quantify the relevant fluorescence parameters that contribute to the steady-state emission parameters [70]. Values of the decay lifetimes are obtained that provide information on the probe distribution and the nature of the local microenvironments. Similarly, the time dependent anisotropy measurements result in the direct quantitation of rotational correlation times [108]. The use

of time-resolved fluorescence methods to find the relationships between the microscopic interactions of proteins and their crystallization behavior should result in a more directed and rational approach for obtaining high quality protein crystals.

Jullien and coworkers previously studied protein interactions in the crystallization of ribonuclease A by monitoring the fluorescence anisotropy of a covalently bound fluorophore [87-89]. The effects of precipitating agents on crystallization were interpreted in terms of the solution non-ideality which increased sharply under conditions that were favorable for protein crystallization. Their subsequent studies using time-resolved methods have shown that species with longer rotational correlation times are present in conditions of high salt concentrations [90]. This species was postulated to be a dimer of ribonuclease. Such results have demonstrated the applicability of fluorescence techniques to the investigation of protein crystallization.

In this study, we measure the time-resolved fluorescence of 1-pyrenebutyric acid (PBA, Figure 5.1) covalently coupled to hen egg-white lysozyme (HEL) to probe the interactions involved in the crystallization process. The fluorescence lifetime of PBA is known to be dependent on microenvironmental parameters such as the polarity and accessibility of the solvent [110]. Rotational correlation times ranging from a few nanoseconds to microseconds may be measured in order to monitor the intermolecular association of proteins in undersaturated and supersaturated solutions [111]. We compare the effects of the salts sodium chloride (NaCl), ammonium acetate (NAc) and ammonium sulfate (NS) on the rotational correlation times and fluorescence lifetimes of HEL solutions containing trace amounts of PBA-HEL. These effects are, in turn, compared to the crystallization behavior of HEL in the presence of these various precipitants.

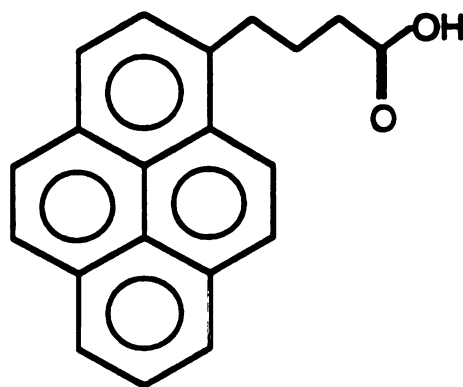


Figure 5.1. The structure of 1-pyrene butyric acid (PBA).

Experimental Methods

Labeling of HEL with PBA

For the labeling of HEL with PBA, succinimidyl 1-pyrenebutyric acid (SPBA) was obtained from Molecular Probes, Inc., and 3X crystallized HEL was obtained from Sigma. 220 mg of HEL was dissolved in 22 ml of sodium borate buffer at pH 8.5 and filtered through a 0.45 μm filter. 11 mg of SPBA was dissolved in 200 μl of dimethyl formamide and then slowly added to the HEL solution while stirring to form a cloudy suspension. The reaction mixture was then stirred for 2 hr at 23° C, after which 2.5 ml of 1.5 M hydroxyl amine at pH 8.3 was added to quench the reaction. After 30 min., the reaction mixture was then passed through a 0.45 μm microfilter. Removal of the unreacted SPBA was accomplished by passing the solution through a G-25 desalting column and eluted with 20mM MES buffer at pH 6.5.

The fractions containing protein, as determined by measuring the absorbance at 280 nm, were collected and applied to a carboxymethyl-sepharose CL-6B cation exchange column equilibrated to pH 6.5 with 20 mM MES buffer. The mixture of unlabeled and labeled HEL were separated by elution with a 0 to 1M NaCl gradient with 10 ml fractions taken. The

absorbance at 280 nm and 341 nm was measured to determine the respective amounts of protein and PBA in each fraction. The fractions determined to contain singly labeled PBA were collected. Final desalting was accomplished by ultrafiltration through a 10,000 MW cutoff filter and equilibrated by washing three times with 50 mM sodium acetate buffer at pH 4.6.

Sample Preparation

All solutions were prepared in 50 mM sodium acetate buffer at pH 4.6 unless otherwise noted. All percent concentrations are expressed as w/v. Stock HEL solutions of 20% were prepared by dissolving the solids in buffer. The HEL solution was then washed three times with buffer using ultrafiltration (10,000 MW cutoff). The concentration was measured by serially diluting the solution 1000 times and measuring the spectrophotometric absorbance at 280 nm using $A^{1\%} = 26.4$ [112]. Stock solutions of 20% NaCl, 40% NS and 20% NAc were prepared in buffer using reagent grade materials. Stock PBA-HEL solutions of 0.2 % w/v were prepared and diluted ten times to obtain a concentration of 0.02% PBA-HEL in the samples. Appropriate amounts of the stock solutions and buffer were mixed together for the samples used in the fluorescence measurements.

Fluorescence Measurements

Steady-state fluorescence measurements were performed using a SPEX Fluorolog spectrofluorimeter. For the time-resolved measurements, a picosecond dye laser system was used as the excitation source and the emission decay data collected using the time-correlated single-photon counting (TCSPC) method [113]. A full description of the TCSPC apparatus has been previously reported [79]. For our measurements, the output from the dye LDS 698 was frequency doubled and passed through a polarization

rotator and a vertically oriented polarizer before impinging upon the sample. Samples were excited with a wavelength of 350 nm and a pulse repetition rate of 760 KHz. The fluorescence emission at 400 nm was collected through collimating lenses, a rotatable emission polarizer and then a depolarizer before entering the monochromator. 4096 channels were used where each channel corresponded to a time interval of 0.197 ns.

All measurements were started within approximately 10 minutes after mixing of the stock solutions and were performed at 23° C. During the time-resolved measurements, the emission polarizer was alternately rotated from a vertical to a horizontal orientation every 120 s to average the effects from fluctuations in the excitation intensity. The vertical and horizontal emission decay profiles were summed until approximately greater than 10,000 counts appeared in the peak channel for a total collection time of about 20 min. for each sample. The instrument response function from the excitation pulse was collected before each sample by measuring light from a scattering solution and was used for subsequent data analysis.

Data Analysis

The analysis of time-resolved fluorescence data involves fitting the fluorescence decay to a sum of exponential components by taking into account the finite pulse shape of the excitation source. The time-dependent fluorescence, $I_{\text{tot}}(t)$, from an initial excited state population, decays exponentially with characteristic lifetimes, τ_i [73],

$$I_{\text{tot}}(t) = \sum_{i=1}^p A_i \exp(-t/\tau_i) \quad (5.1)$$

where i represents a single fluorescence component and p is the number of components. These fluorescence lifetimes are sensitive to the local microenvironment of the probe including quenching effects. When a pulse

with a finite duration is used for excitation, the experimentally observed fluorescence decay profile, $I_{\text{obs}}(t)$, is a convolution of the instrument response function, $L(t)$, with the intrinsic fluorescence response, $I_{\text{tot}}(t)$. $I_{\text{tot}}(s)$ must be extracted from the convoluted fluorescence profile using a least squares fitting procedure [80-83]

Excitation of a population of fluorescence molecules with vertically polarized light preferentially excites the probes which are in a proper orientation thereby inducing fluorescence anisotropy. The induced fluorescence anisotropy decays to a randomly oriented distribution of fluorescing species. This time-dependent induced fluorescence anisotropy is defined by,

$$R(t) = \frac{I_{\text{vv}} - I_{\text{vh}}}{I_{\text{vv}} + 2I_{\text{vh}}} = \frac{I_{\text{diff}}}{I_{\text{tot}}} = \sum_{j=1}^q B_j \exp(-t/\rho_j) \quad (5.2)$$

where I_{vv} and I_{vh} are the vertically and horizontally oriented polarized emission intensities, respectively, for a vertically polarized excitation source. I_{tot} is the time-dependent total fluorescence intensity as before and I_{diff} is the difference fluorescence intensity.

The decay rate of $R(t)$ depends on both the intrinsic properties of the probe molecule and on the interaction between the probe and its local environment [108]. Generally, $R(t)$ can contain up to five exponential components where j represents one decay component, q is the number of components and B_j and ρ_j are the initial anisotropies and rotational correlation times of each component, respectively. $R(t)$ is also distorted by the excitation pulse profile, but $R(t)$ can not be directly fit to the observed decay. Instead, the B_j and ρ_j values are found by numerically fitting the experimentally measured vertically and horizontally polarized emission using previously determined parameters for I_{tot} [83, 84].

Results

Chromatography and PAGE of PBA-Lys

For the ion exchange chromatography of the PBA-HEL reaction, the protein concentration was measured by monitoring the absorbance at 280 nm while the PBA concentration was monitored at 341 nm. Three protein peaks were eluted in the order A, B and C. Peak A showed no absorbance at 341 nm and thus contained unlabeled HEL. Peak B showed approximately half the relative absorbance at 341 nm as peak C. This suggests that peak B contained singly labeled PBA-HEL while peak C contained doubly labeled PBA-lysozyme.

It is known that the succinimidyl group reacts with the free base form of aliphatic amines to form stable carboxamides [114]. On HEL, there are 6 ϵ -amino groups of lysine and the N-terminal amine. At the labeling conditions used (pH 8.5), the N-terminal amine is the most reactive site since the pKa is 7.8-8.0 [115]. The pKa values of the lysine residues are all greater than 10.0 and are less reactive [115]. Thus, it is likely that the N-terminal amine is the singly labeled species in peak B.

Further analysis of samples from the ion-exchange chromatography was performed using polyacrylamide gel electrophoresis (PAGE). Samples corresponding to peaks A, B and C each resulted in a single band on the gel. The band corresponding to the unlabeled HEL showed the greatest mobility followed by the bands corresponding to peaks B and C. Fits to the logarithm of the relative mobility show a linear relationship with respect to the polyacrylamide concentration. All three fits give identical slopes within error but with different intercepts projected to 0% polyacrylamide. These results show that the unlabeled, and the apparently singly labeled and doubly labeled HEL differ in net charge and not size. This result is expected since

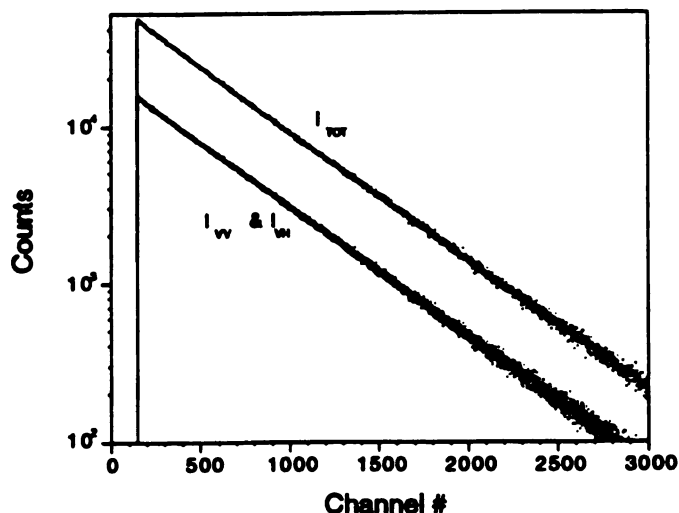


Figure 5.2. Time-dependent fluorescence intensity decays of free PBA at 23°C in 50 mM sodium borate buffer at pH 8.5. Also shown is the fit through the total fluorescence decay data. I_{vv} and I_{vH} are virtually indistinguishable because of the fast rotational rate of the relatively small PBA. Each channel represents a time interval of 0.197 ns.

the reaction of SPBA to an amine will neutralize the charge. All subsequent experiments described use the apparently singly labeled PBA-HEL from peak B as the trace fluorescence probe.

Fluorescence Measurements of PBA-HEL

Steady state peak intensities occur at emission wavelengths near 380 and 400 nm with a shoulder occurring at 417 nm. The emission from PBA-HEL shows a slight 2 nm red shift as compared to unconjugated PBA but the shape of the spectra remains essentially identical. As seen in Figures 5.2 and 5.3, the time-resolved decay of the total fluorescence of free PBA decays at a greater rate than the PBA-HEL. The fluorescence decay of free PBA could be fit by a single exponential term with a fluorescence lifetime of 103 ns.

cons

adeq

is on

shor

medi

conju

conju

solver

collisi

most

conjug

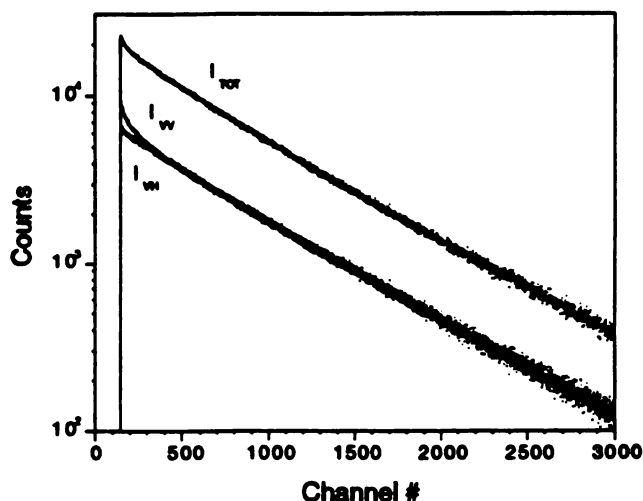


Figure 5.3. Time-dependent fluorescence intensity decays of 0.02% PBA-HEL at 23°C in 50 mM sodium acetate buffer at pH 4.6. The fits are shown as the solid lines through the data points. The difference in I_{vv} and I_{vh} is due to the fluorescence anisotropy of the conjugated PBA. Each channel represents a time interval of 0.197 ns.

As seen in Figure 5.3, the total fluorescence decay of PBA-HEL is considerably more complex. Three exponential terms were required to adequately describe this decay. At a PBA-HEL concentration of 0.02 %, there is one long lifetime component of 151 ns, a medium lifetime of 69 ns and a short lifetime of 6 ns. Because of the long lifetime of PBA, the long and medium lifetime components can be attributed to the fluorescence from the conjugated PBA.

The increase in the value of the long lifetime component of the conjugated PBA as compared to free PBA is likely to result from either solvent polarity effects near the protein surface or decreased accessibility to collisional quenchers, such as oxygen. The medium lifetime component is most likely due to heterogeneity in the microenvironment surrounding the conjugated PBA. The origin of the short lifetime component is not clear, but is

possibly attributable to fluorescence from other sample constituents. Further results will focus on the effects of precipitants on the long component of the fluorescence decay.

Previous investigations have estimated the dimensions of HEL, assuming a prolate ellipsoid shape, to be 5.5 nm and 3.3 nm along the major and minor axis, respectively [116]. Two rotational correlation time components were required to fit the experimental data. The long rotational correlation time of 16.2 ns from a 0.02% PBA-HEL solution agrees well with the expected results for the overall rotation of HEL. This rotational correlation time corresponds to a spherical rotor diameter of 5.0 nm [108]. A short rotational correlation time of 0.13 ns was also present and most likely represents segmental motions of the protein or PBA. For applications to protein crystallization, we are primarily interested in the overall interactions of HEL rather than local conformational changes. Thus, we will examine the effects of the crystallization conditions on the long rotational correlation times.

Effects of NaCl

The effects of NaCl on the long component of the fluorescence lifetimes of 2 and 4% HEL are shown in Figure 5.4a. An increase in the fluorescence lifetimes is seen as the NaCl concentration increases, with a slightly greater increase in the case of 4% HEL than with the 2% HEL. The effects of NaCl on the long component rotational correlation times of 2 and 4% HEL solutions are shown in Figure 5.4b. In this case, the increase in the rotational correlation times of the 4% HEL solutions are significantly greater than the corresponding increase of the 2% solutions.

the

valu

crys

162

to 60

morp

condi

HEL

thoro

warra

the ev

amoun

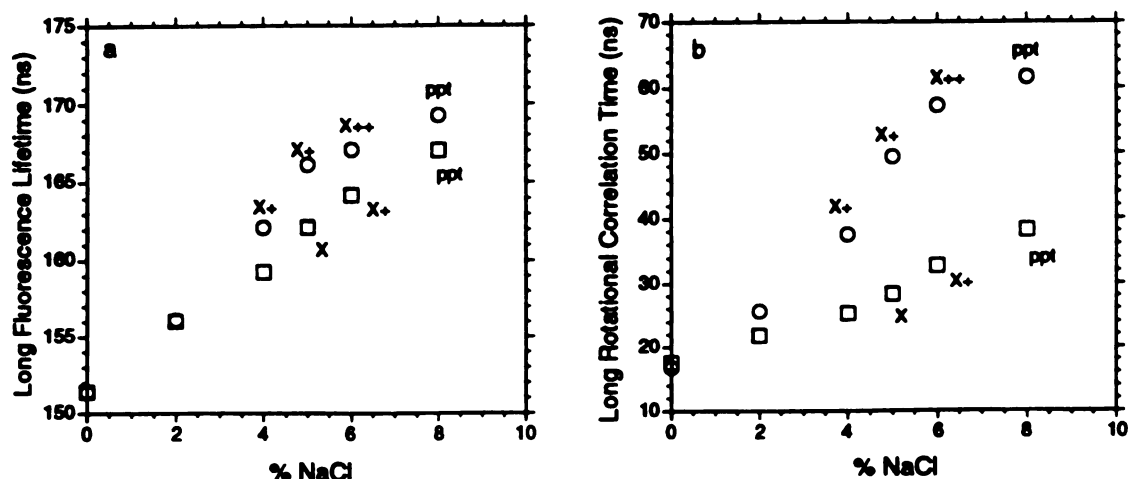


Figure 5.4. Dependence of the a) fluorescence lifetimes of and b) rotational correlation times of PBA-HEL on NaCl concentrations at 2% (□) and 4% (○) HEL. The X and ppt symbols represents crystallization or precipitation, respectively. The + symbols represent the relative amounts formed to show increasing supersaturation.

Under conditions of lower NaCl concentration where no crystals form, the fluorescence lifetimes and rotational correlation times show relatively low values. In the regime where conditions are optimal for producing high quality crystals, the fluorescence lifetimes increase to intermediate values of about 162 to 168 ns while the rotational correlation times increase to a range of 30 to 60 ns. The crystals which formed appeared to be of the familiar tetragonal morphology and exhibited the expected crystallization behavior at the conditions used [8, 36]. Although it did not appear that the presence of PBA-HEL at 0.02 % significantly interfered with the crystallization process, a thorough examination on the kinetic effects of fluorescence additives is warranted in further investigations.

At a NaCl concentration of 8% and greater, rapid aggregation leads to the eventual formation of needle shaped crystals. The presence of large amounts of visible particles at 8 % NaCl interferes with the fluorescence

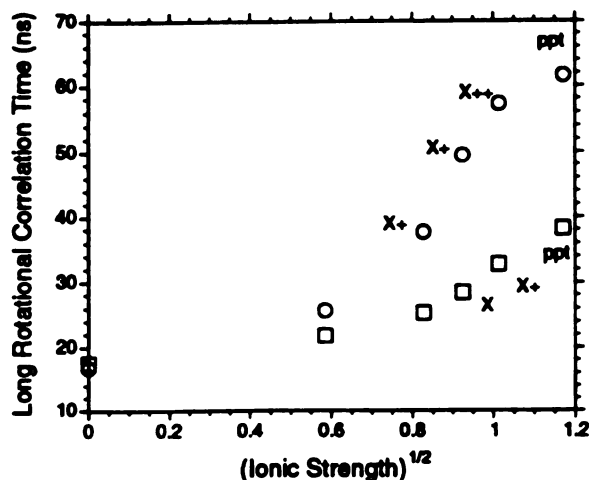


Figure 5.5. Effects of the ionic strength of NaCl on the rotational correlation times of PBA-HEL at 2% (□) and 4% (○) HEL.

measurements due to multiple scattering and result in depressed values for the largest rotational correlation time. Nonetheless, the increasing trend in the rotational correlation time is clear.

Figure 5.5 emphasizes the electrostatic effects of added NaCl by showing the rotational correlation times of PBA-HEL at 2 and 4% HEL as a function of the square root of the ionic strength. The square root of the ionic strength is a more physically meaningful measure of electrostatic effects since it is proportional to the Debye screening length. It is interesting to note that the rotational correlation times increase slowly as the ionic strength increases in undersaturated solution, but shows an increased slope as the solution becomes supersaturated. The greater rate of increase at 4% HEL indicates that the effect of ionic strength is more pronounced at higher protein concentrations.

The effects of HEL concentration at fixed concentrations of 2 and 5% NaCl on the fluorescence lifetimes and rotational correlation times are seen in Figure 5.6. With 2% NaCl, crystals do not appear at HEL concentrations

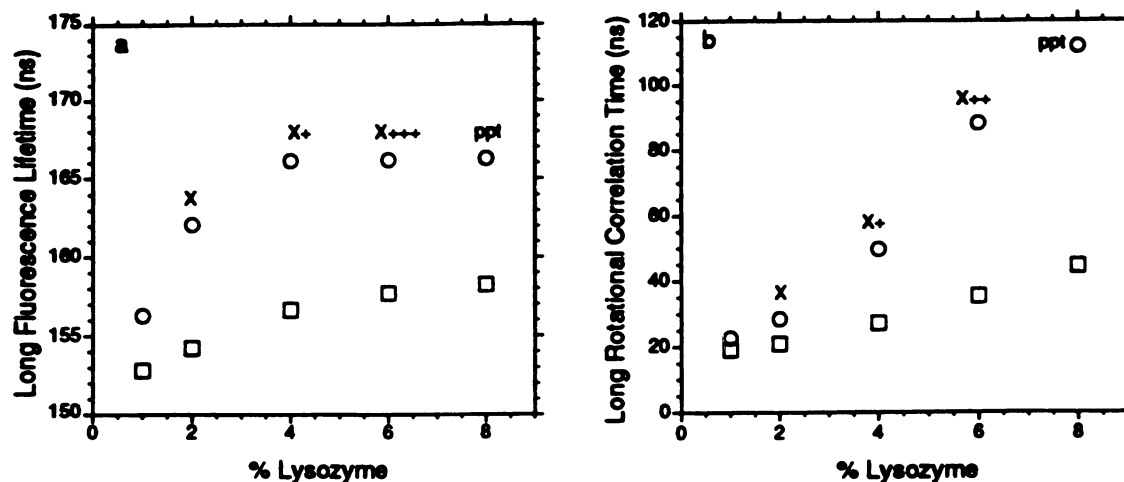


Figure 5.6. Dependence of the a) fluorescence lifetimes and b) rotational correlation times of PBA-HEL on HEL concentrations at 2% (□) and 5% (○) NaCl. See Figure 5.4 for an explanation of the X and ppt symbols.

between 1 and 8%. Solutions containing 5% NaCl are more favorable for crystal growth with the optimal concentrations of HEL lying between 2 and 6%. Rapid nucleation occurs at 8% HEL and 5% NaCl. The fluorescence lifetimes reach a plateau near 167 ns for the 5% NaCl solutions and near 160 ns for the 2% NaCl solutions. It is also seen that as the HEL concentration is increased, greater increases in the rotational correlation times are observed in the presence of 5% NaCl than with 2% NaCl.

Effects of Ammonium Acetate and Ammonium Sulfate

To determine the effects of different salts on the crystallization and fluorescence behavior, the effects of NAc and NS are compared with those of NaCl. In Figure 5.7a, the effects of NS, NAc and NaCl on the fluorescence and crystallization behavior of PBA-HEL in 4% HEL solutions are shown. The fluorescence lifetimes of PBA-HEL in NS solutions show a larger increase as the NS concentration is increased as compared to either the NaCl

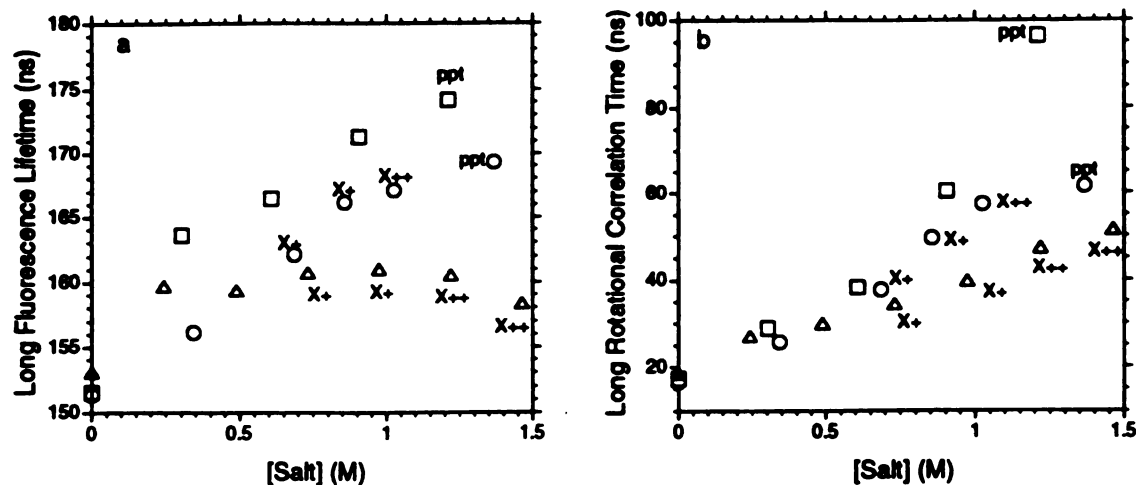


Figure 5.7. Dependence of the a) fluorescence lifetimes and b) rotational correlation times of PBA-HEL on salt concentrations at 4% HEL. The (O), (Δ) and (□) represent solutions containing NaCl, NAc and NS, respectively.

or NAc solutions. The greater increase in the fluorescence lifetimes seen in the presence of NS indicates that the interactions of the conjugated PBA are qualitatively different than the interactions experienced with NaCl and NAc. With NAc, the fluorescence lifetimes show a small increase at the lowest concentration but remain essentially constant as the concentration of NAc increases.

From the relationship of the rotational correlation times to NaCl, NAc and NS concentrations seen in figure 5.7b, ionic effects are observed to cause an increase in the rotational correlation times and thus reflect greater interactions between HEL molecules. The rotational correlation times of PBA-HEL increase as the NS concentration increases and are similar to the values with NaCl at the same molar concentrations. Increases in the NAc concentration also cause increases in the rotational correlation times with crystallization occurring at values greater than 30 ns.

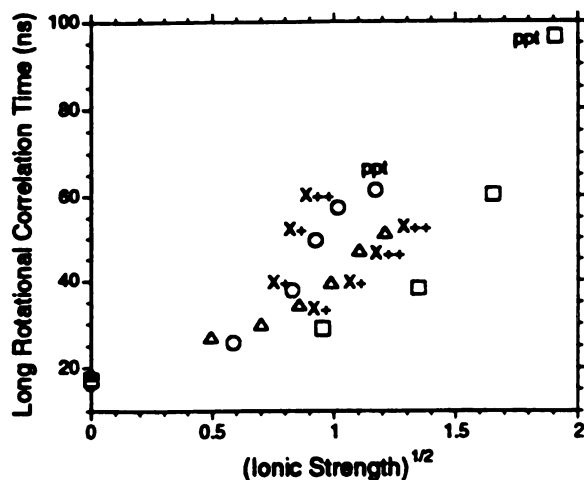


Figure 5.8. Effects of the ionic strength with NaCl (○), NAc (△) and NS (□) on the rotational correlation times of PBA-HEL at 4% HEL.

To further examine the electrostatic effects of salts on the fluorescence and crystallization behavior, Figure 5.8 shows the rotational correlation times of 4% HEL in NaCl, NAc and NS solutions plotted against the square root of the ionic strength. In all three cases, there appears to be a inflection in the slope of the rotational correlation time as the ionic strength increases. However, with NS the change in the slope occurs at a higher ionic strength than with NaCl and NAc. From the different degrees of increase in the rotational correlation times due to NaCl, NAc and NS as a function of ionic strength, it is clear that electrostatic screening is not the only operative effect on the molecular interactions.

It is also clear that these interactions are related to the effectiveness of different concentrations of precipitants on the outcome of the crystallization. This is seen with NaCl and NAc where intermediate values of the rotational correlation times are conducive to the formation of crystals. Conditions which show low values of the rotational correlation times do not exhibit strong enough interactions for crystallization to occur. Conditions which show

rotat

HEL

large

an an

Disc

meth

cryst

polar

soluti

lifetim

the s

appea

HEL

times

rotati

influe

increa

additi

occur.

combin

crystal

additic

times [

in the

rotational correlation times that are too large lead to the rapid aggregation of HEL to form small, intergrown and needle-like crystals. In the case of NS, large increases in the rotational correlation times result in the formation of an amorphous gel.

Discussion

The time-resolved fluorescence of PBA-HEL appears to be a sensitive method for measuring the molecular interactions which lead to the crystallization of HEL. Fluorescence lifetimes provide information on the polarity and solvent accessibility of the conjugated PBA due to changes in the solution constituents. It is unclear whether the differences in the fluorescence lifetimes are due to intramolecular or intermolecular interactions induced by the salt. However, changes in the measured rotational correlation times appear to provide direct information on the intermolecular interactions of HEL under crystallization conditions. In particular, the rotational correlation times have been shown to measure the influence of precipitants on the rotational mobility of HEL.

It is apparent that both the concentrations of NaCl and HEL together influence the crystallization and rotational behavior. The results suggest that increases in the rotational correlation times due to the presence of solution additives are a necessary but not sufficient indication that nucleation will occur. This increase in the rotational correlation time may be attributed to a combination of the different types of interactions which together influence the crystallization behavior. Increases in the viscosity of the solvent due to the addition of precipitants are taken into account in the rotational correlation times [108]. These changes in the bulk viscosity are the result of interactions in the PBA-HEL microenvironment and should also influence the

cry
rot
vis
cor
sta
tra
inc
the
[56]
mea
agg
pro
agg
effe
hyd
Alth
rota
time
exan
rota
preci
the
inter
mobil
degree

crystallization behavior. However, because of the large increases in the rotational correlation times, they can not be attributed to changes in the viscosity alone [117].

A possible explanation for the observed increases in the rotational correlation time is that aggregates of various sizes are formed and remain stable during the time scale of the measurements. Another possibility is that transient interactions occur between the protein molecules and lead to increased frictional resistance. Bishop, et. al. used light scattering to examine the nature of the changes in the translational diffusion coefficients of HEL [56]. The results from those investigations suggested that the decrease in the measured diffusion rates are not due to the formation of discrete isolated aggregates but rather, are due to an increase in the friction factor of the proteins. We observed no direct evidence that distinct populations of aggregates are formed although the possible is not excluded.

The types of interactions between proteins include general electrostatic effects caused by increasing salt concentrations, volume exclusion and hydrodynamic coupling effects from increasing protein concentrations. Although conditions which are conducive for crystallization lead to increasing rotational correlation times, the absolute value of the rotational correlation times do not by themselves indicate whether crystallization will occur. For example, at constant HEL concentrations, rapid aggregation occurs with a rotational correlation time of 62 ns with 4% HEL, while at 2% HEL precipitation occurs at a rotational correlation time of only 38 ns. Increasing the HEL concentration will increase the probability of protein-protein interactions through steric and hydrodynamic coupling resulting in decreased mobility. Increasing salt concentrations should then further influence the degree of these interactions through ionic effects.

The effects of salts on protein association may be classified according to three types of interactions [118]. These are 1) general electrostatic effects, which include ionic screening effects and double-layer interactions, 2) lyotropic salt effects, involved in the salting out of hydrophobic proteins and 3) site-specific ion bonding. Because HEL has a positive charge of about +10 protons at pH 4.6 [39], general and site-specific electrostatic effects are expected to play an important role in the interactions of HEL.

Increasing the salt concentrations results in a shielding of the repulsive electrostatic forces [24]. At higher salt concentrations Van Der Waals attractive forces dominate and nucleation may occur. The specific nature of the anion is known to play an important role in the crystallization process. Riès-Kautt and Ducruix determined that the effectiveness of ions in decreasing the solubility of HEL follows the order $\text{Cl}^- > \text{CH}_3\text{OO}^- > \text{SO}_4^{2-}$ [37]. This effect was explained in terms of the relative ability of different anions to participate in ion pairing with the positively charged protein.

Thus, both general electrostatic and site-specific ion binding effects may be important processes in the crystallization of HEL. The increase in the rotational correlation times at different ionic strengths appear to indicate the effectiveness of the different salts for inducing interactions that lead to crystallization. This retardation of the rotational mobility may allow the formation of specific ionic interactions by NaCl and NAc but not with NS. For HEL, salts that cause an increase in the rotational correlation times at lower ionic strengths appear to be more effective agents for crystallization. A sharper increase in the rotational correlation times is also observed in these salt solutions as the solution becomes supersaturated. Further investigations are required to determine whether this is a general phenomenon.

The ability to measure the nature and magnitudes of the molecular interactions between protein molecules under crystallization conditions should result in a more directed approach in producing high quality crystals for X-ray crystallography. These methods appear to be able to dynamically monitor the supersaturation levels *in situ* and would be useful in the optimization of precipitant and protein concentrations. The ability to characterize the molecular interactions in a particular protein system operating under supersaturated conditions is useful in directing the choice of precipitants. It is important to emphasize that these interactions are evident with fluorescence methods before the appearance of macroscopic crystals. Further work is necessary to establish the detailed protocols for the application of fluorescence spectroscopy to the screening of conditions. However, it is clear that fluorescence spectroscopy holds promise as a valuable aid in the crystallization of proteins.

Chapter 6

Time-Resolved Fluorescence and Anisotropy of Non-Covalently Bound ANS for Monitoring the Crystallization Conditions of Lysozyme*

Abstract

Time-resolved fluorescence measurements and anisotropy measurements of the non-covalently bound probe, 1-anilino-8-naphthalene sulfonic acid (ANS), is demonstrated to be a practical *in situ* method to monitor the solution conditions of hen egg-white lysozyme (HEL). The sensitivity of ANS to the microenvironment of the protein is useful in isolating the fluorescence behavior of the bound fraction. Sodium chloride and ammonium sulfate were found to cause increased binding of ANS to HEL resulting in increased fluorescence intensities. This technique was used to map the response of the total fluorescence and rotational correlation times of ANS to the influence of salt and protein concentrations. ANS fluorescence was then applied to dynamically monitor the progress of protein crystallization in both batch and vapor diffusion experiments.

Introduction

Since the realization that conventional methods for the production of protein crystals were inadequate, there has been a rapid development of new screening and optimization strategies. However, these methods primarily rely on the visual inspection of crystallization trials. Because of the long time

* Submitted to the Journal of Crystal Growth.

periods required to establish solubility relationships for a particular protein-precipitant combination and the insufficient information gained on the molecular processes, this optimization process may be difficult. Methods that could dynamically measure the effects of various precipitants on the interactions of proteins in supersaturated conditions would be helpful in improving the efficiency. Such methods could be used to delineate suitable conditions from which protein nucleation and crystal growth would occur. Furthermore, crystallization conditions could be dynamically monitored to provide for the active control of protein and precipitant concentrations [119].

Previously, we had used a covalently bound probe, 1-pyrenebutyric acid (PBA), to determine the effects of protein crystallization conditions on the fluorescence and anisotropy behavior of hen egg-white lysozyme (HEL) (Chapter 5). Time-resolved methods were used to directly quantify the fluorescence lifetime and rotational correlation times in the presence of precipitating agents. Increases in the rotational correlation times were observed with increasing protein and precipitant concentrations. This decrease in the rotational mobility of the covalently labeled protein was attributed to protein-protein interactions caused by the precipitants. It was shown that such techniques could be used to monitor the solution conditions leading to nucleation and crystallization.

In this work, we investigate a novel application of fluorescence spectroscopic techniques which holds promise for the practical optimization of protein crystallization conditions. Non-covalently bound fluorescence molecules which are able to dynamically monitor the protein-protein and protein-solvent interactions are used. The use of a non-covalently bound probe eliminates the difficulties encountered in labeling procedures. Such difficulties include the consumption of limited protein material and the need

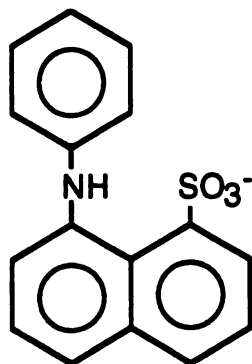


Figure 6.1. Structure of ANS.

to separate the free probes from the protein coupled probes. Because the non-covalently bound probe is directly added to the solution, no extra protein material is used. Interference from free probe molecules is also eliminated by exploiting the properties of fluorescent probes that are sensitive to the local solvent environment. Only the probes which are bound to the protein display significant amounts of fluorescence emission.

1-anilino-8-naphthalene sulfonic acid (ANS, Figure 6.1) was chosen as the non-covalently bound fluorescence probe for this work. This probe has been extensively used in studies of protein folding [120], protein ligand binding [121, 122] and lipid dynamics [123]. In aqueous solutions, ANS displays a weak green emission, but bound to proteins or lipid membranes, an intense blue emission is observed [123-125]. These properties are used to map the response of the time-resolved fluorescence and anisotropy parameters of ANS to varying concentrations of sodium chloride (NaCl) and ammonium sulfate (NS) in HEL solutions. It is also demonstrated using both batch and vapor diffusion experiments that the time evolution of the crystallization trials may be dynamically monitored.

Experimental

Solution Preparation

All solutions were prepared in 50 mM sodium acetate buffer at pH 4.6 unless otherwise noted. Three times crystallized HEL was obtained from Sigma. Stock HEL solutions of 10% were prepared by dissolving the solids in buffer. After a 0.45 μm pore filtration, the lysozyme solution was washed three times with buffer using an ultrafiltration cell (10,000 MW cutoff). Protein concentrations were measured by the spectrophotometric absorbance of a serially diluted solution at 280 nm with $A^{1\%} = 26.4$ [112]. ANS was obtained from Eastman Kodak and was used without further purification. A 10^{-3} M solution of ANS was prepared as the stock solution. This was diluted ten times for a final concentration of 10^{-4} M ANS in the samples. 3.45 M (20 %) NaCl and 3 M NS were also used as stock solutions. The samples were prepared by adding, in order, the appropriate amounts of HEL, buffer, ANS and precipitant with thorough mixing after each addition.

Fluorescence Measurements

Steady-state fluorescence measurements were performed using a SPEX Fluorolog spectrofluorimeter. A picosecond dye laser system was used as the excitation source for the time resolved measurements. The emission decay data was collected using the time-correlated single-photon counting method [113]. More detailed descriptions of the laser system [79] and the measurement procedure (Chapter 3) have previously been reported. Samples were excited with a wavelength of 350 nm and the time-resolved fluorescence decays were collected at 480 nm through a 370 nm cut-off filter and monochromator. A total of 4096 channels was used to record the decay. Each channel corresponded to a time interval of 0.040 ns.

aft

and

For

cul

app

tub

sitt

dro

qua

the

the

solu

becz

alte

aver

instr

each

subs

(Cha

excit

chara

a sin

fluore

The measurements were started within approximately ten minutes after mixing of the stock solutions except for the time-courses of the batch and vapor diffusion experiments. All measurements were performed at 23° C. For the determination of salt effects, 100 μ l samples were prepared in 96 well culture plates. A micro-capacity quartz cuvette was used to hold approximately 70 μ l of each sample.

For the batch time course experiment, a thin walled glass capillary tube, sealed at the ends with Parafilm, was used to contain the sample. A sitting drop vapor diffusion experiment was also performed by placing a 15 μ l drop in a quartz cup. This cup was attached to one corner of a 4 ml capacity quartz cuvette with silicon grease. 1 ml of limiting salt solution was placed in the bottom of the cuvette which was then sealed with a Teflon stopper. In these time course experiments, the laser was directed in a region of the solution that was devoid of crystals. This was easily performed visually because of the intense emission from the crystals.

During the time-resolved measurements, the emission polarizer was alternately rotated from a vertical to a horizontal orientation every 50 s to average the effects from fluctuations in the excitation intensity. The instrument response function from the excitation pulse was collected before each sample by measuring light from a scattering solution and was used for subsequent data analysis.

The data analysis procedure was described in detail previously (Chapter 3). Briefly, the time-dependent fluorescence, $I_{\text{tot}}(t)$, from an initial excited state population, may be fit to a sum of exponential terms with characteristic lifetimes, τ_i , and pre-exponential factors, A_i , where i represents a single fluorescence component [73]. The time-dependent induced fluorescence anisotropy is defined by,

$$R(t) = \frac{I_{vv} - I_{vh}}{I_{vv} + 2I_{vh}} = \frac{I_{dif}}{I_{tot}} = \sum_{j=1}^q B_j \exp(-t/\rho_j) \quad (6.1)$$

where I_{vv} and I_{vh} are the vertically and horizontally oriented polarized emission intensities, respectively, for a vertically polarized excitation source. I_{tot} is the time-dependent total fluorescence intensity as before and I_{dif} is the difference fluorescence intensity. The anisotropic decay is also described by a sum of exponential decays where j represents one decay component and q is the number of components. B_j and ρ_j are the initial anisotropies and rotational correlation times of each component, respectively. The B_j and ρ_j values are found by numerically fitting the experimentally measured vertically and horizontally polarized emission using the determined parameters for I_{tot} [83, 84]. In a mixture of different fluorescent species, each component of the anisotropic decay can be associated with one or several separate components of the total fluorescence decay.

Results

Response of ANS Fluorescence to Solution Conditions

In buffer alone, the steady-state fluorescence intensity from ANS is negligible compared to the intensity observed in the presence of HEL. Further increases in the steady state fluorescence intensity of ANS is observed as the concentration of NaCl is increased. A corresponding blue shift in the fluorescence spectra from approximately 490 nm to 480 nm is also observed. To further investigate the cause of this fluorescence enhancement in the presence of HEL and the increase as salt concentrations increase, the time-resolved fluorescence decays are examined.

An example of the total time-resolved fluorescence decay is shown in Figure 6.2 where the emission from ANS in a 3.6% lysozyme solution is

I
 t
 c
 e
 c
 c
 c
 s
 a
 s
 i
 l
 l
 N

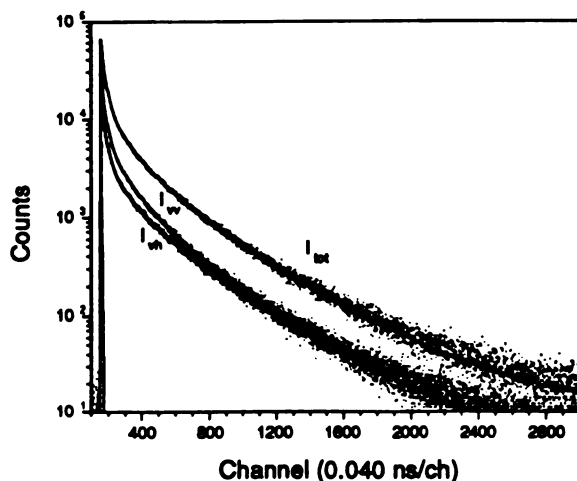


Figure 6.2. Time resolved fluorescence decay curves for 10^{-4} M ANS in 3.6 % HEL.

measured. Four exponential components were required to adequately fit the total fluorescence decay. The fluorescence lifetimes of these components are denoted τ_1 to τ_4 in order of decreasing lifetime, with associated pre-exponential factors A_1 to A_4 . For all of the samples, the total fluorescence decay is found to be due to the combined contributions of two short lifetime components of approximately 0.2 ns and 1.0 ns and to two longer lifetime components of approximately 5 and 17 ns.

We examined the effects of increasing concentrations of NaCl and HEL on the fluorescence lifetimes and pre-exponential factors of ANS. Only a slight increase in the lifetimes of the fluorescence components was observed as the concentration of NaCl increases. There also appeared to be no significant effect from increasing concentrations of HEL. However, as shown in Figure 6.3, we observed that the pre-exponential factors of the two longer lifetime components (A_1 and A_2) increase while those of the two shorter lifetime components (A_3 and A_4) decrease with increasing concentrations of NaCl. From these results, we can conclude that the increase in the steady-

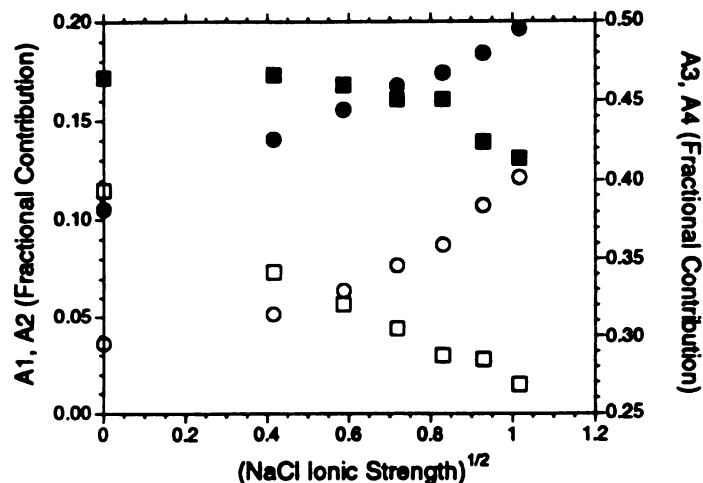


Figure 6.3. Response of the fractional pre-exponential factors A_1 (○), A_2 (●), A_3 (□) and A_4 (■) on NaCl concentrations for 3.6 % HEL.

state fluorescence intensity is due to increases in the relative contributions from A_1 and A_2 .

Because the fractional contributions from both long lifetime components increased concomitantly, it is likely that these components arise from the same or related fluorescent species. From previous investigations using ANS, it has been found that protein bound ANS displays lifetimes of approximately 15 ns [123]. It is likely that the longer lifetime contributions are due to lysozyme bound ANS and that the shorter lifetime components originate from unbound ANS. Because the objective of this study is to map the response of the fluorescence parameters to the crystallization conditions on HEL, we examine the effects of salt on the bound form of ANS.

Figure 6.4 shows the effects of the ionic strength of NaCl and HEL concentrations on the combined fractional contributions of the long lifetime forms ($A_1 + A_2$, denoted FA_{12}) along with the crystallization results. As the NaCl and HEL concentrations become favorable for nucleation and

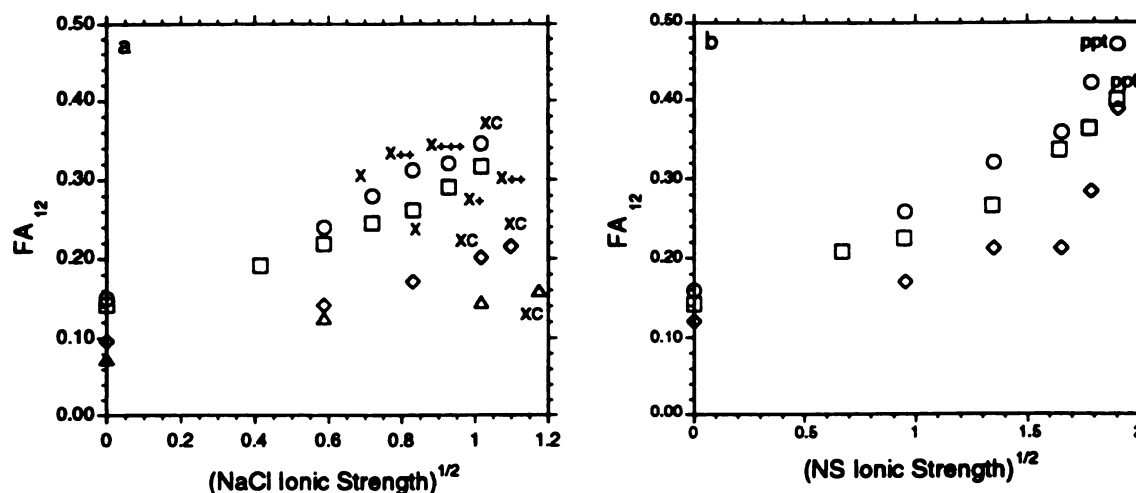


Figure 6.4. Response of the combined fractional contributions from A₁ and A₂ (FA₁₂) of HEL associated ANS to the ionic strength of NaCl (a) and NS (b). For a), symbols represent 1.0 (Δ), 2.0 (◇), 3.6 (□) and 5.0 % (○) HEL. For b), symbols represent 2.1 (◇), 3.6 (□) and 4.3 % (○) HEL. X indicates the formation of crystals, XC indicates crystalline spherulites and ppt indicates precipitation. The + symbols represent relative amounts formed.

subsequent crystallization, the amount of HEL bound ANS is observed to increase. This correlation is stronger at 3.6 and 5% HEL than at the lower protein concentrations. An increase in the slopes appears to occur near the concentration of NaCl which causes saturation. NaCl concentrations greater than approximately 1 M result in the formation of amorphous precipitate which eventually transform into crystalline spherulites. Under such conditions of immediate precipitation, the presence of large visible particles interferes with the fluorescence measurements. At the lower concentrations of HEL, only crystalline spherulites are formed at high NaCl concentrations.

Figure 6.4b shows the effects of the ionic strength of ammonium sulfate (NS) on the bound fraction of ANS in HEL solutions. NS is known to be a salt that is not amenable for the crystallization of HEL [8]. Although the amount of bound ANS increases as the HEL and NS concentrations increase,

no crystallization is observed under these conditions. At high concentrations of NS and HEL, a precipitate forms which gradually transforms into a gel. Again, there appears to be a break in the slopes as the square root of the ionic strength increases. However, in the case of NS, this break appears well below the solubility limit. The change in slope also appears to occur at lower NS concentrations as the HEL concentration increases.

Response of the Rotational Correlation Times to Solution Conditions

The parallel and perpendicular components of the polarized emission decay of ANS in 3.6% HEL solution are shown in Figure 6.2. From the fits to a sum of exponential components, the rotational correlation times from each component are denoted $\rho_1, \rho_2, \rho_3, \dots$, in order of decreasing magnitude with the corresponding initial anisotropies denoted B_1, B_2, B_3, \dots . The rotational correlation times which resulted from the one component fit appeared to describe the overall rotational motions of HEL and showed a strong dependence on the particular solution conditions. Although one component fits were adequate to describe the decays at higher HEL and NaCl concentrations, the initial portion of the decays were not well fit at lower protein concentrations.

The use of two components in the anisotropy decay was judged to provide the most physically meaningful and consistently good fits for the data. The two component fits consisted of a short decay component, ρ_2 , on the order of 1.5 ns and a longer component, ρ_1 , that exhibited a strong dependence on the solution conditions. This component most likely originates from the bound fraction of ANS. For the two component fits, the ρ_1 component was associated with the two longer fluorescence lifetime components in the calculations. This procedure has been shown to provide the

most physically meaningful fits for fluorescence from multiple emitting species [126]. The ρ_2 component was associated with all four total fluorescence decay components. The ρ_1 component appeared homogenous and could not be resolved into additional components representing monomers, dimers or higher aggregates.

Three component fits, with the two longest components associated with the fluorescence from the bound form, resulted in an additional short component on the order of 0.1 ns. The use of three components did not significantly improve the quality of the fits as judged visually and by the reduced sum of squares. One, two and three component fits all yielded similar values for ρ_1 . These results suggest that the ρ_1 component represents the overall rotational motion of ANS bound HEL.

In the absence of salt, the measured long rotational correlation times agrees well with that expected from the overall rotation of HEL in solution. The measured ρ_1 value of 14.8 ns in a 1 % HEL solution corresponds to a rotating sphere with a diameter of 4.8 nm [127]. Using the covalently bound fluorescent probe PBA, a value of 16.2 ns was determined for PBA-HEL. These values agree well with the dimensions of HEL, which can be approximated as a prolate ellipsoid measuring 5.5 nm and 3.3 nm along the major and minor axis, respectively [116]. The effect of NaCl on the measured values for ρ_1 with ANS also agree well with those measured with PBA-HEL, providing further support that ANS is rigidly bound to HEL.

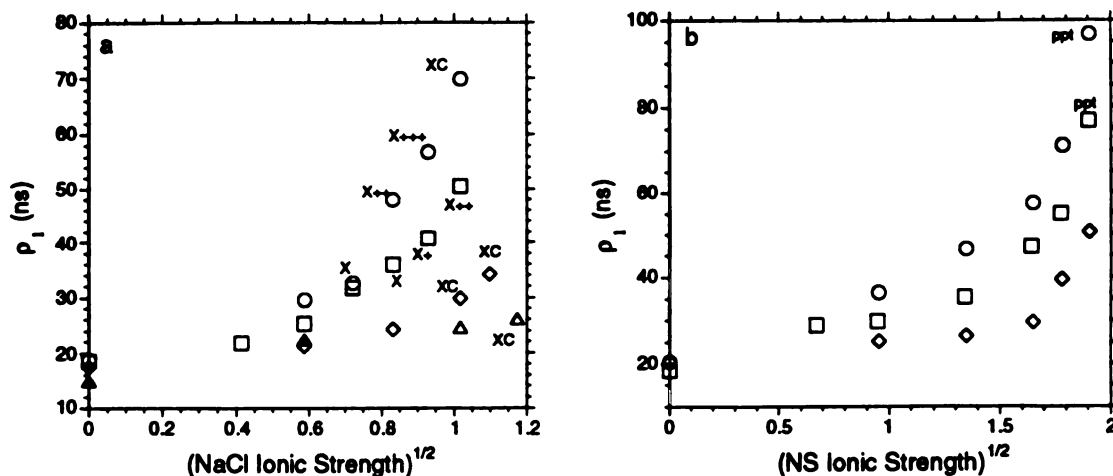


Figure 6.5. Response of the long rotational correlation times (ρ_1) of HEL associated ANS to the ionic strength of NaCl (a) and NS (b). For a), symbols represent 1.0 (Δ), 2.0 (\Diamond), 3.6 (\square) and 5.0 % (\circ) HEL. For b), symbols represent 2.1 (\Diamond), 3.6 (\square) and 4.3 % (\circ) HEL. See Figure 6.4 for explanations of the other symbols.

The effects of NaCl on the ρ_1 values of HEL bound ANS are shown in Figure 6.5a. An increase in ρ_1 is observed as the NaCl and HEL concentrations increase. As plotted against the square root of the ionic strength, three regimes in the ρ_1 values are seen. At low ionic strengths, the rate of increase in ρ_1 is relatively slow and remains below 30 ns. At intermediate ionic strengths, the ρ_1 values show an increased slope similar to the increase observed with the FA₁₂ values. This increase is particularly evident at HEL concentrations greater than 2%. In this region of intermediate ionic strengths, optimal NaCl concentrations for nucleation are seen if the ρ_1 values are in the range of approximately 30 to 60 ns. As the ionic strength of NaCl is further increased, immediate amorphous precipitation results. Measurements that were performed on these highly scattering solutions gave inconsistent results. Presumably, the rotational

correlation times would continue to increase since macroscopic particles are observed visually.

Values for the short rotational correlation times remain at approximately 1.5 ns and showed no significant changes for all NaCl and HEL concentrations. However, the initial anisotropy of the short rotational correlation time (B_2) did show a decrease as the ionic strength increased. The initial anisotropy of the long rotational correlation times (B_1) remains nearly constant at an approximate value of 0.21 for all NaCl and HEL concentrations.

The effects of NS on the ρ_1 values of HEL bound ANS is shown in Figure 6.5b. Similar effects of the ionic strength are seen with NS as with NaCl except that NS did not result in crystallization. The ρ_1 values in NS solutions are seen to be strongly dependent on both the ionic strength and HEL concentrations. Changes in the slopes of ρ_1 also showed increases as the ionic strength increased. As with NaCl, the short rotational correlation time did not vary greatly from 1.5 ns. The values obtained for B_1 did not appear to change significantly from values between 0.20 to 0.24. Again, the B_2 values for ANS in NS solutions decreased as the NS concentration increased.

Monitoring the Progress of Batch Crystallization

The fluorescence parameters of ANS in HEL solutions were measured during the progress of a batch crystallization experiment to demonstrate that the crystallization conditions due to changes in HEL concentration could be dynamically monitored. Changes in the NaCl concentration are expected to be small [128]. Initial concentrations are 4.2 % HEL with 5 % NaCl. Crystals first became clearly visible at approximately 20 hrs at which point the

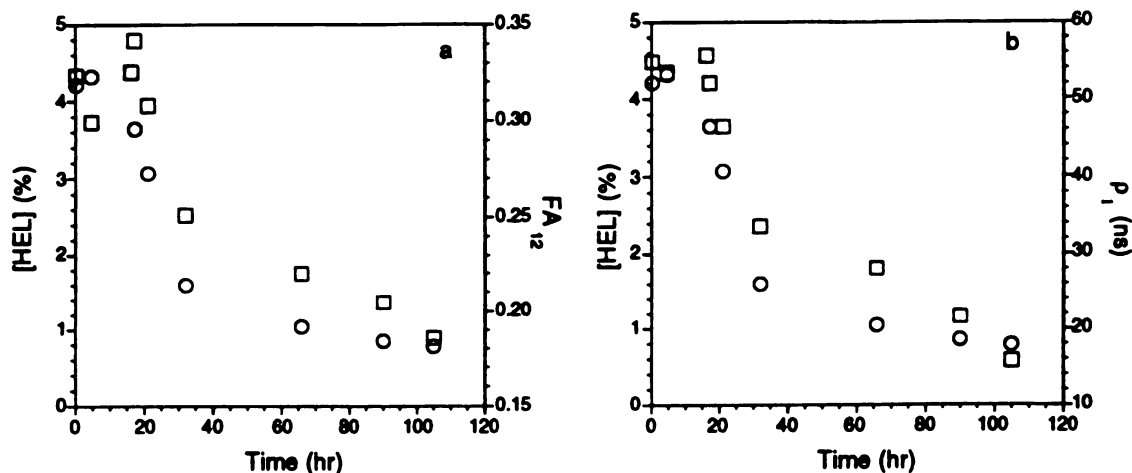


Figure 6.6. Monitoring the batch crystallization of HEL. The (○) symbols represents HEL concentrations from A₂₈₁ measurements of diluted aliquots taken at the indicated times. The (□) symbols are the FA₁₂ values in a) and the ρ_1 values in b) from in situ fluorescence measurements.

concentration of HEL began to decrease. The crystals appeared to be of the familiar tetragonal morphology.

In Figure 6.6a, the FA₁₂ values of ANS is shown together with the spectrophotometrically determined protein concentration. After nucleation, there appears to be an initial fast decrease in the HEL concentration at about 20 to 30 hrs, followed by a slower decrease up to 104 hrs until the solution reached equilibrium at 0.8% HEL. There appears to be a good correlation between the relative amounts of bound ANS with the HEL concentration as the solution becomes depleted. However, the fraction of ANS bound appears to decrease at a faster rate than the HEL concentration in the slow portion of the crystallization. In this experiment, the decrease in the values of FA₁₂ are due primarily to the relative increase in the values of A₄ whereas A₃ remains nearly constant and A₁ and A₂ decrease.

A similar decreasing trend of the ρ_1 values is seen in Figure 6.6b as the crystallization progressed. There is again good agreement with the time profile of the measured HEL concentration. However, from 30 to 104 hrs, the rotational correlation time continues to decrease at a faster rate than the HEL concentration. The ρ_2 values remained constant to about 60 hrs and then began to sharply decrease as the initial anisotropy of this component increases. This behavior is most likely a result of the low concentrations of protein remaining in solution.

At the end of the crystallization, the laser was directed onto a single crystal. Irradiation of the crystal revealed that ANS had been incorporated into the crystal as seen by the intense blue emission. The total fluorescence fits resulted in a FA_{12} value of 0.33 with lifetimes of 12.0, 5.6, 1.4 and 0.11 ns. The longest lifetime component is considerably shorter than that in solution. Fitting of the anisotropic decay resulted in a long rotational correlation time that tended to infinitely large values (>1000 ns). The fits yielded a limiting anisotropy of 0.38 for the long rotational correlation time and 0.14 for the initial anisotropy of the 0.96 ns short rotational correlation time component. As expected, the rotational motion of bound ANS in the crystals is highly constrained.

Monitoring of Vapor Diffusion Crystallization

To determine the response of the fluorescence parameters under conditions where both the protein concentration and NaCl concentrations dynamically change, a vapor diffusion experiment was performed. In this case, the volume of the sitting drop used was too small to collect aliquots of the protein solution. Initially, the 15 μ l sitting drop contained 4 % HEL and 3 % NaCl. This solution was equilibrated against a 6% NaCl reservoir.

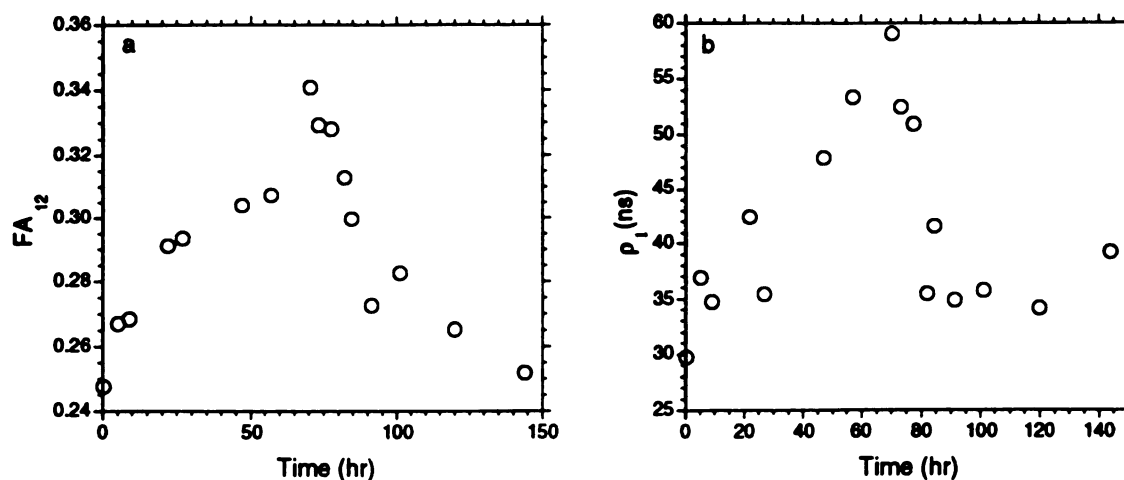


Figure 6.7. Monitoring the progress of a HEL vapor diffusion crystallization trial using ANS fluorescence with a) FA_{12} and b) ρ_1 .

Figure 6.7 shows the time profile of the FA_{12} and the ρ_1 values. As the volume of the sitting drop solution decreased, the solution became supersaturated resulting in the formation of two tetragonal crystals at approximately 70 hrs. A concomitant increase in the bound fraction is observed. Upon crystallization, both the bound fraction and long rotational correlation time follow the decrease in the supersaturation as the crystals grow. The values of the fraction of ANS and the rotational correlation time decrease to near the initial values.

Discussion

Generally, ANS displays substantially increased fluorescence intensities in more nonpolar and viscous solvent microenvironments. It is known that the binding of ANS to proteins causes a substantial increase in the steady-state fluorescence intensity [123]. This behavior has been commonly interpreted to be the result of binding to hydrophobic regions in the protein. However, in the case of chymotrypsin, the crystallographic

structure showed that ANS is bound in a polar region and participates in an alternating charge array [121, 122]. The observed fluorescence enhancement was attributed to the ordering of the polar solvent molecules near the binding site. Furthermore, it has been demonstrated with apomyoglobin that the fluorescence behavior of bound ANS is mainly determined by the restrictions of the probe microenvironment [125].

Free ANS in water exhibits a lifetime of approximately 0.25 ns [129] and corresponds to the shortest lifetime, τ_4 , measured in this study. The two longest lifetime components, τ_1 and τ_2 , are likely to arise from protein bound ANS. The origin of two separate lifetime components may be due to either static or dynamic heterogeneity. There may be different classes of distinct binding sites on HEL corresponding to static heterogeneity, each with different solvent microenvironments affecting the fluorescence lifetime. Alternatively, one class of binding sites may exist which exhibits dynamic heterogeneity due to conformational fluctuations of the protein or the excited state kinetics of ANS.

Kowaser and coworkers have described the photophysical behavior of ANS with the sequential formation of two excited states [130]. Absorption of light first leads to a fluorescent non-planar excited state that displays little sensitivity to solvent polarity. Subsequent conversion to the solvent sensitive charge transfer excited state is then controlled by the local solvent mobility. This two state process suggests that the presence of the two long component fluorescence lifetimes is due to a single class of bound ANS displaying photochemical heterogeneity. However, further physical characterization is required to completely resolve this issue. Regardless of whether the heterogeneity is static or dynamic, the longer lifetime

components do appear to arise from rigidly bound ANS as evidenced by the corresponding rotational correlation times.

The physical interpretation of the τ_3 component is less clear. This lifetime component is intermediate between that of free ANS in the bulk solution and those that are rigidly bound. A possible explanation is that the fraction of ANS corresponding to this fluorescence component may be weakly associated to HEL. This weak association may correspond to the localization of ANS in the bound solvent that is near the vicinity of the protein. The value of the short ρ_2 component at higher lysozyme concentrations is too long to be attributed to free ANS, which is expected to be on the order of 150 ps. At low HEL concentrations, the value of ρ_2 does approach the expected value and may reflect a increase in the mobility of the solvent surrounding HEL. However, this explanation for the origin of the τ_3 component is highly tentative and warrants further investigation.

Previous studies have investigated the binding of other organic anions such as orange II to lysozyme and their influence on lysozyme precipitation and crystallization [41]. Precipitation and equilibrium binding studies performed by Colvin found that the binding of methyl orange to HEL is cooperative and was attributed to interacting hydration effects [131]. According to this model, an inhomogenous electrostatic field about the positive HEL molecule orients the water dipoles in the vicinity of the surface and hinders initial absorption of the anion. At increased concentrations of the anion, an increased probability of Coulomb interactions enables the initial absorption of the anion. This event leads to a decrease in the inhomogenous field further allowing the adsorption of other anions.

From the effects of NaCl and NS on the pre-exponential factors of the HEL bound ANS component, it is apparent that increasing salt

concentrations and HEL concentrations lead to increased amounts of bound ANS. This cooperative behavior suggests that a similar mechanism to that of methyl orange adsorption may occur as the sodium chloride and ammonium sulfate concentrations increase. Binding of the chloride and sulfate ions may disrupt the inhomogeneous field surrounding the HEL molecules thereby increasing the binding of ANS.

The enhanced binding of ANS at higher salt concentrations is also observed to correspond to increases in the ρ_1 times. Decreases in both the rotational and translational mobility of proteins under crystallization conditions is well known [57, 88-90]. Increases in the rotational correlation time appear to be due to increased intermolecular interactions between the HEL molecules (Chapter 5). Binding of anions could provide a mechanism for the observed increase in the long rotational correlation times. Anions bound to specific sites would decrease the net charge on each HEL molecule thereby decreasing the repulsive electrostatic interactions and allowing closer contact. This increased degree of contact between the HEL molecules would result in the decreased mobility of the protein. Although it is clear that the HEL molecules are interacting to a greater degree under crystallization conditions, the precise nature of these interactions and any aggregates that result are at present not well defined.

The time required for nucleation and the number of crystals eventually formed are related to the degree of supersaturation caused by NaCl [128]. There appears to be a strong relationship between the degree of supersaturation, the amount of bound ANS and the rotational correlation time of the HEL associated probe. The nucleation process appears to be influenced by the rotational mobility of HEL in supersaturated solutions. It is likely that the bound anions participate directly in this nucleation process.

The binding of the chloride ions could serve to decrease the mobility of the HEL molecules in solution and enable the specific protein-protein interactions that lead to nucleation.

The results indicate that the applications of non-covalently bound fluorescence probe techniques to the screening and optimization of protein crystallization conditions as well as to the further study of protein crystallization phenomena are diverse. Precipitants that lead to increases in the rotational correlation time and that produce nuclei, such as sodium chloride with HEL, would appear to warrant further optimization of conditions. Plots such as Figures 6.4a and 6.5a, would prove useful in rapidly delineating the optimal protein and precipitant concentrations required to achieve nucleation and subsequent crystal growth. Salts, such as ammonium sulfate, that show increases in the rotational correlation time without subsequent nucleation would not merit further investigation. Further comparisons between different salts will be treated in a subsequent publication (Chapter 7).

As seen in the batch and vapor diffusion experiments, dynamic monitoring of supersaturation has been demonstrated. This technique could be extended to the direct control of crystallization conditions for the optimization of protein crystal growth. Not only are fluorescence techniques able to monitor the bulk kinetics of protein crystallization, but are also able to monitor the spatial properties of the crystal growth solution. With the use of other fluorophores and extensions of the experimental apparatus, it may be possible to directly and simultaneously monitor parameters such as protein and precipitant concentration, temperature and pH. Fluorescence probe techniques appear to offer an extensive potential for improvements in protein crystal growth methodology.

Chapter 7

The Effects of Precipitants on the Time-Resolved Fluorescence and Anisotropy of ANS for Characterizing Lysozyme Crystallization*

Abstract

The spectroscopic behavior of a non-covalently bound fluorescent probe 1-anilino-8-naphthalene sulfonic acid (ANS) was measured to determine the effects of various precipitants and protein concentration on the crystallization of hen egg-white lysozyme (HEL). Increasing concentrations of precipitants and protein caused increases in the binding of ANS and the rotational correlation times. The various precipitants were found to exhibit differing effects on the fluorescence behavior. The results suggest that HEL nucleation involves a two stage process where bound anions cause increased protein interactions followed by the formation of specific protein-protein bonds. The implications of these findings for improving the efficiency screening of crystallization conditions are discussed.

Introduction

The fundamental problems involved in finding protein crystallization conditions are the limitations of the amount of protein material available and the effort involved to screen the possible conditions. Consequently, a more efficient search for protein crystallization conditions depends on reducing the number of experimental trials and the time involved in each trial. Various

* Submitted to the Journal of Crystal Growth.

strategies including factorial [34, 50] and sparse matrix methods [132] have been developed to improve the efficiency of this screening process. All of these strategies rely on the judicious choice of screening conditions.

A more complete understanding of the factors involved in the protein crystallization process would be helpful in guiding the choice of precipitants during crystallization trials. The current approach of such investigations has largely been phenomenological. Typically, a correlation between a measurable property of the solution such as the translational diffusion [55], the polydispersity [54], or the growth kinetics of protein aggregates [8] is sought which will provide a clear indication of whether or not the solution will engender crystallization. Although these physical phenomena are likely to be related to the protein crystallization process, the underlying chemical mechanisms are not well understood.

There have been previous investigations on the nature of the chemical interactions involved in protein crystallization. Because of its ease of crystallization, the protein most encountered in protein crystallization studies is hen egg-white lysozyme (HEL). Reis-Kautt and Ducruix have studied the effects of salts on the crystallization of HEL [37, 97]. Their findings indicate that ion pairing occurs between the protein and the anions in solution. Pusey and coworkers have further investigated the binding of Cl^- ions [133]. The desolubilization of the protein was found to coincide with the saturation of possible binding sites on HEL. As nucleation and crystallization occurred, fewer Cl^- ions were bound. These studies demonstrated that the interactions occurring between the protein and salt precipitants are crucial aspects of crystallization.

We had previously demonstrated that the probe 1-anilino-8-naphthalene sulfonate could be used to dynamically monitor the protein-

protein and protein-solvent interactions of HEL under crystallization conditions (Chapter 6). The increase in the fluorescence intensity of ANS was found to be due to the extent of binding to HEL. Closely related to this increased binding of ANS and the crystallization behavior of HEL are the decreased rotational mobility of the protein. In the current work, we compare the effects of various crystallizing and noncrystallizing precipitants on the time-resolved fluorescence decay and rotational correlation times. The effects of the salts sodium thiocyanate (NaSCN), sodium chloride (NaCl), ammonium acetate (NAc), sodium phosphate (NaP) and ammonium sulfate (NS) on the fluorescence behavior of ANS in HEL solutions are investigated. We also determine the effects of HEL concentration in the presence of these various salts. The findings provide further information on the mechanisms of protein crystallization and the relation to measurements of physical transport properties. The implications of these results to the application of fluorescence techniques for the screening of protein crystallization conditions is also investigated.

Experimental

Solution Preparation

All solutions were prepared in 50 mM sodium acetate buffer at pH 4.6 unless otherwise noted. Three times crystallized HEL was obtained from Sigma. Stock HEL solutions of 10% were prepared by dissolving the solids in buffer and passing through a 0.45 μm pore filter. The HEL solution was then washed three times with buffer using an ultrafiltration cell (10,000 MW cutoff). The protein concentrations were measured by using the spectrophotometric absorbance at 280 nm with $A^{1\%} = 26.4$ [112]. ANS was obtained from Eastman Kodak and was used without further purification. A

10^{-3} M solution of ANS was prepared as the stock fluorescence probe solution. This was diluted ten times for a final concentration of 10^{-4} M ANS in the samples. Stock solutions of NaSCN, NaCl, NAc, NaP and NS were prepared and added to the samples. The samples were prepared by adding, in order, the appropriate amounts of HEL, buffer, ANS and precipitant with mixing after each addition.

Fluorescence Measurements

The steady-state and time-resolved fluorescence measurements and the data analysis were previously described in detail (Chapters 3, 5 and 6, [79]). For the time-resolved measurements, emission decay data were collected using the time-correlated single-photon counting method [113]. Samples were excited with a wavelength of 350 nm and the time-resolved fluorescence decays were collected at 480 nm. A total of 4096 channels was used to record the decay with each channel corresponding to a time interval of 0.040 ns.

The measurements were started within approximately ten minutes after mixing of the stock solutions. All measurements were performed at 23° C. For the determination of salt effects, 100 μ l samples were prepared in 96 well culture plates. A micro-capacity black quartz cuvette was used to hold approximately 70 μ l of each sample. The instrument response function from the excitation pulse was collected before each sample by measuring light from a scattering solution and was used for subsequent data analysis.

The time-dependent fluorescence, $I_{\text{tot}}(t)$, from an initial excited state population, was fit to a sum of exponential terms with characteristic lifetimes, τ_i , and pre-exponential factors, A_i , where i represents a single fluorescence component [73]. A least squares fitting procedure was used to

deconvolute the observed fluorescence decays from the instrument response function [80-83].

The time-dependent induced fluorescence anisotropy is defined by,

$$R(t) = \frac{I_v - I_h}{I_v + 2I_h} = \frac{I_{dif}}{I_{tot}} = \sum_{j=1}^q B_j \exp(-t/\rho_j) \quad (7.1)$$

where I_{vv} and I_{vh} are the vertically and horizontally oriented polarized emission intensities, respectively, for a vertically polarized excitation source. I_{tot} is the time-dependent total fluorescence intensity as before and I_{dif} is the difference fluorescence intensity. The anisotropic decay is also described by a sum of exponential decays where j represents one decay component and q is the total number of components. B_j and ρ_j are the initial anisotropies and rotational correlation times of each component, respectively. The B_j and ρ_j values are found by numerically fitting the experimentally measured vertically and horizontally polarized emission using previously determined parameters for I_{tot} [83, 84].

Results

Fluorescence Properties of ANS in HEL solutions

The total fluorescence decays of all the samples are multiexponential, requiring four exponential components to adequately fit the data. The fluorescence lifetimes are denoted τ_1 to τ_4 in order of decreasing magnitude. In a 3.6% HEL solution, the lifetimes were found to be 16.6, 5.4, 1.0 and 0.2 ns. The corresponding fractional pre-exponential factors, denoted A_1 to A_4 , are 0.04, 0.11, 0.39 and 0.46. Previously, we had assigned the fluorescence lifetime components to fractions of the ANS that are located in different microenvironments in the solution (Chapter 6). τ_1 and τ_2 likely originate from ANS molecules which are bound to HEL, while τ_4 is the lifetime of ANS in the

bulk solution. The origin of τ_3 was less clear but may be due to ANS which is associated with solvent surrounding HEL. Thus, the sum of the pre-exponential factors A_1 and A_2 represent the relative amount of ANS that is bound to the HEL (denoted FA_{12}) whereas A_3 and A_4 represent the remaining fluorescence from species that are either free in solution or weakly associated with HEL.

The I_{VV} and I_{VH} profiles that compose the anisotropic decays were fit using a two rotational correlation time component model as previously described (Chapter 6). The two rotational correlation times are denoted ρ_1 and ρ_2 with corresponding pre-exponential factors B_1 and B_2 . In this model, ρ_1 represents the overall rotational correlation of HEL and is thus associated with the bound lifetime components of ANS (τ_1 and τ_2). This component could not be further decomposed into subcomponents representing monomers and higher aggregates. ρ_1 was found to yield similar values under different methods of analysis. ρ_2 was associated with all four components of the total lifetime decay. Because we are primarily interested in the interactions of HEL, the value of ρ_1 under various crystallization conditions is of the most interest.

Comparison of Salt Effects at 3.6 % HEL

The effects of increasing concentrations of NaSCN, NaCl, NAc, NaP and NS on the crystallization and fluorescence behavior were compared at 3.6 % HEL. NaSCN, NaCl and NAc (at pH 7.7 and 6.4) were found to engender the crystallization of HEL. The 3 M stock NAc solutions exhibited a pH of 7.7. Further adjustments of the pH to 6.4 and 4.6 were made by the addition of acetic acid. Samples using the NAc solutions that were adjusted to pH 4.6 did not produce crystals. NaP was found to be a poor crystallization

agent, at first producing a gel with ensuing disordered crystal growth from the gel. Only gel was formed from the NS solutions. Although the presence of 10^{-4} M ANS did not appear to greatly affect the solubility or crystal morphology of HEL, further study of these effects may be warranted.

The fluorescence lifetimes of ANS as a function of the square root of the ionic strength of the salts did not show appreciable trends. The long lifetime component, τ_1 , was found to range from 16 to 18 ns, while τ_2 varies between 5.5 and 6.5 ns. τ_3 was found to vary between 1.0 and 1.4 ns and τ_4 between 0.1 and 0.2 ns. Although these fluctuations may appear to show slight trends as the concentrations of the salts are increased, they are most likely not significant. Hence, the various microenvironments of ANS do not appear to significantly change in character as the concentrations of salt increases.

In contrast, as seen in Figure 7.1a, the combined fractional pre-exponential contributions ($A_1 + A_2$, denoted FA_{12}) from the components of bound ANS show a strong dependence on the ionic strength of the salts. The different salts appear to influence these values to differing degrees. The behavior of the pH 6.4 NAc solutions appear to be anomalous and are examined in further detail below. For the other salts, the FA_{12} values show increases with increasing ionic strength. In the case of NaSCN and NaCl, further increases in FA_{12} are seen as the supersaturation of the solution increases. In the NaP and NS solutions, this increase in the slope of FA_{12} is observed before saturation is reached. To compensate for the combined increases in A_1 and A_2 , A_3 and A_4 decrease as the concentration of salt increases.

The effects of the pH of NAc solutions on the FA_{12} values of ANS are shown in Figure 7.2a. No significant changes were observed in the

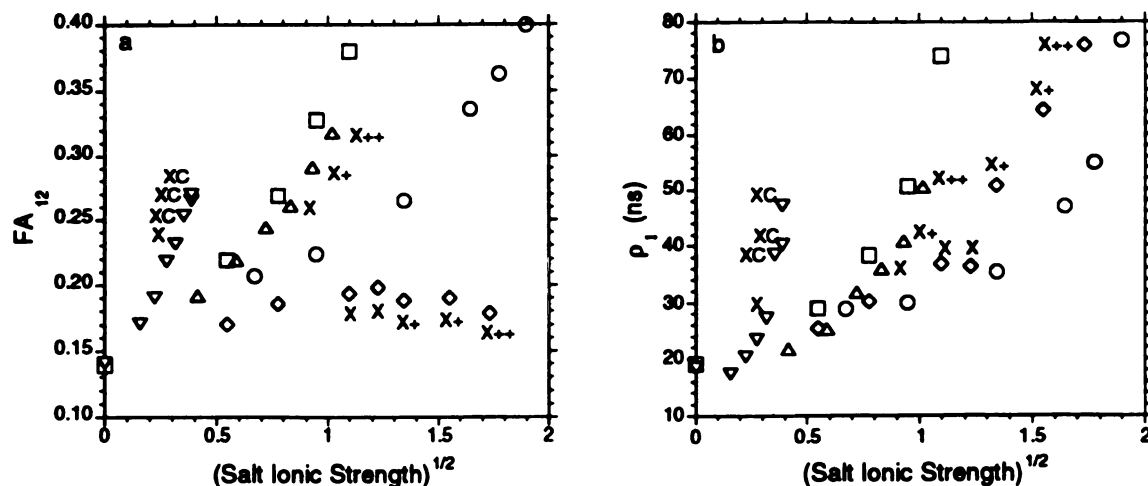


Figure 7.1. Effects of the ionic strength of NS (○), NaP (□), pH 4.6 NAc (◇), NaCl (△) and NaSCN (▽) salts on the a) FA_{12} and b) ρ_1 fluorescence parameters and crystallization behavior of 3.6% HEL solutions. X indicates the formation of crystals and XC indicates crystalline clusters. The + symbols represent relative amounts formed.

fluorescence lifetimes. The greatest changes in FA_{12} are seen at pH 7.7, where no acetic acid was added. Concurrent decreases are seen in the values of A_3 and A_4 . At pH 4.6, the FA_{12} contributions decrease as the concentration of NAc increases. The changes of the fluorescence contributions at pH 6.4 appears to be intermediate between those at pH 4.6 and 7.7.

The effects of the ionic strengths of the precipitants on the long rotational correlation time of ANS (ρ_1) are shown in Figure 7.1b. The ρ_1 times show a strong dependence on the particular salt present and the concentrations of the salts. For NaSCN, NaCl and pH 6.4 NAc, the ρ_1 times rapidly increase as supersaturation occurs. Greater values for ρ_1 also correspond to increased amounts of crystalline material. For these salts with 3.6 % HEL, it appears that a threshold ρ_1 value of approximately 30 ns indicates that nucleation will occur. For NaP and NS, which both form gels at high salt concentrations, large increases in ρ_1 are observed well before

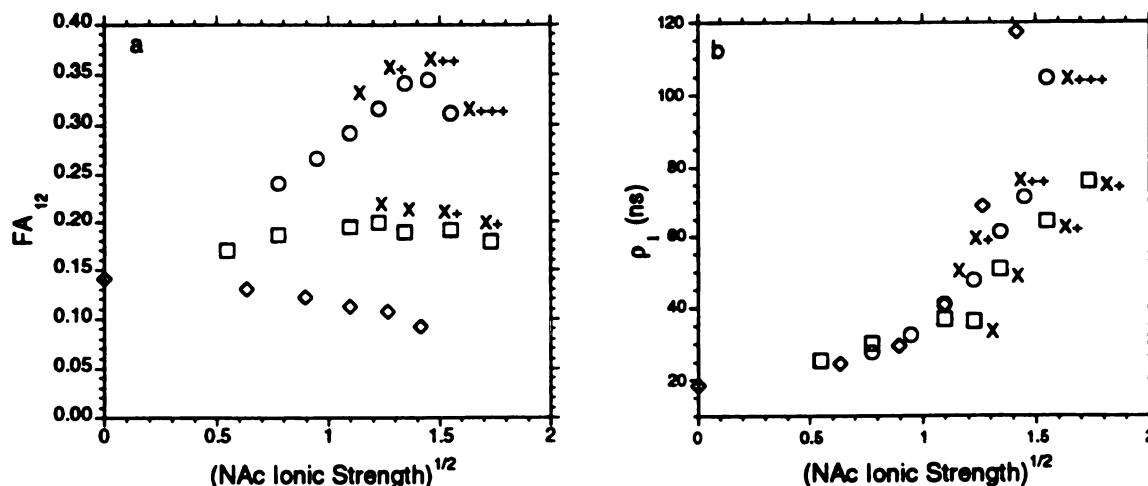


Figure 7.2. Effects of the ionic strengths on the a) FA_{12} and b) ρ_1 fluorescence parameters and crystallization behavior of 3.6% HEL solutions at pH 7.7 (\circ), 6.4 (\square) and 4.6 (\diamond). See Figure 7.1 for an explanation of the other symbols.

saturation is reached. The values of ρ_1 at saturation (not shown) are much greater with NaP and NS than with the crystallizing salts.

It is interesting to note that the values of ρ_1 appear to follow similar trends, with three distinct regions. These values initially fall on a shallow slope as the square root of the ionic strength increases. At higher ionic strengths, an intermediate region displaying a more rapid increase in ρ_1 is observed. A third region, at high salt concentrations which results in immediate precipitation, is also observed. The values of ρ_1 in this region could not be accurately determined because of excessive light scattering and settling of the particles, but are presumably greater than in the intermediate region.

The values for the ρ_2 at 3.6% HEL only show a slight decrease as the ionic strengths of the different salts decrease (not shown). ρ_2 remains in the range of 1.7 to 1.2 ns throughout the range of conditions measured. However, the initial anisotropies corresponding to ρ_1 and ρ_2 showed greater salt effects.

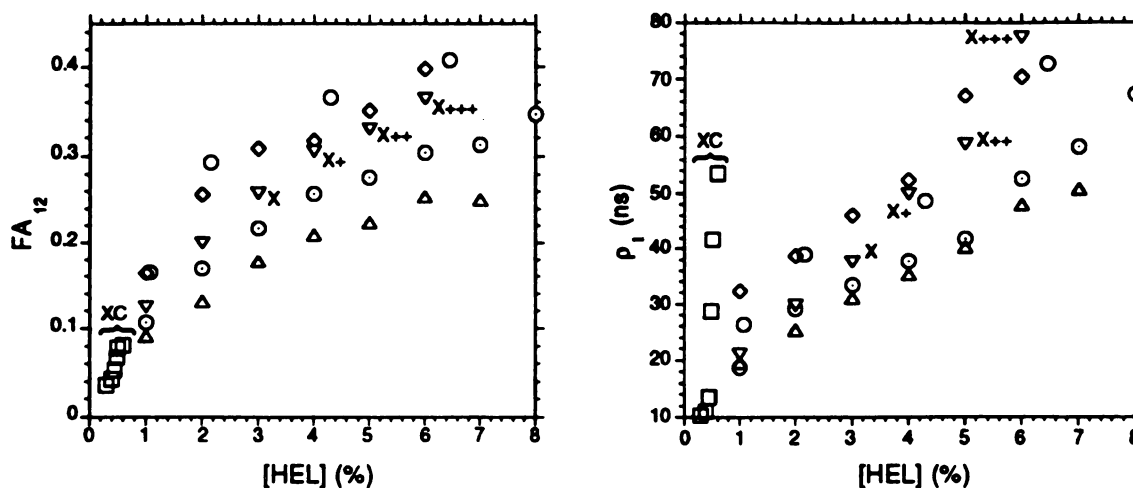


Figure 7.3. Effects of HEL concentrations on the a) FA₁₂ and the b) ρ₁ fluorescence parameters and crystallization behavior of 0.86 ionic strength NS (○), NaP (□), pH6.4 NAc (◇), NaCl (△), NaSCN (▽) and 0.86M concentration NS (○) solutions. See Figure 7.1 for an explanation of the other symbols.

Decreases observed in B2 as the ionic strength increased reflect the behavior of A₃ and A₄. The values of B2 appeared to be dependent on the fraction of ANS that is bound to HEL.

The effect of pH on ρ₁ in NAc solutions is seen in Figure 7.2b. The ρ₁ values at pH 4.6, 6.4 and 7.7 increase as the concentration of NAc increases. NAc appears to show the least effect at pH 6.4 and shows the greatest rate of increase at pH 4.6. Only a slight decrease in ρ₂ is observed at pH 7.7 and 6.4. However, significant decreases in ρ₂, that are concomitant with the increase in ρ₁, were observed at pH 4.6. The B2 values also appears to be reflect the amount of ANS bound to HEL.

Effects of HEL Concentration

To determine the effects of HEL concentration on the crystallization behavior, the fluorescence of ANS solutions were measured at an ionic strength of 0.86 M for NS (molar concentration 0.29 M), NaP, NAc at pH 6.4,

NaCl and NaSCN. The effects of HEL concentration in the presence of 0.86 M NS was also determined. At these salt concentrations, only the solutions containing NaSCN and NaCl produced crystals. In the NaSCN solutions, concentrations of HEL above 0.6 % were not used because of immediate precipitation with subsequent crystal growth from the precipitate. The NaP solutions at 6% HEL also produced a precipitate which subsequently gelled.

As in the case with the precipitants, there also appears to be little dependence of the fluorescence lifetimes on the HEL concentration. Figure 7.3a shows that the values of FA_{12} are observed to increase as a function of the HEL concentration with the extent of increase depending on the particular salt present. These values appear to approach a limiting value, which depends on the particular precipitant, as the concentration of HEL increases above about 3%. In contrast to the effects of increasing salt concentration, A_3 appears to increase as the concentration of HEL approaches 3% and remains near a value of about 0.3 from 3.0 to 8.0 % HEL.

Figure 7.3b shows the effects of HEL concentration on the ρ_1 times of ANS in the presence of the different salts. The greatest effect is seen in the solutions containing NaSCN, with large increases in ρ_1 observed under small increases in the HEL concentration. All the NaSCN solutions eventually yielded crystals but precipitation with subsequent crystallization occurred within minutes in the solutions displaying ρ_1 greater than 25 ns. The rate of increase in the ρ_1 values for the NaCl solutions also appeared to increase at a greater rate than the non-crystallizing precipitants. The ρ_1 values for all the non-crystallizing mediums appeared to increase at a similar rate as a function of the HEL concentration. The ρ_2 values did not reveal any significant trends and remained between 1 and 1.7 ns for all the solutions except with NaSCN. The values of ρ_2 for NaSCN remained at 0.1 to 0.2 ns for

all conditions measured. This low value of ρ_2 for NaSCN appears to be due to the lower protein concentrations.

Discussion

All of the salts except for NAc at pH 4.6 appear to induce some degree of increased ANS binding to HEL. This behavior is likely to be due to a repartitioning of the ANS into the different microenvironments of the protein itself, the solvent surrounding the protein and the bulk solvent (Chapter 6). Although it is commonly assumed that the mechanism of ANS binding to proteins is that of hydrophobic interactions, charge effects are likely to be important as well [121, 122]. The increased degree of ANS binding may be a result of cooperative effects of specific ion binding or alternatively, increased hydrophobic effects due to solvent ordering by the salts. Hydrophobic effects appear to be minimal since NaSCN, which is a chaotropic salt, causes the greatest degree of binding at the lowest concentrations. Because of the positive charges on HEL, anions are expected to interact strongly with HEL [38, 39]. However, structural studies of HEL bound ANS would prove to be helpful in further elucidating the mechanisms of ANS binding.

The rotational correlation times are related to the mobility of the ANS in these various environments. We had shown previously that the ρ_1 times are consistent with the overall rotational mobility of HEL (Chapter 6). Increases in ρ_1 may be attributed to restricted mobility due to increasing protein-protein interactions. The short rotational correlation time is less well defined. It is likely to be a composite of the librational motions of the bound ANS, weakly associated ANS and free ANS. Although it may be possible to further separate the components of the short rotational correlation time, for the purposes of monitoring protein crystallization conditions, there does not appear to be significant advantages in doing so. It also does not appear

feasible to further decompose the long rotational correlation times. Nevertheless, the long rotational correlation time does appear to represent tightly bound ANS and reflects the effects of crystallization agents on the interactions of HEL.

The interactions of anions with HEL are known to play an important role in the crystallization process. According to the results of Reis and Ducruix, the effectiveness of various anions in decreasing the solubility of HEL follows the reverse order $\text{SCN}^- > \text{Cl}^- > \text{AcO}^- \sim \text{H}_2\text{PO}_4^- > \text{SO}_4^{2-}$ [37, 97]. Cations showed similar but smaller effects. This phenomena was attributed to ion pairing between the anions and the positively charged groups on HEL. The results presented here are similar. At constant HEL concentrations, the concentration of salt at the solubility limit increases in the order NaSCN, NaCl, NaAc, NaP and NS. However, increased binding of ANS and increases in the ρ_1 times in the presence of NaP appear at lower salt concentrations than with NaCl or NaAc.

The different processes involved in causing the increased anion binding, increased rotational correlation times and the crystallization of HEL as the salt and protein concentrations increases appear to be related. For all salt conditions except for NAc at pH 4.6 and 6.4, increases in the ANS binding correspond to increases in the rotational correlation times. The binding of anions to HEL is expected to alter the surface properties of the protein by neutralizing the local charges. This decrease in charge would subsequently decrease the repulsive electrostatic forces between the proteins in solution. The decrease in the repulsive electrostatic forces would be expected to enable a greater degree of interaction between the HEL molecules and lead to decreased rotational mobility (Chapter 5 and 6). Because of the different effects between the salts, it appears that specific interactions

between the protein and the anions are more important than general electrostatic effects.

Furthermore, the effect of the protein concentrations appear to be mediated by the presence of precipitants. At low salt concentrations, few anions are likely to be bound on the surface of HEL. Under such conditions, weak interactions occur at all protein concentration. At intermediate salt concentrations, increased anion binding allows greater interactions at higher protein concentrations but are decreased at lower protein concentrations. At higher salt concentrations and in the presence of strong precipitants such as SCN^- , the surface potential of the protein is expected to be completely neutralized by anion binding. Under such conditions, the aggregation appears to be non-specific since the immediate formation of amorphous precipitate is observed.

The effects of NAc at the different pH's appear to be anomalous. This behavior may be explained by considering the solution as a mixture of the two different agents acetic acid and ammonium acetate. At pH 7.7, where only the acetate and ammonium ions are present, the binding of ANS and the rotational correlation times appear to follow the same trends as the other salts. Increasing the concentration of acetic acid to decrease the pH has the effect of decreasing the binding of ANS to HEL. Because the other salts all cause increased binding at pH 4.6, it appears that this decreased binding of ANS can be attributed to the presence of acetic acid in the lower pH solutions. Nonpolar interactions with the acetic acid in the bulk solution may result in the additional solvation of the ANS. However, the rotational correlation times of the bound fraction does show increases as the NAc concentration increases without the formation of crystals.

Previous investigations have suggested that HEL nucleation occurs through the addition of monomer units to growing protein aggregates [14]. However, there appears to be additional processes occurring in the nucleation of HEL. At 3.6% HEL, the rotational correlation times are seen to increase with all of the salts, including those that do not lead to crystallization. This increased degree of association between the proteins appears to enable additional protein-protein reactions leading to nucleation. This nucleation step appears to be mediated by a specific chemical reaction since sulfate and phosphate ions do not produce nuclei under these conditions but do lead to decreased rotational mobilities. It is interesting to compare the precipitation and gelation caused by NS to the phenomena at very high NaCl concentrations, where amorphous aggregates initially form and subsequently nucleate into large numbers of disordered crystals. In the case of NS, the amorphous aggregate appears to follow a separate pathway to the formation of a gel.

The precise nature of these additional nucleation reactions is not clear, but salts that do not lead to crystallization do not appear to participate effectively. Although NS is commonly used as an example of a salt which only induces amorphous aggregation with HEL, tetragonal crystals have been obtained by using ion-exchanged protein [134]. Using mass spectroscopy, preferential non-covalent binding was observed with H_2SO_4 and H_3PO_4 , but not for AcOH and HCl . These results suggest that non-specific bridging of HEL molecules by sulfate and phosphate ions occurs at lower pH. In aqueous solution, chloride ions have been shown to bind to HEL but are released upon subsequent crystallization [133]. There is also prior evidence that HEL nucleation is kinetically, and not transport, limited [135, 136].

These findings, together with our results showing the increasing rotational correlation times in the presence of non-crystallizing agents, suggest that the release of the bound anions is a crucial step in the nucleation process. Under optimal conditions, protein crystallization appears to be composed of two processes. The first process involves the binding of anions allowing increased association between the protein molecules. This decrease in the rotational mobility would permit the formation of specific protein-protein interactions leading to nucleation and the subsequent release of the bound anions. Additives such as NS, NaP and AcOH appear to inhibit this second nucleation step.

From these results, a strategy for screening protein crystallization conditions may be developed. It is apparent that the chemical effects of precipitants are crucial to the nucleation and crystallization of HEL. These chemical effects manifest themselves in the physical interactions indicated by the fluorescence and other physical techniques. By measuring the effects of different salts on the binding and rotational motions of fluorescence probes, the interactions of the proteins may be determined and used to more rationally and efficiently choose proper conditions. Increases in the rotational correlation time appear to be a necessary but not sufficient condition for optimal nucleation and crystal growth.

Once suitable precipitants have been found, the fluorescence methods may be used to map the response of ion binding and rotational correlation times to the precipitant and protein concentrations (Chapter 6). These techniques were also shown to be useful for dynamically monitoring protein crystallization conditions. Used in conjunction with current screening and visual monitoring techniques, fluorescence techniques appear to be a practical method for elucidating the chemical effects responsible for protein

crystallization. Other protein-precipitant systems are currently being investigated to determine the generality of these methods and to further understand the mechanisms of protein nucleation and crystal growth.

Chapter 8

Summary and Conclusions

Conclusions

The goal of this work was to develop techniques that will improve the efficiency of finding optimal protein crystallization conditions. Toward this end, time resolved fluorescence and anisotropy measurements were demonstrated to be a useful technique for monitoring the protein-protein and protein-solvent interactions leading to crystallization. Previously, research along this line had focused on finding a simple diagnostic based on translational diffusion or kinetic measurements to determine whether solution conditions would engender crystallization or amorphous precipitation. Our findings, together with other research, indicate that this strategy is insufficient to explain and predict crystallization behavior. Thus, the application of physical monitoring techniques is incomplete.

To exploit the potential of physical monitoring techniques, a greater understanding of the effects of the solution conditions on the mechanisms of nucleation and crystal growth is required. The chemical interactions of precipitants with proteins and the solvent are ultimately responsible for the events leading to crystallization. These precipitants alter the surface properties of the protein and the solvent resulting in protein-protein and protein-solvent interactions. It is this perturbation in the protein interactions which may be monitored with physical methods to guide the choice of suitable conditions.

The ability to monitor the physical interactions of proteins in conjunction with knowledge of the chemical mechanisms of crystallization will result in the most efficient strategy for finding optimal conditions.

Although such monitoring techniques most likely will not supplant the information gained from macroscopic observations, they will enhance the information gained from the crystallization trials. We have investigated the mechanisms of hen egg-white lysozyme (HEL) crystallization and demonstrated the utility of fluorescence methods for protein crystallization. The following conclusions were reached:

- 1) The crystallographic structure of HEL co-crystallized with the organic ion orange II showed that the ligand was not bound in a specific location on the protein. The structure of the protein itself was not significantly perturbed by the presence of orange II. However, the decrease in the solvent shell indicates that increase hydrophobic interactions resulted from the presence of orange II. These hydrophobic interactions were not considered favorable for crystallization.
- 2) Time-resolved fluorescence and anisotropy measurements of 1-pyrene butyric acid covalently labeled to HEL (PBA-HEL) is useful as a trace fluorescence probe in monitoring the effects of salt precipitants on protein-protein interactions. It was demonstrated that increases in the rotational correlation times of PBA-HEL were able to indicate increases in the protein interactions which are necessary for crystallization.
- 3) A non-covalently bound probe, 1-anilino-8-naphthalene sulfonate (ANS), was shown to be a more practical method for monitoring protein crystallization conditions. The salts were also found to cause cooperative binding of ANS to HEL resulting in increased

fluorescence intensity. The polarity sensitive behavior of ANS was used to eliminate interference from unbound species. This system was used to map the increases in the binding and rotational correlation times to the influence of salt and protein concentrations. It was demonstrated that this technique could be used to dynamically monitor protein crystallization conditions in both batch and vapor diffusion experiments in a practical manner.

- 4) Investigations on the effects of various salts on the fluorescence and anisotropy behavior of the ANS/HEL system were able to provide information on the mechanisms of HEL crystallization. HEL crystallization likely involves a two step process. In this model, binding of the anions acts to reduce the repulsive interactions between the positively charged groups of HEL. For nucleation to occur, specific protein-protein bonds must form. It is likely that the formation of these bonds requires a decrease in the orientational mobility of the HEL molecules and involves a release of the bound anions. The implications of these findings for improving the screening of crystallization conditions were discussed.

From these findings, it appears that the specific interactions between the HEL and the anions is the central phenomenon involved in nucleation and crystallization. These interactions are mediated by the particular chemical properties of the bound anions. As observed with the fluorescence techniques, the binding of these anions cause increased interactions between the protein and leads to a decrease in the rotational mobility. Subsequent nucleation and crystallization depends on the ability of these bound anions to participate during the formation of crystalline contacts between HEL molecules. To

determine whether these findings are generally applicable to the crystallization of other proteins and to develop screening and optimization methods incorporating these results, further work is required.

Recommendations for Further Research

In regards to the crystallization of HEL, further studies which were beyond the scope of the current work may provide useful information on the crystallization process. A more thorough study of the effects of fluorescence probes and other ligands on the crystallization behavior is recommended. Such studies may be classified as investigations on the effects of contaminants on protein crystallization. More detailed investigations on the effects of various concentrations of ANS on the crystallization behavior is recommended to define the perturbations introduced with the use of a fluorescence probe. It is also recommended that the structure of the ANS-HEL conjugate be determined. Structural knowledge of the binding properties of ANS would enhance the interpretation of the fluorescence behavior.

Preliminary investigations have shown that PBA-HEL crystallizes under vastly different conditions than the native form and requires the addition of a detergent and decreased temperatures. More detailed investigations on the crystallization behavior would provide information on the perturbations imposed by the large hydrophobic moiety. It would also prove to be interesting to determine the crystallographic structure of PBA-HEL. Through the structure determination, the specific location and stereochemistry of the PBA group could be identified. Furthermore, it is likely that the interactions of the PBA with detergents could be characterized. This system could provide a useful model system for the crystallization of other hydrophobic proteins.

To generalize the application of fluorescence techniques to the crystallization of different proteins, the spectroscopic behavior of other protein/probe systems should be investigated. These systems should include proteins with properties different from HEL. Such proteins may be classified according to surface properties including acidic, basic or hydrophobic characteristics and according to the size and conformational heterogeneity. Alternatively, different proteins may be chosen according to the types of conditions and precipitants which lead to crystallization. A suitable candidate for further experiments is α -chymotrypsin. The structure of the ANS/ α -chymotrypsin complex has been determined crystallographically and would be helpful in interpreting the results of the fluorescence experiments. The use of other probes could be useful for investigating other probe-protein interactions and may be required for proteins that do not bind ANS.

Improvements in the fluorescence instrumentation are recommended to increase the speed and accuracy of the measurements. These improvements are required for fluorescence spectroscopy to become a routine tool for use by crystallographers. To increase the accuracy of the time anisotropy measurements, an intensity integrator is recommended to monitor intensity fluctuations in the laser excitation source. A laser power integrator which monitors the laser intensity during the measurement of each emission polarizer orientation has been designed and constructed, but has not yet been implemented. The relative intensity of each decay can then be normalized to the excitation power. An electronically controlled polarizer rotator would facilitate the measurement of rotational correlation times. This apparatus would be useful in the automatic monitoring and control of solution conditions during time-course experiments.

To decrease the cost of the instrumentation for routine applications, the use of the frequency modulation techniques should be investigated as an alternative to the time-correlated single photon counting technique. The frequency modulation technique involves the use of a sinusoidally varying excitation source as opposed to the pulsed excitation source currently used. The relative cost and benefits should be examined for each technique. Alternatively, the fluorescence measurements could be performed in steady-state mode. However, resolution of the different decay components would be lost.

After the improvements in the instrumentation and the characterization of other protein/probe systems have been completed, the development of a general crystallization strategy is warranted. It is unlikely that current protocols for previously uncrystallized protein based on the visual observation of crystallization trials will be completely supplanted. However, the incorporation of the fluorescence probe technique into current screening and optimization procedures should be defined to achieve maximum effectiveness. Such procedures would likely involve the proper selection of probes based on the particular properties of the protein and the subsequent characterization of the effects of various precipitants on the protein interactions. Although it is in its infancy, the application of fluorescence techniques to protein crystallization problems shows significant promise.

APPENDIX A

Tabulated Data for Chapter 5

Appendices A, B and C contain the fluorescence and anisotropy parameters from the least squares deconvolution fits of the intensity decays. Total fluorescence parameters are listed first followed by the anisotropy parameters. The first column lists the conditions of each sample, *M* is the molarity, *IS* is the ionic strength and *sqrt(IS)* is the square root of the ionic strength. For the fit parameters, *chisqr* is the reduced sum of squares for the fit, *Scatt* and *Shift* are the scatter and shift parameters for the instrument response function and *Offset* is the zero offset value. For the total fluorescence fits, *A1*, *A2*, *A3*, ..., are the pre-exponential factors and *T1*, *T2*, *T3*, ..., are the fluorescence lifetimes. For the anisotropic fits, *B1*, *B2*, *B3*, ..., are the pre-exponential factors and *R1*, *R2*, *R3*, ..., are the rotational correlation times. Also included with the total fluorescence data are the visual observations made on the solution denoted as *obs*. Please refer to the text for the other symbols and abbreviations.

Total Fluorescence: Set 2, Series 2B. 2% HEL vs. [NaCl]

%NaCl	M	IS	sqrt(IS)	chisqr	Scatt	Shift	Offset	Obs
0.00	0.000	0.000	0.000	1.615	0.000	-0.032	0.000	
2.00	0.342	0.342	0.585	1.713	0.000	-0.019	0.000	
4.00	0.684	0.684	0.827	1.826	0.000	0.004	0.000	
5.00	0.856	0.856	0.925	1.411	0.000	-0.036	0.000	X
6.00	1.027	1.027	1.013	1.838	0.000	-0.016	0.000	X+
8.00	1.369	1.369	1.170	1.744	0.000	-0.019	0.000	PPT+

%NaCl	A1	A2	A3	Sum
0.00	0.678	0.116	0.206	139.8
2.00	0.641	0.152	0.207	110.4
4.00	0.616	0.146	0.238	105.7
5.00	0.609	0.165	0.227	107.6
6.00	0.616	0.161	0.223	91.6
8.00	0.630	0.156	0.214	90.2

%NaCl	T1	T2	T3
0.00	151.4	57.5	2.6
2.00	156.0	65.7	2.6
4.00	159.3	64.9	2.1
5.00	162.1	69.4	2.6
6.00	164.2	70.4	2.4
8.00	167.1	67.4	2.4

Total Fluorescence: Set 2, Series 2A. 4% HEL vs. [NaCl]

%NaCl	M	IS	sqrt(IS)	chisqr	Scatt	Shift	Offset	Obs
0.00	0.000	0.000	0.000	1.907	0.000	-0.033	0.000	
2.00	0.342	0.342	0.585	1.770	0.000	-0.002	0.000	
4.00	0.684	0.684	0.827	1.590	0.000	-0.006	0.000	X+
5.00	0.856	0.856	0.925	1.645	0.000	-0.040	0.000	X+
6.00	1.027	1.027	1.013	1.679	0.000	-0.009	0.000	X++
8.00	1.369	1.369	1.170	1.647	0.000	-0.027	0.000	PPT++

%NaCl	A1	A2	A3	Sum
0.00	0.551	0.115	0.334	125.7
2.00	0.538	0.128	0.334	132.9
4.00	0.525	0.139	0.335	120.7
5.00	0.523	0.147	0.331	120.9
6.00	0.533	0.144	0.323	152.2
8.00	0.532	0.146	0.323	140.4

%NaCl	T1	T2	T3
0.00	151.4	54.3	2.3
2.00	156.1	59.1	2.4
4.00	162.1	63.5	2.3
5.00	166.1	67.5	2.8
6.00	167.1	67.1	2.5
8.00	169.3	68.6	2.7

Total Fluorescence: Set 2, Series 3D. 2% NaCl vs. [HEL]

% Lys	chisqr	Scatt	Shift	Offset	Obs
1.00	1.418	0.000	-0.045	0.000	
2.00	1.595	0.000	-0.027	0.000	
4.00	2.142	0.000	0.019	0.000	
6.00	1.757	0.000	-0.053	0.000	
8.00	2.245	0.000	-0.031	0.000	

% Lys	A1	A2	A3	Sum
1.00	0.692	0.151	0.158	98.1
2.00	0.621	0.138	0.242	99.6
4.00	0.508	0.126	0.366	116.2
6.00	0.439	0.114	0.447	147.8
8.00	0.384	0.101	0.515	167.9

% Lys	T1	T2	T3
1.00	152.8	65.5	2.6
2.00	154.2	62.2	2.6
4.00	156.7	59.8	2.5
6.00	157.7	55.2	2.6
8.00	158.2	50.8	2.5

Total Fluorescence: Set 2, Series 3C. 5% NaCl vs. [HEL]

% Lys	chisqr	Scatt	Shift	Offset	Obs
1.00	1.489	0.000	0.000	0.000	
2.00	1.411	0.000	-0.036	0.000	X
4.00	1.645	0.000	-0.040	0.000	X+
6.00	1.969	0.000	-0.046	0.000	X+++
8.00	2.214	0.000	-0.040	0.000	PPT+

% Lys	A1	A2	A3	Sum
1.00	0.722	0.152	0.126	93.8
2.00	0.609	0.165	0.227	107.6
4.00	0.523	0.147	0.331	120.9
6.00	0.437	0.115	0.448	111.7
8.00	0.385	0.102	0.513	113.3

% Lys	T1	T2	T3
1.00	156.2	66.7	3.4
2.00	162.1	69.4	2.6
4.00	166.1	67.5	2.8
6.00	166.2	59.2	2.6
8.00	166.3	53.3	2.5

Total Fluorescence: Set 2, Series C. 4% HEL vs. [NAc]

%NAc	M	IS	sqrt(IS)	chisqr	Scatt	Shift	Offset	Obs
0.00	0.000	0.000	0.000	1.186	0.000	-0.037	0.000	
2.00	0.244	0.244	0.494	1.314	0.000	0.017	0.000	
4.00	0.488	0.488	0.698	1.384	0.000	-0.008	0.000	
6.00	0.731	0.731	0.855	1.782	0.000	0.004	0.000	
8.00	0.975	0.975	0.988	1.594	0.000	-0.091	0.000	
10.00	1.219	1.219	1.104	1.766	0.000	0.006	0.000	X+
12.00	1.463	1.463	1.209	1.613	0.000	-0.079	0.000	X++

%NAc	A1	A2	A3	Sum
0.00	0.559	0.118	0.324	21.8
2.00	0.537	0.129	0.334	47.4
4.00	0.509	0.137	0.354	68.1
6.00	0.500	0.138	0.362	92.1
8.00	0.499	0.144	0.357	111.1
10.00	0.465	0.153	0.382	96.2
12.00	0.475	0.143	0.381	70.8

%NAc	T1	T2	T3
0.00	153.1	24.4	2.2
2.00	159.7	50.7	3.9
4.00	159.4	46.0	4.0
6.00	160.7	52.0	4.2
8.00	161.0	52.6	4.8
10.00	160.6	50.4	4.7
12.00	158.4	48.5	4.7

Total Fluorescence: Set 2, Series 1K. 4% HEL vs. [NS]

%NS	M	IS	sqrt(IS)	chisqr	Scatt	Shift	Offset	Obs
0.00	0.000	0.000	0.000	1.753	0.000	-0.038	0.000	
4.00	0.303	0.908	0.953	2.042	0.000	-0.010	0.000	
8.00	0.605	1.816	1.348	1.810	0.000	-0.002	0.000	
12.00	0.908	2.724	1.651	1.800	0.000	0.010	0.000	
16.00	1.211	3.633	1.906	1.736	0.000	0.003	0.000	PPT

%NS	A1	A2	A3	Sum
0.00	0.574	0.110	0.317	133.9
4.00	0.520	0.141	0.339	114.4
8.00	0.521	0.144	0.336	104.8
12.00	0.508	0.144	0.349	108.8
16.00	0.519	0.130	0.351	117.7

%NS	T1	T2	T3
0.00	151.6	54.2	2.3
4.00	163.6	61.6	2.5
8.00	166.5	62.4	2.5
12.00	171.3	66.4	2.4
16.00	174.2	61.8	2.5

Fluorescence Anisotropy: Set 2, Series 2B. 2% HEL vs. [NaCl]

%NaCl	M	IS	sqrt(IS)	chisqr	Scatt	Shift	Offset
0.00	0.000	0.000	0.000	1.325	0.000	-0.032	0.000
2.00	0.342	0.342	0.585	1.380	0.000	-0.019	0.000
4.00	0.684	0.684	0.827	1.448	0.000	0.003	0.000
5.00	0.856	0.856	0.925	1.238	0.000	-0.037	0.000
6.00	1.027	1.027	1.013	1.481	0.000	-0.016	0.000
8.00	1.369	1.369	1.170	1.418	0.000	-0.019	0.000

%NaCl	B1	B2	Sum	R1	R2
0.00	0.127	0.073	0.199	17.508	0.940
2.00	0.131	0.088	0.219	21.820	0.549
4.00	0.133	0.097	0.230	25.366	0.404
5.00	0.131	0.091	0.222	28.396	0.810
6.00	0.128	0.081	0.210	32.738	0.794
8.00	0.099	0.098	0.197	38.239	0.498

Fluorescence Anisotropy: Set 2, Series 2B. 4% HEL vs. [NaCl]

%NaCl	M	IS	sqrt(IS)	chisqr	Scatt	Shift	Offset
0.00	0.000	0.000	0.000	1.473	0.000	-0.032	0.000
2.00	0.342	0.342	0.585	1.440	0.000	-0.002	0.000
4.00	0.684	0.684	0.827	1.377	0.000	-0.006	0.000
5.00	0.856	0.856	0.925	1.389	0.000	-0.041	0.000
6.00	1.027	1.027	1.013	1.415	0.000	-0.011	0.000
8.00	1.369	1.369	1.170	1.399	0.000	-0.028	0.000

%NaCl	B1	B2	Sum	R1	R2
0.00	0.137	0.113	0.250	16.749	0.564
2.00	0.138	0.139	0.277	25.622	0.561
4.00	0.131	0.129	0.260	37.621	0.741
5.00	0.123	0.105	0.228	49.526	1.837
6.00	0.120	0.097	0.217	57.288	1.736
8.00	0.121	0.145	0.266	61.549	0.781

Fluorescence Anisotropy: Set 2, Series 3D. 2% NaCl vs. [HEL]

%HEL	chisqr	Scatt	Shift	Offset
1.00	1.219	0.000	-0.045	0.000
2.00	1.317	0.000	-0.028	0.000
4.00	1.656	0.000	0.019	0.000
6.00	1.445	0.000	-0.054	0.000
8.00	1.760	0.000	-0.033	0.000
10.00	1.631	0.000	-0.051	0.000

%HEL	B1	B2	Sum	R1	R2
1.00	0.135	0.065	0.200	18.955	0.570
2.00	0.136	0.089	0.225	20.744	0.522
4.00	0.137	0.121	0.258	27.210	0.807
6.00	0.138	0.148	0.286	35.057	1.123
8.00	0.138	0.157	0.294	44.222	1.325
10.00	0.130	0.158	0.288	56.686	1.700

Fluorescence Anisotropy: Set 2, Series 3C. 5% NaCl vs. [HEL]

% HEL	chisqr	Scatt	Shift	Offset
1.00	1.261	0.000	0.000	0.000
2.00	1.238	0.000	-0.037	0.000
4.00	1.389	0.000	-0.041	0.000
6.00	1.620	0.000	-0.050	0.000
8.00	1.728	0.000	-0.044	0.000
10.00	2.477	0.000	-0.038	0.000

% HEL	B1	B2	Sum	R1	R2
1.00	0.128	0.051	0.180	22.417	0.788
2.00	0.131	0.091	0.222	28.396	0.810
4.00	0.123	0.105	0.228	49.526	1.837
6.00	0.120	0.138	0.257	87.921	2.072
8.00	0.116	0.177	0.293	111.954	1.584
10.00	0.112	0.217	0.329	127.075	1.574

Fluorescence Anisotropy: Set 2, Series C. 4%HEL vs. [NAc]

%NAc	M	IS	sqrt(IS)	chisqr	Scatt	Shift	Offset
0.00	0.000	0.000	0.000	1.114	0.000	-0.036	0.000
2.00	0.244	0.244	0.494	1.167	0.000	0.017	0.000
4.00	0.488	0.488	0.698	1.217	0.000	-0.008	0.000
6.00	0.731	0.731	0.855	1.355	0.000	0.004	0.000
8.00	0.975	0.975	0.988	1.330	0.000	-0.091	0.000
10.00	1.219	1.219	1.104	1.413	0.000	0.006	0.000
12.00	1.463	1.463	1.209	1.352	0.000	-0.079	0.000

%NAc	B1	B2	Sum	R1	R2
0.00	0.150	0.144	0.294	18.539	0.436
2.00	0.133	0.160	0.293	27.007	0.591
4.00	0.135	0.163	0.298	29.958	0.577
6.00	0.104	0.151	0.255	34.430	0.531
8.00	0.125	0.150	0.275	39.621	0.715
10.00	0.122	0.188	0.310	47.156	0.540
12.00	0.116	0.173	0.289	51.426	0.722

Fluorescence Anisotropy: Set 2, Series 1K. 4%HEL vs. [NS]

%NS	M	IS	sqrt(IS)	chisqr	Scatt	Shift	Offset
0.00	0.000	0.000	0.000	1.428	0.000	-0.038	0.000
4.00	0.303	0.908	0.953	1.591	0.000	-0.010	0.000
8.00	0.605	1.816	1.348	1.491	0.000	-0.002	0.000
12.00	0.908	2.724	1.651	1.470	0.000	0.008	0.000
16.00	1.211	3.633	1.906	1.460	0.000	0.000	0.000

%NS	B1	B2	Sum	R1	R2
0.00	0.141	0.099	0.240	17.291	0.612
4.00	0.137	0.100	0.237	28.986	0.847
8.00	0.130	0.087	0.217	38.239	1.713
12.00	0.118	0.079	0.198	60.458	4.739
16.00	0.109	0.076	0.184	96.454	7.503

APPENDIX B

Tabulated Data for Chapter 6

See Appendix A for an explanation of the header abbreviations and symbols.

Total Fluorescence: Set 3, Series 2L 1%HEL vs. NaCl

%NaCl	M	IS	SqIs	chisqr	Scatt	Shift	Offset	Obs
0.00	0.000	0.000	0.000	1.985	0.000	0.006	2.897	
2.00	0.345	0.345	0.587	1.507	0.000	0.004	2.665	
6.00	1.034	1.034	1.017	1.437	0.000	0.008	0.851	
8.00	1.379	1.379	1.174	1.506	0.000	0.009	2.977	XC

%NaCl	A1	A2	A3	A4	A1+A2	Sum
0.00	0.017	0.056	0.324	0.603	0.073	1885
2.00	0.036	0.089	0.227	0.648	0.125	1113
6.00	0.046	0.099	0.224	0.631	0.145	1054
8.00	0.052	0.107	0.242	0.599	0.159	817

%NaCl	T1	T2	T3	T4
0.00	17.030	5.192	0.946	0.183
2.00	17.513	5.839	1.071	0.180
6.00	17.752	6.128	1.124	0.184
8.00	17.549	5.847	1.042	0.165

Total Fluorescence: Set 3, Series 3B. 2%HEL vs. NaCl

%NaCl	M	IS	SqIs	chisqr	Scatt	Shift	Offset	Obs
0.00	0.000	0.000	0.000	1.726	0.000	0.005	3.521	
2.00	0.345	0.345	0.587	1.553	0.000	0.007	2.095	
4.00	0.690	0.690	0.830	1.423	0.000	0.011	1.647	
6.00	1.034	1.034	1.017	1.440	0.000	0.007	0.440	XC
7.00	1.207	1.207	1.099	1.277	0.000	0.013	1.005	XC

%NaCl	A1	A2	A3	A4	A1+A2	Sum
0.00	0.024	0.071	0.378	0.527	0.095	1495
2.00	0.039	0.103	0.291	0.568	0.142	964
4.00	0.052	0.120	0.284	0.544	0.171	831
6.00	0.068	0.133	0.265	0.534	0.201	730
7.00	0.080	0.136	0.263	0.521	0.216	578

%NaCl	T1	T2	T3	T4
0.00	16.961	5.146	0.918	0.147
2.00	17.199	5.621	1.014	0.161
4.00	17.244	5.744	1.013	0.145
6.00	17.731	6.176	1.148	0.164
7.00	17.344	5.729	0.998	0.116

Total Fluorescence: Set 3, Series 2G. 3.6%NaCl vs. NaCl

%NaCl	M	IS	SqIs	chisqr	Scatt	Shift	Offset	Obs
0.00	0.000	0.000	0.000	1.306	0.000	-0.007	6.403	
1.00	0.172	0.172	0.415	1.468	0.000	0.007	1.837	
2.00	0.345	0.345	0.587	1.326	0.000	0.002	0.252	
3.00	0.517	0.517	0.719	1.293	0.000	0.011	1.480	
4.00	0.690	0.690	0.830	1.404	0.000	0.013	-0.484	X
5.00	0.862	0.862	0.928	1.208	0.000	0.023	-1.344	X+
6.00	1.034	1.034	1.017	1.159	0.000	0.032	-0.211	X++

%NaCl	A1	A2	A3	A4	A1+A2	Sum
0.00	0.036	0.105	0.394	0.465	0.141	962.18
1.00	0.051	0.141	0.342	0.467	0.192	834.49
2.00	0.064	0.156	0.321	0.460	0.219	658.13
3.00	0.077	0.168	0.305	0.451	0.245	570.29
4.00	0.087	0.174	0.288	0.451	0.261	571.72
5.00	0.107	0.184	0.285	0.424	0.291	399.98
6.00	0.121	0.196	0.269	0.414	0.318	419.87

%NaCl	T1	T2	T3	T4
0.00	16.600	5.420	1.035	0.189
1.00	17.085	5.738	1.079	0.163
2.00	17.323	6.024	1.188	0.185
3.00	17.336	6.042	1.196	0.170
4.00	17.426	6.040	1.202	0.157
5.00	17.460	6.029	1.148	0.140
6.00	17.918	6.531	1.330	0.169

Total Fluorescence: Set 3, Series 3A. 5%HEL vs. NaCl

%NaCl	M	IS	SqIs	chisqr	Scatt	Shift	Offset	Obs
0.00	0.000	0.000	0.000	1.472	0.000	0.010	-1.020	
2.00	0.345	0.345	0.587	1.305	0.000	0.008	-0.245	
3.00	0.517	0.517	0.719	1.554	0.000	-0.025	-2.004	X
4.00	0.690	0.690	0.830	1.197	0.000	0.006	0.591	X++
5.00	0.862	0.862	0.928	1.278	0.000	0.009	0.527	X+++
6.00	1.034	1.034	1.017	1.149	0.000	0.007	0.748	XC

%NaCl	A1	A2	A3	A4	A1+A2	Sum
0.00	0.037	0.113	0.386	0.464	0.150	1166
2.00	0.071	0.169	0.323	0.437	0.240	689
3.00	0.092	0.188	0.301	0.419	0.280	496
4.00	0.108	0.205	0.284	0.404	0.313	508
5.00	0.120	0.202	0.274	0.404	0.322	413
6.00	0.134	0.213	0.269	0.384	0.347	412

%NaCl	T1	T2	T3	T4
0.00	16.456	5.245	0.962	0.124
2.00	16.875	5.714	1.100	0.131
3.00	17.253	6.173	1.393	0.215
4.00	17.346	5.994	1.219	0.156
5.00	17.497	6.077	1.187	0.114
6.00	17.860	6.279	1.198	0.111

Total Fluorescence: Set 3, Series 1E. 2.1%HEL vs. NS

%NS	M	IS	SqIs	chisqr	Scatt	Shift	Obs
0.00	0.000	0.000	0.000	1.501	0.000	0.009	
4.00	0.303	0.908	0.953	1.387	0.000	0.019	
8.00	0.605	1.816	1.348	1.314	0.000	0.001	
12.00	0.908	2.724	1.651	1.540	0.000	0.009	
14.00	1.060	3.179	1.783	1.425	0.000	0.015	
16.00	1.211	3.633	1.906	1.371	0.000	0.007	

%NS	A1	A2	A3	A4	A1+A2	Sum
0.00	0.033	0.088	0.380	0.500	0.120	1362
4.00	0.052	0.117	0.266	0.564	0.170	968
8.00	0.072	0.139	0.267	0.522	0.211	729
12.00	0.075	0.136	0.261	0.528	0.211	741
14.00	0.125	0.159	0.235	0.482	0.283	565
16.00	0.177	0.211	0.226	0.386	0.388	462

%NS	T1	T2	T3	T4	Offset
0.00	17.229	5.529	0.990	0.167	2.178
4.00	17.636	5.776	1.017	0.152	9.647
8.00	17.772	6.040	1.082	0.145	4.863
12.00	17.381	5.786	0.989	0.133	-6.135
14.00	17.078	5.625	0.894	0.066	-3.796
16.00	17.241	6.230	1.079	0.110	-4.881

Total Fluorescence: Set 3, Series 3H. 3.6% HEL vs. NS

%NS	M	IS	SqIs	chisqr	Scatt	Shift	Offset	Obs
0.00	0.000	0.000	0.000	1.306	0.000	-0.007	6.403	
1.98	0.150	0.450	0.671	1.312	0.000	0.001	2.256	
3.96	0.300	0.900	0.949	1.270	0.000	0.016	1.683	
7.92	0.600	1.800	1.342	1.255	0.000	0.010	0.548	
11.88	0.900	2.700	1.643	1.272	0.000	0.011	0.103	
13.86	1.050	3.150	1.775	1.184	0.000	0.016	0.876	
15.84	1.200	3.600	1.897	1.226	0.000	0.013	-0.758	

%NS	A1	A2	A3	A4	A1+A2	Sum
0.00	0.036	0.105	0.394	0.465	0.141	962
1.98	0.062	0.145	0.302	0.491	0.208	778
3.96	0.067	0.157	0.304	0.472	0.224	760
7.92	0.090	0.175	0.296	0.439	0.265	565
11.88	0.136	0.200	0.264	0.400	0.336	462
13.86	0.155	0.208	0.252	0.385	0.363	340
15.84	0.186	0.214	0.226	0.374	0.400	406

%NS	T1	T2	T3	T4
0.00	16.600	5.420	1.035	0.189
1.98	17.800	6.165	1.248	0.202
3.96	17.732	6.016	1.117	0.160
7.92	17.745	6.121	1.125	0.148
11.88	17.810	6.524	1.276	0.153
13.86	17.771	6.566	1.239	0.112
15.84	17.689	6.492	1.162	0.085

Total Fluorescence: Set 3, Series 1D. 4.3% HEL vs. NS

%NS	M	IS	SqIs	chisqr	Scatt	Shift	Offset	Obs
0.00	0.000	0.000	0.000	1.475	0.000	0.002	4.337	
4.00	0.303	0.908	0.953	1.400	0.000	0.008	-0.389	
8.00	0.605	1.816	1.348	1.172	0.000	0.013	6.330	
12.00	0.908	2.724	1.651	1.240	0.000	0.002	5.642	
14.00	1.060	3.179	1.783	1.171	0.000	-0.005	3.658	
16.00	1.211	3.633	1.906	1.166	0.000	-0.006	3.734	PPT

%NS	A1	A2	A3	A4	A1+A2	Sum
0.00	0.042	0.116	0.391	0.451	0.159	1017
4.00	0.087	0.171	0.287	0.455	0.258	499
8.00	0.125	0.196	0.274	0.406	0.321	506
12.00	0.152	0.206	0.235	0.408	0.358	371
14.00	0.192	0.229	0.235	0.344	0.421	309
16.00	0.219	0.251	0.215	0.314	0.471	302

%NS	T1	T2	T3	T4
0.00	16.868	5.504	1.013	0.144
4.00	17.632	5.980	1.142	0.138
8.00	17.742	6.373	1.287	0.170
12.00	17.895	6.467	1.198	0.102
14.00	17.833	6.714	1.315	0.116
16.00	18.205	7.172	1.518	0.153

Total Fluorescence: Set 3, Series 1T. Batch Time Course

Time (hr)	A278	HEL	chisqr	Scatt	Shift	Offset
0.25	0.222	4.213	1.196	0.000	0.003	14.291
4.50	0.228	4.326	1.159	0.000	-0.009	3.710
16.00			1.250	0.000	-0.001	4.129
17.00	0.192	3.643	1.201	0.000	0.001	0.330
21.00	0.162	3.074	1.217	0.000	0.011	2.393
32.00	0.084	1.594	1.178	0.000	-0.011	4.278
66.00	0.055	1.044	1.261	0.000	-0.009	3.395
90.00	0.045	0.854	1.644	0.000	-0.014	-1.870
105.00	0.041	0.778	1.261	0.000	-0.042	4.249
Crystal at 105hr			1.220	0.000	-0.002	0.561

Time (hr)	A1	A2	A3	A4	A1+A2	Sum
0.25	0.125	0.198	0.260	0.417	0.323	481
4.50	0.115	0.184	0.238	0.463	0.299	653
16.00	0.126	0.199	0.261	0.414	0.325	463
17.00	0.133	0.209	0.268	0.390	0.342	355
21.00	0.119	0.189	0.258	0.434	0.308	493
32.00	0.095	0.156	0.259	0.490	0.251	563
66.00	0.081	0.139	0.251	0.529	0.220	654
90.00	0.076	0.129	0.241	0.555	0.205	978
105.00	0.062	0.124	0.219	0.595	0.186	678
XTAL105	0.106	0.227	0.317	0.350	0.333	574

(Continued...)

Time (hr)	T1	T2	T3	T4
0.25	17.844	6.191	1.161	0.105
4.50	17.835	6.639	1.478	0.179
16.00	18.086	6.578	1.343	0.158
17.00	17.889	6.491	1.393	0.190
21.00	17.711	6.096	1.171	0.136
32.00	18.124	6.393	1.237	0.180
66.00	18.010	6.161	1.124	0.161
90.00	17.771	5.918	1.062	0.165
105.00	18.891	6.889	1.365	0.213
XTAL105	12.029	5.634	1.468	0.111

Total Fluorescence: Set 3, Series 4T. Vapor Diffusion Time Course

Time (hr)	chisqr	Scatt	Shift	Offset
0.25	1.265	0.000	0.011	1.958
5.00	1.282	0.000	0.003	1.736
9.00	1.356	0.000	0.006	1.702
22.00	1.257	0.000	0.004	0.440
27.00	1.279	0.000	-0.003	1.346
47.00	1.296	0.000	0.010	0.034
57.00	1.349	0.000	0.002	-0.279
70.50	1.302	0.000	0.002	1.890
73.25	1.245	0.000	-0.008	-0.178
77.50	1.206	0.000	-0.010	0.739
82.25	1.292	0.000	-0.006	-0.766
84.50	1.203	0.000	-0.014	0.223
91.50	1.177	0.000	-0.011	1.396
101.00	1.142	0.000	-0.011	1.158
101.00	1.239	0.000	-0.012	1.754
120.00	1.130	0.000	-0.013	8.014
144.00	1.288	0.000	0.002	1.942

(Continued...)

Time (hr)	A1	A2	A3	A4	FA12	Sum
0.25	0.078	0.170	0.298	0.455	0.248	692
5.00	0.087	0.180	0.301	0.433	0.267	643
9.00	0.087	0.181	0.298	0.434	0.268	525
22.00	0.097	0.194	0.288	0.421	0.291	416
27.00	0.099	0.195	0.285	0.421	0.294	573
47.00	0.104	0.200	0.268	0.428	0.304	489
57.00	0.107	0.201	0.277	0.416	0.307	482
70.50	0.122	0.218	0.277	0.382	0.341	476
73.25	0.118	0.211	0.276	0.395	0.329	475
77.50	0.119	0.208	0.277	0.395	0.328	537
82.25	0.116	0.197	0.276	0.411	0.313	466
84.50	0.112	0.188	0.274	0.426	0.300	474
91.50	0.102	0.171	0.268	0.460	0.272	493
101.00	0.112	0.171	0.244	0.473	0.283	434
101.00	0.109	0.171	0.256	0.464	0.280	459
120.00	0.105	0.160	0.234	0.500	0.265	518
144.00	0.095	0.157	0.228	0.520	0.252	594

(Continued...)

Time (hr)	T1	T2	T3	T4
0.25	17.717	6.323	1.287	0.178
5.00	17.573	6.202	1.245	0.164
9.00	17.558	6.227	1.253	0.160
22.00	17.683	6.388	1.316	0.168
27.00	17.604	6.300	1.324	0.167
47.00	17.670	6.120	1.146	0.102
57.00	17.723	6.410	1.291	0.127
70.50	17.892	6.631	1.380	0.161
73.25	17.671	6.175	1.186	0.127
77.50	17.670	6.298	1.298	0.167
82.25	17.797	6.454	1.296	0.160
84.50	17.840	6.426	1.292	0.180
91.50	17.903	6.514	1.303	0.183
101.00	18.213	6.771	1.355	0.177
101.00	18.062	6.440	1.184	0.165
120.00	18.078	6.691	1.250	0.174
144.00	17.905	6.639	1.234	0.147

Fluorescence Anisotropy: Set 3, Series 2L 1%HEL vs. NaCl

%NaCl	M	IS	SqIs	chisqr	Scatt	Shift	Offset
0.00	0.000	0.000	0.000	1.850	0.000	0.005	0.000
2.00	0.345	0.345	0.587	1.495	0.000	0.003	0.000
6.00	1.034	1.034	1.017	1.394	0.000	0.006	0.000
8.00	1.379	1.379	1.174	1.401	0.000	0.007	0.000

%NaCl	B1	B2	FB1	Sum	R1	R2
0.00	0.166	0.154	0.520	0.320	14.805	1.611
2.00	0.198	0.137	0.591	0.335	22.398	1.480
6.00	0.194	0.140	0.581	0.334	24.554	1.467
8.00	0.196	0.141	0.582	0.337	26.075	1.291

Fluorescence Anisotropy: Set 3, Series 3B. 2%HEL vs. NaCl

%	M	IS	SqIs	chisqr	Scatt	Shift	Offset
0.00	0.000	0.000	0.000	1.634	0.000	0.004	0.000
2.00	0.345	0.345	0.587	1.419	0.000	0.006	0.000
4.00	0.690	0.690	0.830	1.332	0.000	0.010	0.000
6.00	1.034	1.034	1.017	1.366	0.000	0.006	0.000
7.00	1.207	1.207	1.099	1.241	0.000	0.012	0.000

%	B1	B2	FB1	Sum	R1	R2
0.00	0.175	0.165	0.514	0.340	17.458	1.624
2.00	0.193	0.147	0.568	0.340	21.132	1.634
4.00	0.199	0.145	0.579	0.344	24.190	1.453
6.00	0.204	0.137	0.597	0.341	29.800	1.692
7.00	0.208	0.143	0.593	0.351	34.183	1.201

Fluorescence Anisotropy: Set 3, Series 2G. 3.6%NaCl vs. NaCl

%	M	IS	SqIs	chisqr	Scatt	Shift	Offset
0.00	0.000	0.000	0.000	1.345	0.000	-0.008	0.000
1.00	0.172	0.172	0.415	1.361	0.000	0.006	0.000
2.00	0.345	0.345	0.587	1.259	0.000	0.001	0.000
3.00	0.517	0.517	0.719	1.270	0.000	0.010	0.000
4.00	0.690	0.690	0.830	1.321	0.000	0.012	0.000
5.00	0.862	0.862	0.928	1.243	0.000	0.022	0.000
6.00	1.034	1.034	1.017	1.185	0.000	0.031	0.000
7.00	1.207	1.207	1.099	2.268	0.000	-0.022	0.000

%	B1	B2	FB1	Sum	R1	R2
0.00	0.186	0.166	0.529	0.353	18.478	1.681
1.00	0.206	0.155	0.571	0.361	21.846	1.416
2.00	0.207	0.146	0.587	0.353	25.357	1.517
3.00	0.207	0.145	0.589	0.352	31.718	1.558
4.00	0.212	0.142	0.598	0.354	35.950	1.472
5.00	0.212	0.135	0.611	0.347	40.800	1.299
6.00	0.211	0.130	0.618	0.341	50.505	1.514
7.00	0.113	0.095	0.544	0.208	51.294	0.807

Fluorescence Anisotropy: Set 3, Series 3A. 5%HEL vs. NaCl

%NaCl	M	IS	SqIs	chisqr	Scatt	Shift	Offset
0.00	0.000	0.000	0.000	1.341	0.000	0.009	0.000
2.00	0.345	0.345	0.587	1.276	0.000	0.007	0.000
3.00	0.517	0.517	0.719	1.471	0.000	-0.026	0.000
4.00	0.690	0.690	0.830	1.190	0.000	0.004	0.000
5.00	0.862	0.862	0.928	1.206	0.000	0.009	0.000
6.00	1.034	1.034	1.017	1.155	0.000	0.005	0.000
7.00	1.207	1.207	1.099	1.524	0.000	-0.017	0.000

%NaCl	B1	B2	FB1	Sum	R1	R2
0.00	0.199	0.173	0.535	0.371	18.812	1.375
2.00	0.208	0.149	0.583	0.357	29.554	1.392
3.00	0.221	0.148	0.600	0.369	32.662	1.354
4.00	0.209	0.133	0.612	0.342	47.862	1.419
5.00	0.211	0.130	0.618	0.341	56.841	1.440
6.00	0.220	0.129	0.630	0.350	69.822	1.307
7.00	0.098	0.143	0.406	0.241	86.007	0.176

Fluorescence Anisotropy: Set 3, Series 1E. 2.1%HEL vs. NS

%NS	M	IS	SqIs	chisqr	Scatt	Shift	Offset
0.00	0.000	0.000	0.000	1.572	0.000	0.009	0.000
4.00	0.303	0.908	0.953	1.655	0.000	0.018	0.000
8.00	0.605	1.816	1.348	1.547	0.000	-0.001	0.000
12.00	0.908	2.724	1.651	1.689	0.000	0.007	0.000
14.00	1.060	3.179	1.783	1.624	0.000	0.014	0.000
16.00	1.211	3.633	1.906	1.497	0.000	0.006	0.000

%NS	B1	B2	FB1	Sum	R1	R2
0.00	0.191	0.185	0.507	0.376	20.676	1.894
4.00	0.216	0.161	0.573	0.376	25.184	1.387
8.00	0.221	0.160	0.580	0.380	26.378	1.058
12.00	0.227	0.159	0.589	0.385	29.576	1.193
14.00	0.231	0.136	0.630	0.367	39.359	0.935
16.00	0.218	0.123	0.639	0.341	50.493	1.057

Fluorescence Anisotropy: Set 3, Series 3H. 3.6% HEL vs. NS

%NS	M	IS	SqIs	chisqr	Scatt	Shift	Offset
0.00	0.000	0.000	0.000	1.345	0.000	-0.008	0.000
1.98	0.150	0.450	0.671	1.285	0.000	0.000	0.000
3.96	0.300	0.900	0.949	1.253	0.000	0.015	0.000
7.92	0.600	1.800	1.342	1.241	0.000	0.009	0.000
11.88	0.900	2.700	1.643	1.215	0.000	0.010	0.000
13.86	1.050	3.150	1.775	1.173	0.000	0.015	0.000
15.84	1.200	3.600	1.897	1.206	0.000	0.012	0.000
17.82	1.350	4.050	2.012	1.364	0.000	-0.011	0.000

%NS	B1	B2	FB1	Sum	R1	R2
0.00	0.186	0.166	0.529	0.353	18.478	1.681
1.98	0.211	0.162	0.566	0.372	28.851	1.551
3.96	0.205	0.152	0.574	0.357	29.906	1.375
7.92	0.220	0.148	0.598	0.368	35.339	1.377
11.88	0.224	0.135	0.625	0.359	47.010	1.465
13.86	0.224	0.125	0.642	0.348	54.894	1.315
15.84	0.217	0.105	0.673	0.322	76.715	1.405
17.82	0.029	0.290	0.092	0.319	73.337	0.001

Fluorescence Anisotropy: Set 3, Series 1D. 4.3% HEL vs. NS

%NS	M	IS	SqIs	chisqr	Scatt	Shift	Offset
0.00	0.000	0.000	0.000	1.551	0.000	0.001	0.000
4.00	0.303	0.908	0.953	1.546	0.000	0.007	0.000
8.00	0.605	1.816	1.348	1.275	0.000	0.015	0.000
12.00	0.908	2.724	1.651	1.259	0.000	0.001	0.000
14.00	1.060	3.179	1.783	1.269	0.000	-0.007	0.000
16.00	1.211	3.633	1.906	1.182	0.000	-0.007	0.000

%NS	B1	B2	FB1	Sum	R1	R2
0.00	0.219	0.193	0.532	0.412	20.499	1.419
4.00	0.230	0.158	0.592	0.388	36.473	1.348
8.00	0.234	0.140	0.625	0.374	46.504	1.725
12.00	0.234	0.128	0.646	0.362	57.302	1.308
14.00	0.236	0.120	0.663	0.356	70.868	1.205
16.00	0.204	0.095	0.682	0.299	96.775	1.353

Fluorescence Anisotropy: Set 3, Series 1T. Batch Time Course

Time	A278	HEL	chisqr	Scatt	Shift	Offset
0.25	0.222	4.213	1.340	0.000	0.002	0.000
4.50	0.228	4.326	1.352	0.000	-0.011	0.000
16.00			1.256	0.000	-0.002	0.000
17.00	0.192	3.643	1.532	0.000	0.000	0.000
21.00	0.162	3.074	1.364	0.000	0.009	0.000
32.00	0.084	1.594	1.249	0.000	-0.012	0.000
66.00	0.055	1.044	1.384	0.000	-0.010	0.000
90.00	0.045	0.854	2.017	0.000	-0.015	0.000
105.00	0.041	0.778	3.449	0.000	-0.028	0.000
Crystal-105			1.330	0.000	-0.004	0.000

Time	B1	B2	FB1	Sum	T1	T2
0.25	0.243	0.147	0.623	0.391	54.856	1.171
4.50	0.241	0.158	0.604	0.398	53.532	1.289
16.00	0.233	0.140	0.624	0.373	55.643	1.518
17.00	0.238	0.154	0.608	0.392	52.099	1.231
21.00	0.230	0.149	0.606	0.379	46.472	1.092
32.00	0.219	0.153	0.589	0.372	33.596	1.505
66.00	0.212	0.158	0.574	0.370	27.974	1.212
90.00	0.219	0.186	0.541	0.405	21.539	0.745
105.00	0.280	0.413	0.404	0.694	15.667	0.149
Crystal-105	0.379	0.250	0.603	0.628	>10E3	1.673

Fluorescence Anisotropy: Set 3, Series 4T. Vapor Diffusion Time Course

Time (hr)	chisqr	Scatt	Shift	Offset
0.25	1.238	0.000	0.010	0.000
5.00	1.240	0.000	0.002	0.000
9.00	1.267	0.000	0.006	0.000
22.00	1.203	0.000	0.003	0.000
27.00	1.219	0.000	-0.003	0.000
47.00	1.211	0.000	0.010	0.000
57.00	1.234	0.000	0.001	0.000
70.50	1.237	0.000	0.001	0.000
73.25	1.221	0.000	-0.009	0.000
77.50	1.227	0.000	-0.011	0.000
82.25	1.212	0.000	-0.007	0.000
84.50	1.225	0.000	-0.015	0.000
91.50	1.156	0.000	-0.012	0.000
101.00	1.140	0.000	-0.012	0.000
101.00	1.222	0.000	-0.013	0.000
120.00	1.146	0.000	-0.014	0.000
144.00	1.262	0.000	0.001	0.000

(Continued...)

Time (hr)	B1	B2	FB1	Sum	R1	R2
0.25	0.191	0.130	0.595	0.322	29.753	1.412
5.00	0.187	0.128	0.594	0.315	36.854	1.530
9.00	0.177	0.120	0.595	0.297	34.735	1.554
22.00	0.180	0.117	0.607	0.297	42.454	1.555
27.00	0.170	0.109	0.610	0.279	35.414	1.328
47.00	0.183	0.113	0.618	0.296	47.937	1.209
57.00	0.188	0.116	0.618	0.304	53.336	1.525
70.50	0.198	0.122	0.619	0.320	59.008	1.530
73.25	0.181	0.114	0.613	0.295	52.487	1.395
77.50	0.189	0.119	0.615	0.308	50.927	1.428
82.25	0.165	0.099	0.626	0.264	35.373	1.312
84.50	0.195	0.128	0.604	0.323	41.550	1.262
91.50	0.181	0.117	0.607	0.299	34.837	1.556
101.00	0.175	0.113	0.608	0.288	35.690	1.375
101.00	0.184	0.123	0.599	0.307	35.006	1.221
120.00	0.175	0.120	0.593	0.295	34.130	1.346
144.00	0.168	0.122	0.579	0.291	39.252	1.389

APPENDIX C

Tabulated Data for Chapter 7

See Appendix A for an explanation of the header abbreviations and symbols.

Total Fluorescence: Set 3, Series 2A. 3.6%HEL vs. NaSCN

%NaSCN	M	IS	SqIs	chisqr	Scatt	Shift	Offset	Obs
0.00	0.000	0.000	0.000	1.306	0.000	-0.007	6.403	
0.20	0.025	0.025	0.158	1.416	0.000	0.011	7.822	
0.41	0.050	0.050	0.224	1.410	0.000	0.017	7.711	
0.61	0.075	0.075	0.274	1.545	0.000	0.009	-2.816	
0.81	0.100	0.100	0.316	1.401	0.000	0.013	2.071	X
1.01	0.125	0.125	0.354	1.336	0.000	0.015	1.285	XC
1.22	0.150	0.150	0.387	1.389	0.000	0.010	1.332	XC
1.22	0.150	0.150	0.387	1.340	0.000	0.012	1.792	XC

%NaSCN	A1	A2	A3	A4	A1+A2	Sum
0.00	0.036	0.105	0.394	0.465	0.141	962
0.20	0.044	0.126	0.366	0.464	0.171	964
0.41	0.051	0.140	0.345	0.464	0.191	1035
0.61	0.058	0.160	0.336	0.446	0.218	1093
0.81	0.061	0.171	0.311	0.457	0.232	612
1.01	0.071	0.183	0.296	0.450	0.254	580
1.22	0.074	0.191	0.292	0.442	0.266	674
1.22	0.079	0.192	0.292	0.438	0.270	701

%NaSCN	T1	T2	T3	T4
0.00	16.600	5.420	1.035	0.189
0.20	15.940	5.390	1.034	0.167
0.41	15.812	5.513	1.034	0.139
0.61	16.050	5.787	1.104	0.156
0.81	16.571	6.118	1.211	0.174
1.01	16.496	6.109	1.183	0.146
1.22	16.679	6.255	1.267	0.173
1.22	16.604	6.257	1.237	0.150

Total Fluorescence: Set 3, Series 2G. 3.6%HEL vs. NaCl

See Appendix C.

Total Fluorescence: Set 3, Series 3G. 3.6%HEL vs. NAc pH6.4

%NAc	M	IS	SqIs	chisqr	Scatt	Shift	Offset	Obs
0.00	0.000	0.000	0.000	1.306	0.000	-0.007	6.403	
2.31	0.300	0.300	0.548	1.358	0.000	0.012	1.202	
4.63	0.600	0.600	0.775	1.462	0.000	0.008	1.235	
9.25	1.200	1.200	1.095	1.491	0.000	0.011	1.276	X
11.56	1.500	1.500	1.225	1.476	0.000	-0.003	1.100	X
13.88	1.800	1.800	1.342	1.474	0.000	0.013	1.708	X+
18.50	2.400	2.400	1.549	1.578	0.000	0.007	1.164	X+
23.13	3.000	3.000	1.732	1.452	0.000	0.011	1.729	X++

%NAc	A1	A2	A3	A4	A1+A2	Sum
0.00	0.036	0.105	0.394	0.465	0.141	962
2.31	0.044	0.127	0.333	0.497	0.170	865
4.63	0.050	0.137	0.317	0.497	0.186	872
9.25	0.054	0.140	0.302	0.504	0.194	840
11.56	0.055	0.144	0.297	0.504	0.198	864
13.88	0.053	0.136	0.291	0.520	0.189	856
18.50	0.053	0.138	0.295	0.514	0.191	932
23.13	0.049	0.130	0.297	0.525	0.179	993

%NAc	T1	T2	T3	T4
0.00	16.600	5.420	1.035	0.189
2.31	16.791	5.673	1.032	0.140
4.63	17.006	5.877	1.097	0.148
9.25	16.878	5.884	1.111	0.145
11.56	17.081	6.160	1.269	0.200
13.88	16.579	5.617	1.030	0.114
18.50	16.465	5.759	1.125	0.138
23.13	15.765	5.173	1.010	0.125

Total Fluorescence: Set 3, Series 2B. 3.6%HEL vs. NaP

%NaP	M	IS	SqIs	chisqr	Scatt	Shift	Offset	Obs
0.00	0.000	0.000	0.000	1.702	0.000	0.013	2.333	
3.60	0.300	0.300	0.548	1.360	0.000	0.014	-0.134	
7.20	0.600	0.600	0.775	1.323	0.000	0.011	1.847	
10.80	0.900	0.900	0.949	1.240	0.000	0.016	0.584	
14.40	1.200	1.200	1.095	1.198	0.000	0.010	0.937	
18.00	1.500	1.500	1.225	1.144	0.000	0.010	0.249	PPT

%NaP	A1	A2	A3	A4	A1+A2	Sum
0.00	0.034	0.105	0.391	0.470	0.139	1157
3.60	0.067	0.152	0.323	0.458	0.219	669
7.20	0.096	0.173	0.295	0.436	0.269	620
10.80	0.131	0.197	0.278	0.395	0.328	457
14.40	0.173	0.207	0.235	0.385	0.380	321
18.00	0.235	0.227	0.204	0.334	0.462	253

%NaP	T1	T2	T3	T4
0.00	17.033	5.609	1.017	0.159
3.60	17.260	6.004	1.102	0.146
7.20	17.777	6.421	1.213	0.143
10.80	17.949	6.445	1.163	0.111
14.40	18.017	6.530	1.180	0.079
18.00	18.315	6.996	1.352	0.088

Total Fluorescence: Set 3, Series 3H. 3.6%HEL vs. NS

See Appendix C.

Total Fluorescence: Set 3, Series 3E. 3.6% HEL vs. NAc, pH 4.6

%NS	M	IS	SqIs	chisqr	Scatt	Shift	Offset	Obs
0.00	0.000	0.000	0.000	1.306	0.000	-0.007	6.403	
3.08	0.400	0.400	0.632	1.526	0.000	0.010	0.765	
6.17	0.800	0.800	0.894	1.634	0.000	0.007	1.195	
9.25	1.200	1.200	1.095	1.859	0.000	0.000	0.551	
12.33	1.600	1.600	1.265	1.777	0.000	0.002	1.701	
15.42	2.000	2.000	1.414	1.923	0.000	0.016	0.723	

%NS	A1	A2	A3	A4	A1+A2	Sum
0.00	0.036	0.105	0.394	0.465	0.141	962
3.08	0.030	0.101	0.351	0.518	0.130	1235
6.17	0.026	0.096	0.342	0.536	0.122	1208
9.25	0.020	0.092	0.354	0.534	0.112	1462
12.33	0.016	0.091	0.378	0.515	0.107	1716
15.42	0.012	0.081	0.342	0.565	0.093	2734

%NS	T1	T2	T3	T4
0.00	16.600	5.420	1.035	0.189
3.08	16.538	4.962	0.990	0.153
6.17	15.721	4.569	0.964	0.158
9.25	15.072	4.121	0.880	0.157
12.33	13.757	3.391	0.682	0.082
15.42	13.520	3.287	0.654	0.050

Total Fluorescence: Set 3, Series 2F. 3.6% HEL vs. NAc, pH 7.7

%NAc	M	IS	SqIs	chisqr	Scatt	Shift	Offset	Obs
0.00	0.000	0.000	0.000	1.304	0.000	-0.007	0.005	
4.63	0.600	0.600	0.775	1.389	0.000	0.005	0.712	
6.94	0.900	0.900	0.949	1.318	0.000	0.009	-2.782	
9.25	1.200	1.200	1.095	1.345	0.000	0.016	-1.190	
11.56	1.500	1.500	1.225	1.347	0.000	0.002	-3.478	X
13.88	1.800	1.800	1.342	1.312	0.000	0.006	-2.074	X+
16.19	2.100	2.100	1.449	1.302	0.000	0.008	-1.436	X++
18.50	2.400	2.400	1.549	1.223	0.000	0.016	0.743	X+++

%NAc	A1	A2	A3	A4	A1+A2	Sum
0.00	0.036	0.105	0.394	0.465	0.141	962
4.63	0.069	0.172	0.300	0.459	0.241	663
6.94	0.081	0.185	0.287	0.447	0.266	630
9.25	0.095	0.197	0.271	0.438	0.292	519
11.56	0.110	0.206	0.253	0.430	0.316	469
13.88	0.126	0.215	0.242	0.417	0.341	423
16.19	0.132	0.213	0.243	0.413	0.345	384
18.50	0.124	0.188	0.197	0.492	0.311	571

%NAc	T1	T2	T3	T4
0.00	16.600	5.420	1.035	0.189
4.63	17.251	6.323	1.165	0.174
6.94	17.171	6.214	1.105	0.143
9.25	17.306	6.401	1.119	0.134
11.56	17.261	6.407	1.168	0.134
13.88	17.150	6.423	1.173	0.132
16.19	17.099	6.316	1.070	0.098
18.50	17.186	6.508	1.131	0.074

Total Fluorescence: Set 3, Series 4B. 0.862 IS NaSCN vs. HEL

%HEL	M	IS	SqIs	chisqr	Scatt	Shift	Offset	Obs
0.30	0.000	0.000	0.014	2.360	0.000	0.000	1.631	XC
0.40	0.000	0.000	0.017	2.463	0.000	-0.002	2.130	XC
0.45	0.000	0.000	0.018	2.383	0.000	0.005	1.595	XC
0.48	0.000	0.000	0.018	1.882	0.000	-0.003	1.147	XC
0.50	0.000	0.000	0.019	1.948	0.000	-0.001	2.847	XC
0.60	0.000	0.000	0.020	2.031	0.000	0.066	1.855	XC

%HEL	A1	A2	A3	A4	A1+A2	Sum
0.30	0.009	0.027	0.116	0.848	0.036	3642
0.40	0.012	0.031	0.121	0.836	0.043	2818
0.45	0.012	0.041	0.158	0.789	0.053	2770
0.48	0.021	0.047	0.143	0.790	0.067	2561
0.50	0.022	0.056	0.143	0.778	0.078	2027
0.60	0.023	0.058	0.250	0.669	0.081	1222

%HEL	T1	T2	T3	T4
0.30	16.350	5.020	0.792	0.199
0.40	16.435	5.196	0.847	0.198
0.45	16.081	4.776	0.781	0.186
0.48	15.960	5.338	0.868	0.194
0.50	16.003	5.573	0.928	0.191
0.60	14.915	4.595	0.541	0.122

Total Fluorescence: Set 3, Series 4A. 0.862 IS NAc pH 6.4 vs. HEL

%HEL	chisqr	Scatt	Shift	Offset	Obs
1.00	1.592	0.000	0.004	1.766	
2.00	1.299	0.000	0.005	2.951	
3.00	1.347	0.000	0.014	0.806	X
4.00	1.262	0.000	0.007	1.013	X+
5.00	1.166	0.000	0.014	0.392	X++
6.00	1.192	0.000	0.010	0.052	X++

%HEL	A1	A2	A3	A4	A1+A2	Sum
1.00	0.036	0.089	0.232	0.643	0.125	1193
2.00	0.066	0.135	0.275	0.525	0.200	716
3.00	0.089	0.169	0.288	0.455	0.258	641
4.00	0.112	0.193	0.280	0.415	0.306	552
5.00	0.123	0.207	0.282	0.388	0.330	518
6.00	0.139	0.225	0.278	0.358	0.364	509

%HEL	T1	T2	T3	T4
1.00	17.342	5.809	1.050	0.177
2.00	17.388	5.817	1.066	0.157
3.00	17.701	6.137	1.152	0.143
4.00	17.697	6.326	1.290	0.165
5.00	17.798	6.373	1.277	0.140
6.00	17.983	6.611	1.391	0.155

Total Fluorescence: Set 3, Series 4F. 0.862 IS NaP vs. HEL

%HEL	chisqr	Scatt	Shift	Offset	Obs
1.00	1.763	0.000	0.001	-0.923	
2.00	1.373	0.000	0.005	1.385	
3.00	1.435	0.000	0.012	-0.186	
4.00	1.397	0.000	0.004	-0.571	
5.00	1.360	0.000	0.018	0.902	
6.00	1.262	0.000	0.010	0.173	
7.00	1.359	0.000	0.010	-0.151	

%HEL	A1	A2	A3	A4	A1+A2	Sum
1.00	0.021	0.071	0.232	0.677	0.091	1630
2.00	0.033	0.098	0.290	0.579	0.131	656
3.00	0.047	0.131	0.309	0.513	0.178	828
4.00	0.058	0.152	0.309	0.482	0.209	710
5.00	0.063	0.161	0.310	0.466	0.223	716
6.00	0.073	0.180	0.303	0.444	0.253	567
7.00	0.075	0.175	0.300	0.450	0.250	572

%HEL	T1	T2	T3	T4
1.00	15.942	5.222	0.966	0.177
2.00	16.449	5.460	0.968	0.155
3.00	16.785	5.760	1.058	0.151
4.00	16.920	5.870	1.121	0.152
5.00	16.915	5.809	1.100	0.125
6.00	17.176	6.071	1.232	0.146
7.00	16.790	5.673	1.050	0.087

Total Fluorescence: Set 3, Series 4G. 0.862 IS NS vs. HEL

%HEL	chisqr	Scatt	Shift	Offset	Obs
1.00	1.316	0.000	0.004	2.001	
2.00	1.242	0.000	0.011	0.986	
3.00	1.135	0.000	0.010	2.084	
4.00	1.274	0.000	0.013	0.874	
5.00	1.176	0.000	0.018	1.076	
6.00	1.159	0.000	-0.001	-1.235	PPT

%HEL	A1	A2	A3	A4	A1+A2	Sum
1.00	0.062	0.102	0.252	0.584	0.164	819
2.00	0.101	0.155	0.282	0.462	0.256	513
3.00	0.127	0.182	0.274	0.418	0.309	394
4.00	0.133	0.185	0.257	0.425	0.317	412
5.00	0.154	0.198	0.234	0.415	0.351	322
6.00	0.177	0.221	0.249	0.353	0.398	357

%HEL	T1	T2	T3	T4
1.00	17.232	6.115	1.084	0.169
2.00	17.635	6.289	1.131	0.153
3.00	17.904	6.538	1.209	0.127
4.00	18.047	6.579	1.220	0.098
5.00	18.004	6.452	1.221	0.088
6.00	17.799	6.257	1.158	0.086

Total Fluorescence: Set 3, Series 1F. 0.862 M NS vs. HEL

%HEL	chisqr	Scatt	Shift	Offset	Obs
1.08	1.489	0.000	0.011	-6.597	
2.15	1.282	0.000	0.001	-1.760	
4.30	1.637	0.000	0.012	-12.128	
6.45	1.539	0.000	0.013	-8.922	
8.60	1.231	0.000	0.016	0.869	
10.75	1.129	0.000	0.018	-0.024	

%HEL	A1	A2	A3	A4	A1+A2	Sum
1.08	0.058	0.107	0.217	0.619	0.165	799
2.15	0.113	0.180	0.274	0.433	0.293	543
4.30	0.164	0.202	0.242	0.392	0.366	469
6.45	0.187	0.221	0.225	0.367	0.408	412
8.60	0.188	0.218	0.215	0.380	0.405	380
10.75	0.199	0.221	0.184	0.396	0.420	293

%HEL	T1	T2	T3	T4
1.08	17.264	5.634	0.915	0.103
2.15	17.619	6.127	1.074	0.130
4.30	17.179	5.803	1.074	0.098
6.45	17.517	6.011	1.106	0.085
8.60	17.981	6.752	1.306	0.087
10.75	18.017	6.616	1.333	0.086

Fluorescence Anisotropy: Set 3, Series 2A. 3.6%HEL vs. NaSCN

%NaSCN	M	IS	SqIs	chisqr	Scatt	Shift	Offset
0.00	0.000	0.000	0.000	1.345	0.000	-0.008	0.000
0.20	0.025	0.025	0.158	1.427	0.000	0.010	0.000
0.41	0.050	0.050	0.224	1.396	0.000	0.016	0.000
0.61	0.075	0.075	0.274	1.604	0.000	0.008	0.000
0.81	0.100	0.100	0.316	1.321	0.000	0.011	0.000
1.01	0.125	0.125	0.354	1.299	0.000	0.014	0.000
1.22	0.150	0.150	0.387	1.345	0.000	0.009	0.000
1.22	0.150	0.150	0.387	1.305	0.000	0.011	0.000
1.42	0.175	0.175	0.418	1.579	0.000	-0.018	0.000

%NaSCN	B1	B2	FB1	Sum	R1	R2
0.00	0.186	0.166	0.529	0.353	18.478	1.681
0.20	0.205	0.159	0.564	0.363	17.406	1.307
0.41	0.202	0.155	0.566	0.357	20.400	1.317
0.61	0.205	0.151	0.576	0.356	23.452	1.327
0.81	0.206	0.145	0.587	0.351	27.298	1.492
1.01	0.204	0.136	0.599	0.340	38.448	1.536
1.22	0.196	0.133	0.595	0.328	40.236	1.611
1.22	0.203	0.134	0.602	0.336	47.198	1.614
1.42	0.053	0.049	0.520	0.101	85.712	0.782

Fluorescence Anisotropy: Set 3, Series 2G. 3.6%HEL vs. NaCl

See Appendix C.

Fluorescence Anisotropy: Set 3, Series 3G. 3.6%HEL vs. NAc pH6.4

%NAc	M	IS	SqIs	chisqr	Scatt	Shift	Offset
2.31	0.300	0.300	0.548	1.345	0.000	0.011	0.000
4.63	0.600	0.600	0.775	1.290	0.000	0.007	0.000
9.25	1.200	1.200	1.095	1.341	0.000	0.010	0.000
11.56	1.500	1.500	1.225	1.818	0.000	-0.004	0.000
13.88	1.800	1.800	1.342	1.317	0.000	0.012	0.000
18.50	2.400	2.400	1.549	1.417	0.000	0.006	0.000
23.13	3.000	3.000	1.732	1.344	0.000	0.010	0.000

%NAc	B1	B2	FB1	Sum	R1	R2
2.31	0.211	0.170	0.554	0.380	25.464	1.441
4.63	0.210	0.158	0.571	0.369	30.206	1.483
9.25	0.209	0.154	0.575	0.363	36.792	1.439
11.56	0.217	0.164	0.569	0.381	36.249	1.173
13.88	0.217	0.157	0.581	0.374	50.754	1.291
18.50	0.216	0.156	0.581	0.372	64.310	1.340
23.13	0.213	0.157	0.576	0.369	75.894	1.190

Fluorescence Anisotropy: Set 3, Series 2B. 3.6%HEL vs. NaP

%NaP	M	IS	SqIs	chisqr	Scatt	Shift	Offset
0.00	0.000	0.000	0.000	1.507	0.000	0.012	0.000
3.60	0.300	0.300	0.548	1.272	0.000	0.013	0.000
7.20	0.600	0.600	0.775	1.268	0.000	0.010	0.000
10.80	0.900	0.900	0.949	1.174	0.000	0.015	0.000
14.40	1.200	1.200	1.095	1.193	0.000	0.009	0.000
18.00	1.500	1.500	1.225	1.180	0.000	0.009	0.000

%NaP	B1	B2	FB1	Sum	R1	R2
0.00	0.182	0.169	0.519	0.351	19.081	1.549
3.60	0.210	0.156	0.574	0.366	29.006	1.387
7.20	0.214	0.142	0.601	0.356	38.235	1.512
10.80	0.220	0.128	0.632	0.349	50.545	1.410
14.40	0.225	0.116	0.660	0.341	73.887	1.262
18.00	0.232	0.101	0.698	0.333	122.637	1.377

Total Fluorescence: Set 3, Series 3H. 3.6%HEL vs. NS

See Appendix C.

Fluorescence Anisotropy: Set 3, Series 3E. 3.6% HEL vs. NAc, pH 4.6

%NAc	M	IS	SqIs	chisqr	Scatt	Shift	Offset
0.00	0.000	0.000	0.000	1.345	0.000	-0.008	0.000
3.08	0.400	0.400	0.632	1.479	0.000	0.009	0.000
6.17	0.800	0.800	0.894	1.531	0.000	0.005	0.000
9.25	1.200	1.200	1.095	1.652	0.000	-0.001	0.000
12.33	1.600	1.600	1.265	1.598	0.000	0.001	0.000
15.42	2.000	2.000	1.414	1.703	0.000	0.015	0.000

%NAc	B1	B2	FB1	Sum	R1	R2
0.00	0.186	0.166	0.529	0.353	18.478	1.681
3.08	0.194	0.166	0.538	0.360	24.574	1.419
6.17	0.196	0.160	0.550	0.357	29.456	1.315
9.25	0.180	0.160	0.530	0.340	40.825	1.034
12.33	0.173	0.181	0.489	0.354	68.633	0.525
15.42	0.156	0.191	0.449	0.347	117.354	0.415

Fluorescence Anisotropy: Set 3, Series 2F. 3.6% HEL vs. NAc, pH 7.7

%NAc	M	IS	SqIs	chisqr	Scatt	Shift	Offset
4.63	0.600	0.600	0.775	1.345	0.000	0.003	0.000
6.94	0.900	0.900	0.949	1.296	0.000	0.008	0.000
9.25	1.200	1.200	1.095	1.308	0.000	0.015	0.000
11.56	1.500	1.500	1.225	1.318	0.000	0.001	0.000
13.88	1.800	1.800	1.342	1.253	0.000	0.004	0.000
16.19	2.100	2.100	1.449	1.271	0.000	0.007	0.000
18.50	2.400	2.400	1.549	1.221	0.000	0.015	0.000

%NAc	B1	B2	FB1	Sum	R1	R2
4.63	0.206	0.145	0.587	0.350	27.693	1.562
6.94	0.212	0.143	0.597	0.355	32.608	1.418
9.25	0.220	0.137	0.617	0.357	40.889	1.386
11.56	0.228	0.132	0.633	0.360	47.360	1.248
13.88	0.222	0.125	0.641	0.347	61.159	1.369
16.19	0.234	0.124	0.654	0.357	71.357	1.114
18.50	0.216	0.112	0.659	0.328	104.531	1.241

Fluorescence Anisotropy: Set 3, Series 4B. 0.862 IS NaSCN vs. HEL

%HEL	chisqr	Scatt	Shift	Offset
0.30	2.064	0.000	0.000	0.000
0.40	2.177	0.000	-0.002	0.000
0.45	2.181	0.000	0.005	0.000
0.48	2.005	0.000	-0.003	0.000
0.50	2.004	0.000	-0.002	0.000
0.60	1.693	0.000	0.066	0.000

%HEL	B1	B2	FB1	Sum	R1	R2
0.30	0.232	0.247	0.485	0.479	10.223	0.097
0.40	0.234	0.264	0.470	0.499	10.990	0.094
0.45	0.218	0.231	0.486	0.449	13.508	0.117
0.48	0.205	0.246	0.454	0.451	28.673	0.117
0.50	0.184	0.198	0.481	0.382	41.612	0.188
0.60	0.184	0.237	0.437	0.421	53.485	0.106

**Fluorescence Anisotropy: Set 3, Series 4A. 0.862 IS NAc pH 6.4 vs.
HEL**

%HEL	chisqr	Scatt	Shift	Offset
1.00	1.521	0.000	0.003	0.000
2.00	1.290	0.000	0.004	0.000
3.00	1.240	0.000	0.013	0.000
4.00	1.221	0.000	0.006	0.000
5.00	1.192	0.000	0.013	0.000
6.00	1.193	0.000	0.009	0.000

%HEL	B1	B2	FB1	Sum	R1	R2
1.00	0.193	0.142	0.577	0.334	21.072	1.321
2.00	0.207	0.147	0.584	0.354	29.691	1.343
3.00	0.213	0.145	0.595	0.358	37.625	1.421
4.00	0.219	0.139	0.612	0.358	49.827	1.473
5.00	0.218	0.133	0.622	0.351	58.611	1.583
6.00	0.221	0.125	0.638	0.346	77.391	1.624

Fluorescence Anisotropy: Set 3, Series 4F. 0.862 IS NaP vs. HEL

%HEL	chisqr	Scatt	Shift	Offset			
1.00	1.756	0.000	0.000	0.000			
2.00	1.326	0.000	0.003	0.000			
3.00	1.344	0.000	0.011	0.000			
4.00	1.336	0.000	0.003	0.000			
5.00	1.271	0.000	0.017	0.000			
6.00	1.254	0.000	0.008	0.000			
7.00	1.269	0.000	0.009	0.000			

%HEL	B1	B2	FB1	Sum	R1	R2
1.00	0.193	0.145	0.571	0.338	19.597	1.001
2.00	0.202	0.150	0.573	0.352	25.384	1.319
3.00	0.209	0.157	0.571	0.366	31.027	1.455
4.00	0.215	0.155	0.581	0.371	35.172	1.480
5.00	0.214	0.156	0.578	0.369	40.113	1.385
6.00	0.215	0.154	0.583	0.368	47.857	1.593
7.00	0.212	0.154	0.578	0.366	50.568	1.432

Fluorescence Anisotropy: Set 3, Series 4G. 0.862 IS NS vs. HEL

%HEL	chisqr	Scatt	Shift	Offset
1.00	1.350	0.000	0.003	0.000
2.00	1.214	0.000	0.010	0.000
3.00	1.178	0.000	0.009	0.000
4.00	1.194	0.000	0.012	0.000
5.00	1.135	0.000	0.017	0.000
6.00	1.165	0.000	-0.002	0.000

%HEL	B1	B2	FB1	Sum	R1	R2
1.00	0.214	0.147	0.594	0.361	32.208	1.581
2.00	0.224	0.142	0.611	0.366	38.582	1.332
3.00	0.227	0.135	0.627	0.362	45.954	1.283
4.00	0.224	0.131	0.631	0.354	52.328	1.358
5.00	0.232	0.125	0.650	0.356	66.988	1.204
6.00	0.229	0.113	0.670	0.341	70.235	1.173

Fluorescence Anisotropy: Set 3, Series 1F. 0.862 M NS vs. HEL

%HEL	chisqr	Scatt	Shift	Offset
1.08	2.331	0.000	0.010	0.000
2.15	1.502	0.000	0.000	0.000
4.30	2.089	0.000	0.011	0.000
6.45	1.696	0.000	0.012	0.000
8.60	1.212	0.000	0.015	0.000
10.75	1.156	0.000	0.017	0.000

%HEL	B1	B2	FB1	Sum	R1	R2
1.08	0.218	0.156	0.583	0.373	26.287	1.000
2.15	0.228	0.145	0.611	0.373	38.891	1.219
4.30	0.237	0.127	0.651	0.364	48.489	1.050
6.45	0.245	0.119	0.674	0.364	72.591	1.038
8.60	0.248	0.121	0.671	0.369	115.258	1.195
10.75	0.250	0.116	0.683	0.366	237.034	1.241

LIST OF REFERENCES

1. C. E. Bugg, *J. Cryst. Growth* 76 (1986) 535.
2. A. McPherson, *J. Cryst. Growth* 110 (1991) 1.
3. Hunefeld, *Die Chemismus in der Thierischen Organization* (Leipzig, 1840).
4. E. J. Cohn and J. D. Ferry, Eds., *Proteins, Amino Acids and Peptides* (Rheinhold, New York, 1950).
5. J. B. Sumner, *J. Biol. Chem.* 37 (1919) 359.
6. J. B. Sumner and S. F. Howell, *J. Biol. Chem.* 113 (1936) 607.
7. T. Arakawa and S. N. Timasheff, *Methods in Enzymology* 114 (1985) 49.
8. G. Feher and Z. Kam, *Methods in Enzymology* 114 (1985) 77.
9. R. Boistelle and J. P. Astier, *J. Cryst. Growth* 90 (1988) 14.
10. A. McPherson, *Methods in Enzymology* 114 (1985) 112.
11. A. McPherson, *Preparation and Analysis of Protein Crystals* (Wiley, New York, 1982).
12. D. Ollis and S. White, *Methods in Enzymology* 182 (1990) 646.
13. R. S. Feigelson, *J. Cryst. Growth* 90 (1988) 1.
14. Z. Kam, H. B. Shore and G. Feher, *J. Mol. Biol.* 123 (1978) 539.
15. P. Hartman and P. Bennema, *J. Cryst. Growth* 49 (1980) 145.
16. P. Hartman and W. G. Perdock, *Acta Cryst.* 8 (1955) 49.
17. P. Hartman, in: *Crystal Growth: an Introduction*, Ed. P. Hartman (North-Holland, Amsterdam, 1973) p. 367.
18. S. D. Durbin and G. Feher, *J. Cryst. Growth* 76 (1986) 583.
19. R. W. Fiddis, R. A. Longman and P. D. Calvert, *Trans. Faraday Soc.* 75 (1979) 2753.
20. S. D. Durbin and G. Ferher, *J. Mol. Biol.* 212 (1990) 763.

21. E. Forsythe and M. L. Pusey, *J. Cryst. Growth* 139 (1994) 89.
22. L. C. Sieker, *J. Cryst. Growth* 90 (1988) 31.
23. M. Pusey, W. K. Witherow and R. J. Naumann, *J. Cryst. Growth* 90 (1988) 105.
24. C. C. Young, R. C. De Mattei, R. S. Feigelson and W. A. Tiller, *J. Cryst. Growth* 90 (1988) 79.
25. A. A. Green, *J. Biol. Chem.* 95 (1932) 47.
26. J. G. Kirkwood, *Proteins, Amino Acids and Peptides*. E. J. Cohn, J. T. Edsall, Eds., (Van Nostrand-Reinhold, Princeton, New Jersey, 1943).
27. W. Eberstein, Y. Georgalis and W. Saenger, *J. Cryst. Growth* 143 (1994) 71.
28. W. A. Tiller, *J. Cryst. Growth* 76 (1986) 607.
29. E. J. W. Verwey and J. T. G. Overbeek, *Theory of Stability of Lyophobic Colloids* (Elsevier, Amsterdam, 1948).
30. J. A. McCammon and P. G. Wolynes, *Nature* 262 (1976) 325.
31. S. D. Durbin and W. E. Carlson, *J. Cryst. Growth* 122 (1992) 71.
32. F. R. Salemme, L. Genieser, B. C. Finzel, R. M. Hilmer and J. J. Wendoloski, *J. Cryst. Growth* 90 (1988) 273.
33. P. C. Weber, *Advan. Protein Chem.* 41 (1991) 1.
34. C. W. Carter Jr. and C. W. Carter, *J. Biol. Chem.* 254 (1979) 12219.
35. G. L. Gilliland, M. Tung, D. M. Blakeslee and J. Ladner, *Data. Acta Crystallogr. D* 50 (1994) 408.
36. S. B. Howard, T. P. J., J. K. Baird and E. J. Meehan, *J. Cryst. Growth* 90 (1988) 94.
37. M. M. Ries-Kautt and A. F. Ducruix, *J. Cryst. Growth* 110 (1991) 20.
38. R. Roxby and C. Tanford, *Biochem.* 11 (1972) 2193.
39. R. Roxby and C. Tanford, *Biochem.* 10 (1971) 3348.
40. M. L. Pusey, *J. Cryst. Growth* 122 (1992) 1.

41. M. J. Conroy and R. E. Lovrien, *J. Cryst. Growth* 122 (1992) 213.
42. U. Derewenda, et al., *Nature* 338 (1989) 594.
43. N. E. Chayen, L. F. Lloyd, C. A. Collyer and D. M. Blow, *J. Cryst. Growth* 97 (1989) 367.
44. L. F. Lloyd, P. Brick and D. M. Blow, *J. Cryst. Growth* 122 (1992) 355.
45. E. A. Stura, G. R. Nemerow and I. A. Wilson, *J. Cryst. Growth* 122 (1992) 273.
46. W. Ruf and E. A. Stura, *J. Cryst. Growth* 122 (1992) 253.
47. C. R. Cantor and P. R. Schimmel, *Biophysical Chemistry Part II: Techniques for the Study of Biological Structure and Function* (W. H. Freeman and Co., San Francisco, 1980).
48. M. L. Pusey, *J. Cryst. Growth* 110 (1991) 60.
49. R. Pecora, *Dynamic Light Scattering: Applications of Photon Correlation Spectroscopy* (Plenum Press, New York, 1985).
50. C. W. Carter Jr., E. T. Baldwin and L. Frick, *J. Cryst. Growth* 90 (1988) 60.
51. V. Mikol, P. Vincendon, G. Eriani and E. Hirsch, *J. Cryst. Growth* 110 (1991) 195.
52. W. Kadima, A. McPherson, M. Dunn F. and F. Jurnak, *J. Cryst. Growth* 110 (1991) 188.
53. W. Kadima, A. McPherson, M. F. Dinn and F. A. Jurnak, *Biophysics. J.* 57 (1990) 371.
54. M. Zulaf and A. D'Arcy, *J. Cryst. Growth* 122 (1992) 102.
55. V. Mikol, E. Hirsch and R. Giege, *FEBS Letters* 258 (1989) 63.
56. J. B. Bishop, W. J. Fredericks, S. B. Howard and T. Sawada, *J. Cryst. Growth* 122 (1992) 41.
57. M. Skouri, J. P. Munch, B. Lorber and R. Giege, *J. Cryst. Growth* 122 (1992) 14.
58. Y. Georgalis, A. Zouni and W. Saenger, *J. Cryst. Growth* 118 (1992) 360.

59. Y. Georgalis, A. Zouni, W. Eberstein and W. Saenger, *J. Cryst. Growth* 126 (1993) 245.
60. W. W. Wilson, *Methods: A Companion to Methods in Enzymology* 1 (1990) 110.
61. A. J. Malkin and A. McPherson, *Acta Cryst.* D50 (1994) 385.
62. G. Sazaki, H. Ooshima, J. Kato, Y. Harano and N. Hirokawa, *J. Cryst. Growth* 130 (1993) 357.
63. B. R. Ware, in: *Optical Techniques in Biological Research*, Ed. D. L. Rousseau (Academic Press, Orlando, 1984) p. 1.
64. N. C. Ford, in: *Measurement of Suspended Particles by Quasi-Elastic Light Scattering*, Ed. B. E. Dahneke (John Wiley and Sons, New York, 1983) p. 32.
65. B. R. Ware, D. Cyr, S. Gorti and F. Lanni, in: *Measurement of Suspended Particles by Quasi-Elastic Light Scattering*, Ed. B. E. Dahneke (John Wiley & Sons, New York, 1983) p. 255.
66. J. M. Beechem and L. Brand, *Ann. Rev. Biochem.* 54 (1985) 43.
67. R. F. Chen, in: *Practical Fluorescence*, Ed. G. G. Guilbault (Marcel Dekker, New York, 1990) p. 575.
68. T. G. Dewey, Ed., *Biophysical and Biochemical Aspects of Fluorescence Spectroscopy* (Plenum Press, New York, 1991).
69. T. Gulik-Krzywicki, E. Shecter and M. Iwatsubo, *Biochim. Biophys. Acta.* 219 (1970) 1.
70. D. M. Jameson and T. L. Hazlett, in: *Biophysical and Biochemical Aspects of Fluorescence Spectroscopy*, Ed. T. G. Dewey (Plenum Press, New York, 1991) p. 105.
71. K. Kalyanasundaram, *Photochemistry in Microheterogeneous Systems* (Academic Press, Orlando, 1987).
72. K. Kalyanasundaram, in: *Photochemistry in Organized and Constrained Media*, Ed. V. Ramamurthy (VCH, New York, 1991) p. 39.
73. J. R. Lakowicz, *Principles of Fluorescence Spectroscopy* (Plenum Press, New York, 1983).
74. J. R. Lakowicz, *Methods in Enzymology* 131 (1986) 518.

75. J. M. Schurr, B. S. Fujimoto, P. Wu and L. Song, in: **Topics in Fluorescence Spectroscopy**, vol. 3, Ed. J. R. Lakowicz (Plenum Press, New York, 1992) p. 137.
76. A. Szabo, *J. Chem. Phys.* 81 (1984) 150.
77. J. Yguerabide and E. E. Yguerabide, in: **Optical Techniques in Biological Research**, Ed. D. L. Rousseau (Academic Press, Orlando, 1984) p. 181.
78. T. Tao, *Biopolymers* 8 (1969) 609.
79. L. E. Bowman, K. A. Berglund and D. G. Nocera, *Rev. Sci. Instrum.* 64 (1993) 338.
80. A. Grinvald and I. Z. Steinburg, *Anal. Biochem.* 75 (1976) 260.
81. A. Grinvald and I. Z. Steinburg, *Anal. Biochem.* 59 (1974) 583.
82. J. N. Demas, **Excited State Lifetime Measurements** (Academic Press, New York, 1983).
83. A. J. Cross and G. R. Fleming, *Biophys. J.* 46 (1984) 45.
84. P. Wahl, *Biophys. Chem.* 10 (1979) 91.
85. W. H. Press, B. P. Flannery, S. A. Teukolsky and W. T. Vetterling, **Numerical Recipes in C: The Art of Scientific Computing** (Cambridge, Cambridge, 1988).
86. L. M. Loew, Ed., **Spectroscopic Membrane Probes** (CRC Press, Inc., Boca Raton, 1988).
87. M. P. Crosio and M. Jullien, *J. Cryst. Growth* 122 (1992) 66.
88. M. Jullien, *FEBS Letters* 253 (1989) 38.
89. M. Jullien and M. P. Crosio, *J. Cryst. Growth* 110 (1991) 182.
90. M. Jullien, M. P. Crosio, B.-N. Sylvie, F. Merola and J.-C. Brochon, *Acta Cryst. D50* (1994) 398.
91. T. Imoto, L. N. Johnson, A. C. T. North, D. C. Phillips and J. A. Rupley, in: **The Enzymes**, vol. VII, Ed. P. D. Boyer (Academic Press, New York, 1972) p. 665.
92. A. Fleming and V. D. Allison, *Brit. J. Exp. Path.* 3 (1922) 252.
93. C. C. F. Blake, et al., *Nature* 206 (1965) 757.

94. T. Imoto and L. S. Forster, *Proc. Natl. Acad. Sci. USA* 69 (1971) 1151.
95. K. Vos, A. V. Hoek and A. J. W. G. Visser, *Eur. J. Biochem.* 165 (1987) 55.
96. A. McPherson, *Eur. J. Biochem.* 189 (1990) 1.
97. M. M. Ries-Kautt and A. F. Ducruix, *J. Biol. Chem.* 264 (1989) 745.
98. K. P. Wilson, B. A. Malcolm and B. W. Mathews, *J. Biol. Chem.* 267 (1992) 10842.
99. A. J. Howard, et al., *J. Appl. Crystallogr.* 20 (1987) 383-387.
100. A. T. Brunger, *X-PLOR Manual (Version 2.1)* (Yale University, New Haven, 1990).
101. B. C. Finzel, *J. Appl. Crystallogr.* 20 (1987) 53.
102. J. A. Bell, et al., *Proteins: Structure, Function and Genetics* 10 (1991) 10.
103. A. Wlodawer, J. Deisenhofer and R. Huber, *J. Mol. Biol.* 193 (1987) 145.
104. J. Moult, et al., *J. Mol. Biol.* 100 (1976) 179.
105. R. Kodandapnai, C. G. Suresh and M. Vijayan, *J. Biol. Chem.* 265 (1990) 16126.
106. R. G. Pearson, *J. Am. Chem. Soc.* 85 (1963) 3533.
107. H. Michel, Ed., *Crystallization of Membrane Proteins* (CRC Press, Boca Raton, 1991).
108. A. Kawski, *Crit. Rev. Anal. Chem.* 23 (1993) 459.
109. E. Bucci and R. F. Steiner, *Biophys. Chem.* 30 (1988) 199.
110. W. M. Vaughan and G. Weber, *Biochem.* 9 (1970) 464.
111. B. Pan, R. Chakraborty and K. A. Berglund, *J. Crystal Growth* 130 (1993) 587.
112. A. J. Sophianopoulous, C. K. Rhodes, D. N. Holcomb and K. E. Vac Holde, *J. Biol. Chem.* 237 (1962) 1107.

113. D. J. S. Birch and R. E. Imhof, in: *Topics in Fluorescence Spectroscopy*, vol. 1, Ed. J. R. Lakowicz (Plenum Press, New York, 1991) p. 1.
114. R. P. Haugland, *Handbook of Fluorescent Probes and Research Chemicals* (Molecular Probes, Inc., Eugene, 1992).
115. S. Kurimatsu and K. Hamaguchi, *J. Biochem.* 87 (1980) 1215.
116. S. B. Dubin, N. A. Clark and G. B. Benedek, *J. Chem. Phys.* 54 (1971) 5158.
117. W. J. Fredericks, M. C. Hammonds, S. B. Howard and F. Rosenberger, *J. Cryst. Growth* 141 (1994) 183.
118. L. Picullel and S. Nilsson, *Progr. Colloid Polym. Sci.* 82 (1990) 198.
119. R. C. DeMattei and R. S. Feigelson, *J. Cryst. Growth* 122 (1992) 21.
120. B. E. Jones, J. M. Beecham and C. R. Matthews, *Biochem.* 34 (1995) 1867.
121. J. D. Johnson, M. A. El-Bayoumi, L. D. Weber and A. Tulinsky, *Biochem.* 18 (1979) 1292.
122. L. D. Weber, A. Tulinsky, J. D. Johnson and M. A. Bayoumi, *Biochem.* 18 (1979) 1297.
123. J. Slavík, *Biochim. et Biophys. Acta* 694 (1982) 1.
124. L. Brand and J. R. Gohlke, *Ann. Rev. Biochem.* 41 (1972) 83.
125. H. Dodiuk, H. Hanety and E. M. Kosower, *J. Phys. Chem.* 83 (1979) 1979.
126. H. Szmecinski, R. Jayaweera, H. Cherek and J. R. Lakowicz, *Biophys. Chem.* 27 (1987) 233.
127. P. Debye, *Polar Molecules* (Leipzig and Rheinhold, New York, 1929).
128. A. V. Elgersma, M. Ataka and T. Katsura, *J. Cryst. Growth* 122 (1992) 31.
129. G. W. Robinson, et al., *J. Am. Chem. Soc.* 100 (1978) 7146.
130. E. M. Kosower and H. Kanety, *J. Am. Chem. Soc.* 105 (1983) 6236.
131. J. R. Colvin, *Can. J. Biochem. and Physiol.* 32 (1954) 109.
132. J. Jancarik and S.-H. Kim, *J. Appl. Cryst.* 24 (1991) 409.

- 133. L. Sabelle and M. L. Pusey, *Acta Cryst. D50* (1994) 396.
- 134. M. Ries-Kautt and A. Ducruix, *Acta. Cryst. D50* (1994) 366.
- 135. M. L. Pusey and R. J. Naumann, *J. Cryst. Growth* 76 (1986) 593.
- 136. L. A. Monaco and F. Rosenberger, *J. Cryst. Growth* 129 (1993) 465.

MICHIGAN STATE UNIV. LIBRARIE



31293014101772